Quantitative analysis of self-potential anomalies: Review of case studies from various SP applications

Lev V. Eppelbaum (levap@tauex.tau.ac.il)
Tel Aviv University https://orcid.org/0000-0001-6540-0150

Research Article

Keywords: disturbances, quantitative analysis, complex physical-geological environments, self-potential moment, ore deposits, archaeological sites, underground caves, underground pipes

Posted Date: March 17th, 2021

DOI: https://doi.org/10.21203/rs.3.rs-305402/v1

Quantitative analysis of self-potential anomalies: Review of case studies from various SP applications

Lev V. Eppelbaum

Dept. of Geophysics, School of Earth Sciences, Faculty of Exact Sciences, Tel Aviv University, Ramat Aviv *6997801*, Tel Aviv, Israel; Email: levap@tauex.tau.ac.il

Data Availability Statement

The field examples presented in the paper are author's data (Caucasus, Israel) or were reproduced from the published sources (with citation) and with following analysis

Abstract

Self-potential (SP) method is one of the most non-expensive and unsophisticated geophysical methods. However, its application limits absence of reliable interpreting methodology, first for the complex geological-environmental conditions. The typical disturbances appearing in the SP method are discussed. To exclude these noise components before the quantitative analysis, some ways for their removing (elimination) are presented. Some brief review of the available interpretation methods is presented. For the magnetic method of geophysical prospecting, special quantitative procedures applicable under complex physical-geological environments (oblique polarization, uneven terrain relief and unknown level of the normal field), have been recently developed. Earlier detected common peculiarities between the magnetic and SP fields have been extended. These common aspects make it possible to apply the advanced procedures developed in magnetic prospecting to SP method. Besides the reliable determination of the depth of anomalous targets, these methodologies enable to calculate the corrections for non-horizontal SP observations and direction of polarization vector. For classification of SP-anomalies is proposed to use a new parameter – 'self-potential moment'. These quantitative procedures (improved modifications of characteristic point, tangent techniques and areal method) have been successfully tested on SP models and employed in real situations in mining, archaeological, environmental and technogenic geophysics. The obtained results indicate practical importance of the developed methodologies.

Keywords: disturbances, quantitative analysis, complex physical-geological environments, self-potential moment, ore deposits, archaeological sites, underground caves, underground pipes

1. INTRODUCTION

The Self-Potential (SP) method is based on the study of natural electric field (in some sources this method is named as 'spontaneous polarization'). The term "natural" here means that the field does not create by an external artificial source. Permanent electric fields arise in the course of redox, filtration, and diffusion-adsorption processes in the upper part of geological section. The registration of these fields is the goal of the SP method, and the geophysical interpretation of the parameters generating this field is the main purpose of SP data examination. An oxidizing object (e.g., ore body, archaeological or other target) is a galvanic cell, the occurrence of which requires: (1) the contact of electric conductors with different types of conductivity (electronic and ionic), and (2) the difference in the redox conditions at different contact points of these conductors. An appearance of these conditions is usually impossible without the underground water contact (Sato and Mooney, 1960).

In the geological section, the conditions for the formation of a galvanic cell arise on targets with electronic conductivity, if these bodies are in the water-saturated rocks with ionic conductivity. The change in the redox conditions at the contact of the electronic conductor (anomalous target) and the surrounding medium is associated with a decrease in the oxygen content with a depth.

Fox's (1830) SP observations at copper vein deposits in Cornwall (England) laid the foundation of the application of all electric methods in geophysics as a whole. SP is an effective, prompt and comparatively simple geophysical method. Equipment for SP method is one of the most non-expensive in the field geophysics (Table 1).

58 **Table 1**. Averaged prices for geophysical potential field equipment

Method	Gravity	Magnetic	Resistivity	Self-Potential
Price of equipment, US $	60,000 – 110,000	20,000 – 25,000	35,000 – 55,000	150 – 200

59

60 Conventional equipment employed in the SP method consists of
61 microVoltmeter, pair of non-polarizable electrodes, cable and $CuSO_4$ solution (the
62 latter is necessary for the better contact of employed electrodes with the environment).
63 Without hesitation, ground penetration radar (GPR) and electric resistivity
64 tomography (ERT) are more powerful geophysical tools which can theoretically
65 produce a lot more detailed geophysical-archaeological information. However, they
66 are much more expensive and, what is the most important, water content in subsurface
67 strongly complicates application of these methods. At the same time, presence of water
68 is only positive factor for the SP method, since it enables to increase SP anomaly
69 intensity (Semenov, 1980; Parasnis, 1986).
70 SP method is employed in mining geophysics (e.g., Semenov, 1980; Corry,
71 1985; Babu and Rao, 1988; Lile, 1996; Golkdie, 2002; Bhattacharya et al., 2007;
72 Dmitriev, 2012; Fedi and Abbas, 2013; Biswas and Sharma, 2016; Eppelbaum,
73 2019a,b), archaeological geophysics (e.g., Wynn and Sherwood, 1984; Mauriello et
74 al., 1998; Eppelbaum et al., 2003a, b; Drahor 2004; Di Maio et al., 2010; Shevnin et
75 al., 2014; De Giorgi and Leucci, 2017, 2019), environmental geophysics (e.g., Corwin,
76 1990; Quarto and Schiavone, 1996; Jardani et al., 2006a; Eppelbaum, 2007; Srigutomo
77 et al., 2010; Chen et al., 2018; Gusev et al., 2018; Oliveti and Cardarelli, 2019) and
78 technogenic geophysics (e.g., Castermant et al., 2008; Fomenko, 2010; Onojasun and

79 Takum, 2015; Cui et al., 2017). Application of quantitative analysis in the SP method
80 for solving other geological-geophysical problems is beyond the scope of this study.

81

82 **2. SELF-POTENTIAL OBSERVATIONS: AVAILABLE DISTURBANCES**

83 ***2.1. Different kinds of noise in SP observations***

84 Main kinds of noise appearing in the SP method are shown in a block-scheme (Figure
85 1). Some of these noise effects are considered below in detail.

86 *2.1.1. Electrode noise in SP method*

87 Although the fact that SP electrode is called as "non-polarizable", after some time it
88 accomplishes some polarization effects from the surrounding media. However, taking
89 into account that we measure the value ΔU ($U_1 - U_2$), the most is important is to keep
90 not absolute non-polarizability, but an equivalent polarization on the both applied
91 electrodes. For checking this equivalent, the following procedure can be employed in
92 field conditions (of course, measurements in a physical laboratory are more precise).
93 We can write a trivial equation for first electrode: $U_1 + e_1$ (U_1 is the first "medium"
94 signal, and e_1 is the noise accumulated in the first electrode). For second electrode,
95 correspondingly we have $U_2 + e_2$ (U_2 is the second "medium" signal, and e_2 is the noise
96 of accumulated in the second electrode). According to (Semenov, 1980), we measure

97 $$\Delta U_1 = (U_1 + e_1) - (U_2 + e_2). \quad (1)$$

98 Let us will change electrodes by their places. In this case we will obtain

99 $$\Delta U_2 = (U_1 + e_2) - (U_2 + e_1). \quad (2)$$

100 After this, calculating a difference between ΔU_1 and ΔU_2, we receive

101 $$\partial U = \Delta U_1 - \Delta U_2 = [U_1 + e_1 - U_2 - e_2] - [U_1 + e_2 - U_2 - e_1] = 2(e_1 - e_2) \quad (3)$$

102 or

$$\left(e_1 - e_2\right) = \frac{\partial U}{2}. \quad (4)$$

If the value $\left(e_1 - e_2\right)$ is significant (e.g., ≥ 3 mV), the noised electrodes must be replaced by new ones.

A similar methodology for the electrode noise detection was suggested by Perrier and Pant (2005).

2.1.2. Temporal variations in SP method

Parasnis (1986) has been carried out SP measurements in Akulla region (Sweden) seven times during the period of 1960-1967 years. These measurements indicate a good repeatability despite of the fact that they were conducted under different climatic conditions. Similar investigations performed by other researchers (e.g., Semenov, 1980) generally confirm good repeatability of the SP different time observations.

For estimation of accuracy ε of SP field measurements the following trivial formula often employed in various geophysical methods may be applied

$$\varepsilon = \sqrt{\frac{\sum_{i=1}^{N}\left(\Delta U_{SP}^{init} - \Delta U_{SP}^{rep}\right)^2}{N}},$$

where N is the total number of SP observations, 'init' means the ordinary measurements, and 'rep' means the repeated measurements. The number of repeated measurements should be at least 8-10% of the total number pf observations. If the value of ε exceeds some *a priori* assumed value (this value usually depend on the concrete spread of the SP amplitudes), results of SP survey can be rejected as non-reliable ones.

2.1.3. Terrain relief correction

In the SP method, terrain relief influence is two-fold. On the one hand, over the positive topographic forms can be created negative SP anomalies caused by

126 electromotive force (this phenomena strongly depends on the peculiarities of
127 underground water circulations). Comparison of the SP graphs with topographic data
128 usually allows to identifying anomalies of this type by the characteristic mirror image
129 of the terrain in them (Khesin et al., 1996).

130 From other side, as follows from the very detailed SP measurements of Ernstson
131 and Schrerer (1986), at the inclined topographic surface the SP field directly increases
132 with relief form heightening (Figure 2). In the last case, for elimination of the terrain
133 relief influence, a correlation method developed in magnetic prospecting (Khesin et
134 al., 1996) and VLF studies (Eppelbaum and Mishne, 2011) can be applied
135 (employment of other methods to reduce the relief influence is also possible). The
136 essence of this method is following. The method employs for removing the terrain
137 relief effect from the observed field ΔU_{obser} a linear least-squares relation ΔU_{appr}
138 (application of more complex equations is also possible):

139 $$\Delta U_{appr} = c + bh,$$

140 where h is the height of relief, b is the angle coefficient, and c is the free member.

141 Value ΔU_{appr} approximates the observed field as a function of elevation h
142 (anomalous zones usually do not include to the correlation field) and then we obtain
143 corrected (residual) field ΔU_{corr}, where the relief influence is essentially eliminated:

144 $$\Delta U_{corr} = \Delta U_{obser} - \Delta U_{appr}.$$

145 Wang and Geng (2015) studied the problem of terrain correction in SP method
146 in detail on several field examples. They noted that the mechanism of SP anomalies
147 formed by terrains is rather complex, and therefore is difficult to obtain the
148 corresponding analytical formulas. The authors applied three types of relief fitting:
149 (1) linear, (2) quadratic and (3) exponential. After careful analysis, Wang and Geng

(2015) concluded that the linear fitting is more optimal since it not creates factious anomalies. Thus, the aforementioned investigation confirms application of the aforementioned linear least-squares relation.

2.1.4. Calculation of SP anomaly distortion due to observations on uneven surface

SP anomalies (as and anomalies of other potential fields) distort due to observations on uneven surface (and correspondingly, different distances to anomalous object). This disturbing effect usually is calculated at the end of interpretation process (see section 2.4).

2.1.5. Net justification in areal observations

Net justification of SP data is conventionally performed by the use of procedure identical to justification of observations in gravity and magnetic prospecting (e.g., Telford et al., 1990). Some other strategies for removing this effect are presented, for instance, in Revil and Jardani (2013).

2.1.6. Influence of meteorological factors

Many scientists note that after rains the intensity of SP anomalies increases (e.g., Semenov, 1980; Parasnis, 1986; Revil and Jardani, 2013). Therefore, occasionally an artificial irrigation of site intended for SP research is recommended.

2.1.7. Presence of magmatic associations

Obviously development of magmatic associations (or other kinds of hard geological rocks) in a site destined for field investigations does not allow to grounding SP electrodes. The same reason may limit the water circulation at subsurface, which can weaken, or even to cancel completely generation of the SP anomalies.

2.1.8. Some environmental factors

SP anomaly level may affect some environmental factors. One of these factors is shadowing of part of the investigated area. For instance, Revil and Jardani (2013) have

documented the fact that difference between the SP electrodes placed in cold and warm media may exceed 10 mV. Other factor is a presence of some hygrophilous plants (e.g., hazel and almonds) whose roots can pick over a lot of moisture from the upper part of the geological section (thereby hindering the generation of SP anomalies).

Ernstson and Schrerer (1986) have been monitored SP and temperature anomalies during 15 months (in 1980-1981) (Figure 3). The correlation between SP and soil temperature is interpreted as result of influence of thermal diffusivity and convection processes in subsurface (Ernstson and Schrerer, 1986). Between these parameters a correlation of $r = 0.6$ has been established. It is not a high relationship, but in any case should be taken into account.

Perrier and Morat (2000) also detected a correlation between the amplitudes of the SP variations and soil temperatures. According to these authors, state of the soil in the first 30 cm seems to play an important role. Perrier and Morat (2000) concluded that the joint monitoring of electric potential and temperature appears to be a powerful tool to monitor the underlying soil processes.

An essential relationship between the SP data and temperature values recorded in boreholes at intermediate and large depths was established by Jardani and Revil (2009) in the Cerro Prieto geothermal field (Baja California, USA). Existence of this phenomenon under normal thermophysical conditions is not studied yet in detail.

3. REVIEW OF QUANTITATIVE INTERPRETATION METHODS

An extensive literature is devoted to the interpretation of self-potential anomalies. Unfortunately, it is not possible to cite even all the most important publications in this review, and the author apologizes to those researchers whose excellent publications were not included in this review.

199 The calculation of theoretical anomalies due to SP has long been based primarily
200 on Petrovsky's (1928) solution derived for a vertically polarized sphere (Zaborovsky,
201 1963). Later on, some substantial solutions for sheet-like bodies and inclined plates
202 were obtained (Semenov, 1980). The electric polarization vector was generally
203 considered to be directed along the sheet-like body dipping (along the longer axis of
204 the conductive body).

205 Other method of SP anomaly quantitative interpretation includes anomalous
206 body with a simple geometrical shape which approximates the anomaly source. Its
207 parameters (i.e. the occurrence depth, the angle between the horizon and the direction
208 of the polarization vector) are usually determined: (1) graphically using characteristic
209 points of the anomaly plot, or (2) by trial-and-error method consisting of visual
210 comparison of the observed anomaly with a set of master curves (Semenov, 1980).

211 Zaborovsky (1963), Semenov (1980) and Murty and Haricharan (1984) applied
212 to SP anomaly, generated by plate and calculated along the profile across its strike, the
213 following formula:

214 $$U(x) = \frac{j\rho}{2\pi} \ln \frac{r_1^2}{r_2^2}, \qquad (5)$$

215 where j is the current per unit length, ρ is the host medium resistivity, r_1 and r_2 are the
216 distances from the plate left and right ends to the observation point.

217 Fitterman (1979) gave a method of SP anomaly calculation for field sources of
218 an arbitrary shape based on numerical integration using Green's function. This
219 potentially promising approach is highly computer intensive and not provides
220 sufficient accuracy.

221 There are a number of recent interpretation techniques based on minimizing the
222 difference between observed and theoretical anomalies. The minimization is achieved

223 by sequential optimization of the interpretation parameters through computer-aided
224 iterations. These techniques are also complicated and time consuming.

225 A few groups of authors have performed spatial-frequency analysis of SP
226 anomalies produced by polarized bodies of various geometrical shapes: Rao et al.
227 (1982), Rao and Mohan (1984), Banerjee and Pal (1990), Skianis et al. (1991, 1995).

228 A series of publications (Abdelrahman and Sharafeldin, 1997; Abdelrahman et
229 al., 1997, 1998; El-Araby, 2004; Essa et al., 2008) provided a large number of
230 methodological approaches. However, these approaches (based mainly on application
231 of the gradient analysis and calculation of derivatives) by their general usefulness,
232 have not caused a quantitative jump in this field.

233 Gibert and Pessel (2001) have applied the continuous wavelet transform for
234 localization of SP anomalies. The wavelet analysis provided both an estimate of the
235 location and of the nature of the target responsible for a given self-potential signal.
236 The wavelet-based techniques as well as analytic signals were employed by Sailhac
237 and Marquis (2001) to interpret SP anomalies caused by subsurface fluid flow in the
238 Mt. Etna.

239 Patella (1997) suggested an application a tomographic presentation of SP
240 images. It consisted of scanning the section through SP profiles, by the unit strength
241 elementary charge, which is given a regular grid of coordinates within the section. At
242 the each point of the section the charge occurrence probability function is calculated.
243 The complete set of calculated grid values is employed to draw colored sections. This
244 method was evaluated by Di Maio et al. (2016).

245 Mendonça (2008) has employed the Green's functions to simplify the evaluation
246 of SP anomalies from buried conductors. This approach was used by this author to

247 simulate geoelectric targets in mineral exploration and to obtain current source terms
248 by inverting an SP data set.

249 Srivastava and Agarwal (2009) developed Enhanced Local Wave number
250 technique where nature of the causative source has been determined by computing
251 structural indices based on its horizontal location and depth. This approach was tested
252 on several mineral deposits with complex ore body distribution.

253 An attempt to apply the neural network approach to compute the shape factor
254 and depth of the causative target from SP anomaly was undertaken in Al-Garni (2017).
255 Without denying the general promising of this approach, it should be noted some
256 inconclusiveness of the examples given in this work.

257 Gobashy et al. (2019) proposed a method based on utilizing while optimization
258 algorithm, which as an effective heuristic solution to the inverse problem of SP field
259 due to a 2D inclined bed. Realization of this algorithm in complex physical-geological
260 conditions is under question. Rao et al. (2020) proposed a global optimization
261 methodology expressed in development of inversion algorithm for 2D inclined plates.
262 Absence of geological sections in the mentioned work complicates examination of this
263 methodology.

264 Hristenko and Stepanov (2012) have demonstrated a system of 2D modeling of
265 SP field from several different anomalous bodies with introduced Gaussian noise
266 under conditions of uneven relief. Some applied transformations allowed to exclude
267 effect of near-surface geological inhomogeneties from the total SP field and to enhance
268 anomalies from the buried targets.

269 The procedure based on interpretation of self-potential anomalies due to simple
270 geometrical structures using Fair function minimization (Tlas and Asfahani, 2013), is of
271 certain interest. Giannakis et al. (2019) suggested a hybrid optimization scheme for SP

measurements due to multiple sheet-like bodies. This procedure demands a wide verification on concrete field examples. A special interest presents the recent research of Oliveti and Cardarelli (2019) who developed the least square subspace preconditioned method to compute the known Tikhonov solution to reliable detecting the depth and the shape of shallow electrical current density sources.

Fedi and Abbas (2013) proposed the 'depth from extreme points method' and employed it on several models and field examples. The method yields estimates of the source horizontal location, depth (top or center), and geometry.

Kilty (1984) published a paper which acknowledged the analogy between the current density of SP and magnetic induction. This author suggested interpreting SP anomalies based on the conventional methods developed for magnetic prospecting. However, the trivial methodologies are not acceptable for complex physical-geological conditions. A similar approach, but with the improved interpretation methodology was proposed by Khesin et al. (1996). Eppelbaum and Khesin (2012) proposed a new elaboration of the interpretation process. The present paper shows a final generalization of this approach.

4. SOME COMMON ASPECTS OF MAGNETIC AND SP FIELDS

The magnetic field is a potential one (when value of target's magnetization is not very high) and satisfies Poisson's equation:

$$\mathbf{U}_a = -\,\mathrm{grad}\, V, \tag{6}$$

where $\mathbf{U_a}$ is the anomalous magnetic field and V represents the magnetic potential.

SP polarization is generated by the spontaneous manifestation of electric double layers on contacts of various geological (or environmental and artificial) objects. The electric fields **E** of the electric double layer l caused by natural electric polarization are defined as the gradient of a scalar potential Π_i:

$$\mathbf{E}_{SP} = -\mathrm{grad}\ \Pi_i . \tag{7}$$

The potential Π_i satisfies Laplace's equation everywhere outside the layer l (Zhdanov and Keller, 1994).

Jardani et al. (2008), in addition to equation (7), proposed the following model for explanation of SP pattern generating by geothermal flow:

$$\mathrm{grad}\cdot\left(\sigma\,\mathrm{grad}\Pi\right) = \mathrm{grad}\cdot\mathbf{J}_s = \zeta, \tag{8}$$

where σ is the conductivity (in S/m), $\mathbf{J}_s$ is the current density vector (in A/m^2), and ζ is the volumetric current density (in A/m^3).

Analytical expressions for some interpreting models for magnetic and SP fields are presented in Table 2.

Table 2. Magnetic and SP fields: Comparison of analytical expressions for some interpreting models

Field	*Analytical expression*	
Magnetic	*Thin bed* (*TB*) (9)	*Point source* (*rod*) (10)

	$Z_v = 2J2b\frac{z}{x^2+z^2}$	$Z_v = \frac{mz}{\left(x^2+z^2\right)^{3/2}}$
Self-Potential	*Horizontal circular cylinder* (*HCC*) (11) $\Delta U = 2\frac{\rho_1}{\rho_1+\rho_2}U_0 r_0 \frac{z}{x^2+z^2}$	*Sphere* (12) $\Delta U = \frac{2\rho_1}{2\rho_2+\rho_1}U_0 R^2 \frac{z}{\left(x^2+z^2\right)^{3/2}}$

Here Z_v is the vertical magnetic field component at vertical magnetization; J is the magnetization; b is the horizontal semi-thickness of *TB*; m is the magnetic mass (point pole magnetic charge); ρ_1 is the host medium resistivity; ρ_2 is the anomalous object (*HCC* or sphere) resistivity; U_0 is the potential jump at the source body/host medium interface; r_0 is the polarized cylinder radius; R is the sphere radius; x is the current coordinate; z is the depth of the upper edge of *TB* (center of *HCC* or sphere) occurrence.

Formulas describing potential character of magnetic (eq. (7)) and SP (eq. (8)) fields are identical ones. The proportionality of analytical expressions (9) and (11), (10) and (12) for magnetic and SP fields is obvious. It allows to employing in SP data analysis advanced interpretation methods developed in magnetic prospecting (we assume that the SP polarization vector is analogue of the vector of magnetization). It is supposed that the majority of interpretation methodologies developed for magnetic and gravity fields are applicable for the SP method. However, practical application of such procedures as upward and downward continuation for SP method needs some further research.

In several works was demonstrated application of some advanced procedures from the most developed potential fields (gravity and magnetics), to the self-potential data. Akgün (2001) applied the Hilbert transform (usually employed in gravity and magnetic prospecting) for analysis of SP data. Sindirgi et al. (2008) successfully tested on SP anomalies method of the total normalized gradient developed in gravity

prospecting. This investigation has been continued in (Sindirgi and Özyalin, 2019) with application of the Euler deconvolution. Extended Euler deconvolution techniques was successfully tested by Agarwal and Srivastava (2009) in some mineral deposits and observation in deep borehole. Biswas (2018) suggested to studying SP anomalies using 2D analytic signal developed in magnetic prospecting.

Of special interest is the recently published research of Sungkono (2020), where the author proposed to employ posterior distribution model of the SP anomaly inversion**.** The advantages of this approach are that the SP data may contain single and multiples of SP sources and this method does not require prior assumptions over the shape of the anomaly source.

4.1. Quantitative analysis of SP anomalies by the use of advanced methodologies developed in magnetic prospecting

The improved methods for SP anomaly analysis include characteristic point, tangent and areal methods (these methods are described in detail in the publications suggested to magnetic anomaly interpretation: e.g., Khesin et al., 1996; Eppelbaum et al., 2001; Eppelbaum and Mishne, 2011; Eppelbaum and Khesin, 2012; Eppelbaum, 2015). Formulas for interpretation SP anomalies by the use of characteristic point method are shown in Table 3. Several figures below display some peculiarities of the characteristic point and tangent methods application.

Table 3. Formulas for quantitative interpretation of magnetic anomalies from bodies approximated by thin bed (TB) and horizontal circular cylinder (HCC) using the improved characteristic point method (after Eppelbaum and Mishne (2011), with modifications)

Parameters necessary for examination	**Parameters derived from anomalies from models**		**Formulas for calculation of parameters necessary for quantitative analysis**	
	Thin bed	HCC	Thin bed	HCC

Generalized angle θ	d_1, d_2 d_{1r} d_1, d_5 d_{1r}, d_5 $d_1 = x_{\min} - x_{\max}$ $d_2 = (x_{0.5\Delta U_A})_r - (x_{0.5\Delta U_A})_l$ $d_5 = x_r - x_l$ $\Delta U_A = \Delta U_{\max} - \Delta U_{\min}$	$\tan(\theta) = d_2 / d_1$ $\sin(\theta/3) = d_5 / \sqrt{3} d_1$	$\cot(\theta/3) = \sqrt{3}\dfrac{(d_{1l} + d_{1r})}{(d_{1l} - d_{1r})}$ $\dfrac{d_5}{d_{1r}} = \dfrac{\sqrt{2}\cos(\theta/2) - 1}{\sqrt{3}\cos(60^\circ + \theta/3)}$
Depth h_0, h_c	d_1, d_2, θ d_{1r}, θ d_5, θ	$h_0 = \sqrt{d_1 d_2} / k_{1,2}$, where $k_{1,2}$ $= \dfrac{2}{\sqrt{\sin\theta\cos\theta}}$ $k_5 = 2\sqrt{3}\dfrac{\sin(\theta/3)}{\sin\theta}$	$h_c = d_{1r} / k_{1r}$, where k_{1r} $= 2\sqrt{3}\dfrac{\cos(60^\circ + \theta/3)}{\cos\theta}$ $h_c = \dfrac{d_{1r}}{d_{1r} - d_{1r}(\Delta h)}\Delta h$ $h = d_5 / k_5$, where $k_5 = 2\sqrt{2}\dfrac{\cos(\theta/2) - 1}{\cos\theta}$
Horizontal displacement x_0, x_c	h, θ, $x_{\max}$, $x_{\min,r}$ $(x_{0.5\Delta U_A})_r$, $(x_{0.5\Delta U_A})_l$	$x_0 = 0.5(x_{\max} + x_{\min,r}) - h\cot\theta$ $x_0 = h\tan\left(\dfrac{\theta}{2}\right)$	$x_c = 0.5(x_{\max} + x_{\min,r}) - h_c\dfrac{\sin(60^\circ + \theta/3)}{\cos\theta} + h_c\tan\theta$ $x_c = 0.5(x_r + x_l) + h_c\tan\theta - \sqrt{2}h_c\dfrac{\sin(\theta/2)}{\cos\theta}$
Normal background ΔU_{backgr}	$\Delta U_{\min}$, ΔU_A, θ	$\Delta U_{\text{backr}} = \Delta U_{\min} + \Delta U_A\dfrac{k_0}{1 + k_0}$, where $k_0 = \dfrac{1 - \cos\theta}{1 + \cos\theta}$,	$k_0 = \dfrac{\cos^3(60^\circ + \theta/3)}{\cos^3(\theta/3)}$
Self-potential moment	ΔU_a, h_0, h_c, Q	$M_{\Delta U} = \dfrac{1}{2}\Delta U_a h_0$	$M_{\Delta U} = \dfrac{\Delta U_a h_c^2}{(3\sqrt{3}/2)\cos(30^\circ - \theta/3)}$

Indices "0" and "c" designate the thin bed (TB) and horizontal circular cylinder (*HCC*) models, respectively. Values h_0 and h_c are the depths to upper edge of TB and center of the *HCC*, respectively. Parameter Δh designates measurements of self-potential field at different depths of the electrodes' grounding

Preliminary results for SP anomalies to estimating HCC radius and length of horizontal upper edge may be obtained from 3D magnetic field modeling (taking into account a common similarity of these fields).

Table 4. Nomenclature of variables applied for quantitative analysis of SP anomalies due to model of thin bed and horizontal circular cylinder (see Table 3).

Variable	Description
θ	Generalized angle reflecting the degree of SP anomaly asymmetry as a function relation of an anomalous body depth of occurrence, geometric form, value of polarization
x_0	Horizontal displacement of projection of the middle of the upper edge of thin bed to the earth's surface due to oblique polarization
x_c	Horizontal displacement of projection of the center of the *HCC* to the earth's surface due to oblique polarization
h_0	Depth to the upper edge of thin bed
h_c	Depth to the center of *HCC*
ΔU_{max}	Maximum value of SP anomaly
ΔU_{min}	Minimum value of SP anomaly
ΔU_A	Total amplitude of SP anomaly
d_1	Difference of extremum abscissae for thin bed
d_{1r}	Difference of extremum abscissae for *HCC*
d_2	Difference of semiamplitude point abscissae
d_5	Difference of inflection point abscissae
x_r	Right inflection abscissae point
x_l	Left inflection abscissae point
ΔU_{backr}	Normal background level of SP anomaly
$M_{\Delta U}$	Self-potential moment for the models of thin bed or *HCC*

The improved versions of tangent and areal methods are presented in detail in Eppelbaum et al. (2001), Eppelbaum and Mishne (2011) and Eppelbaum (2015).

4.2. SP observations on an inclined profile

When potential geophysical anomalies are observed on an inclined profile, the obtained parameters characterize some fictitious body (Eppelbaum, 2019a). The transition from the parameters of fictitious target to those of real target is realized using the following expressions:

$$\left.\begin{aligned} h_r &= h_f + x_{0f}\tan\omega_0 \\ x_r &= -h_f\tan\omega_0 + x_{0f} \end{aligned}\right\}, \qquad (13)$$

where h is the depth of the body upper edge occurrence (or HCC (sphere) center), x_0 is the shifting of the anomaly maximum from the projection of the center of the anomalous body to the earth's surface (produced by an oblique polarization), and ω_0 is the angle of the terrain relief inclination ($\omega_0 > 0$ when the inclination is toward the positive direction of the x-axis), the subscripts "r" and "f" stand for parameters of real and fictitious bodies, respectively.

The direction of the electric self-polarization vector ϕ_p is calculated from the expression

$$\phi_p = 90^{\circ} - \theta, \tag{14}$$

and on an inclined relief

$$\phi_p, _r = 90^{\circ} - \theta + \omega_0. \tag{15}$$

Performed calculation of the vector ϕ_p direction on concrete field examples indicates that for the interpreting models closed to the model of thin bed, direction of this vector approximately coincides with the anomalous body dipping. It enables to obtain an supplementary interpretation parameter.

Besides the geometric parameters of anomalous target, the self-potential moment can also be determined (see Table 3). For the models of thin bed and HCC, the self-potential moment can be calculated by the use of Eq. (16a) and (16b), respectively (see also Tables 3 and 4)

$$M_{\Delta U} = \frac{1}{2}\Delta U_a h_0, \tag{16a}$$

$$M_{\Delta U} = \frac{\Delta U_a h_c^2}{\left(3\sqrt{3}/2\right)\cos\left(30^{\circ} - \theta/3\right)}, \tag{16b}$$

where ΔU_a is the amplitude of SP anomaly (in mV), h_0 is the occurrence depth of the upper edge of thin bed (in meters), h_c^2 is the squared depth to the center of the HCC (in

396 m^2), and θ is the some generalized angle (see Tables 3 and 4). The self-potential moment,
397 by analogy with the magnetic field analysis, can be used for classification of various SP
398 anomalies (and, correspondingly, hidden targets).

399 Initial methodologies for quantitative analysis of magnetic anomalies under
400 complex physical-geological conditions for the model of thick bed were presented in
401 Khesin et al. (1996) and its significant evaluation (including the intermediate models
402 between the thick and thin beds) – in Eppelbaum (2015).

403 For observation on inclined profile, the real self-potential moment can be
404 calculated as follows:

405 $$M_{\Delta U,r} = M_{\Delta U,f} \cos\omega_0 \,. \qquad (17)$$

406 Here the subscripts "*r*" and "*f*" stand for a parameter of real and fictitious self-potential
407 moments, respectively.

408 Undoubtedly, calculation of all aforementioned parameters from SP data
409 should be joined to a unified computerized system with a minimal participation of an
410 interpreter.

411 For testing some SP anomalies, software for 3D computation of magnetic field
412 may be applied. In this case, magnetic vector orientation can be utilized as analogue
413 of self-potential vector.

414

415 **5. QUANTITATIVE ANALYSIS OF SP ANOMALIES**

416 Thus, the developed interpretation system in the SP method is applicable for complex
417 physical-geological conditions: oblique polarization, inclined relief and unknown level
418 of the SP normal field.

419 **5.1. Testing on theoretical models**

First of all the aforementioned interpretation methods were successfully tested on the SP anomalies from models presented in Semenov (1980), Göktürkler and Balkaya (2012) and Hristenko and Stepanov (2012).

5.2. Mining geophysics

Self-potential method often enough has been employing in ore deposits of different kind (e.g., Stern, 1945; Yüngül, 1954; Sengupta et al., 1969; Logn and Bolviken, 1974; Cowan et al., 1975; Semenov, 1980; Nayak, 1981; Corry, 1985; Babu and Rao, 1988; Lile, 1996; Goldie, 2002; Bhattacharya et al., 2007; Mendonça, 2008; Srivastava and Agarwal, 2009; Dmitriev, 2012; Fedi and Abbas, 2013; Biswas and Sharma, 2016; Alizadeh et al., 2017; Erofeev et al., 2017; Safipour et al., 2017; Eppelbaum, 2019a,b; Zhu et al., 2020).

5.2.1. Chyragdere sulfur deposit (central Azerbaijan)

It is interesting to compare SP studies carried out over the Ghyragdere sulfur deposit (central Azerbaijan) during several years: 1930, 1937 and 1938 (Figure 4). This figure shows that the mining works in the underground shaft (1930 – 1938) strongly distort the SP field observed at the earth's surface (distance from the observation points to ore deposit consisted several tens of meters). This testifies to the tight correlation between the mining processes and SP anomalies. It would be fascinating to compare the volumes and contours of the mined ore with the SP isolines, separately for the abovementioned years, but over the past years, these documents have been lost.

5.2.2. Sariyer sulphide-pyrite deposit (near Istanbul, Turkey)

Yüngül (1954) documented the results of the survey in the Sariyer area (Istanbul). The performed interpretation indicates that the obtained position of *HCC* center is in the line with geometrical and physical parameters of the sulphide-pyrite ore body (Figure 5). Here and in some other figures, displayed parameters d_3 and d_4 relate to the

445 improved tangent method (this method is described in detail, for instance, in
446 Eppelbaum et al. (2001)). Calculating the self-potential moment by the use of Eqs.
447 (16b) and (17), we obtain $M_{\Delta U} = 31800\,\mathrm{mV}\cdot\mathrm{m}^2$. The calculated direction of self-
448 potential vector by use of Eq. (15) is vertical one.

449 *5.2.3. Polymetallic deposit (Russia)*

450 Figure 6 displays results of SP anomaly quantitative interpretation using characteristic
451 points and tangent methods (areal method based on the calculation of the area occupied
452 by SP anomaly has also been applied). The interpretation results, as can easily see from
453 Figure 6, have a good agreement with the location of ore body. Self-potential moment
454 (here model of thin bed was selected and Eqs. (16a) and (17) were applied)
455 $M_{\Delta U} = \frac{1}{2}60\,\mathrm{mV}\cdot 6.5\,\mathrm{m}\cdot 0.93 = 181\mathrm{mV}\cdot\mathrm{m}$. The calculated direction of self-potential
456 vector (Eq. (15)) practically coincides with the polymetallic body dipping.

457 *5.2.4. Katsdag polymetallic deposit (Azerbaijan)*

458 Three SP anomalies were successfully interpreted in the Katsdag copper-polymetallic
459 deposit (southern slope of the Greater Caucasus, Azerbaijan) under conditions of
460 rugged terrain relief (Figure 7). Anomalies 1 and 2 are intensive ones, but anomaly 3
461 is comparatively small. It is important to underline here an essential difference
462 between the quantitative results of SP anomalies analysis calculated without and with
463 estimation of the rugged relief influence. The SP moment calculated for anomaly 1
464 (after applying Eqs. (16a) and (17)) is $M_{\Delta U} = \frac{1}{2}180\,\mathrm{mV}\cdot 20\,\mathrm{m}\cdot 0.984 = 3450\,\mathrm{mV}\cdot\mathrm{m}$.

465 *5.2.5. Filizchai polymetallic deposit (Azerbaijan)*

466 A very intensive SP anomaly (almost 500 mV) was observed in the portion of Filizchai
467 copper-polymetallic field (southern slope of the Greater Caucasus, Azerbaijan) under
468 conditions of highly complex terrain relief (Figure 8). Results of interpretation

(improved methods of characteristic points and tangents were applied) also indicate significant difference of position of the upper edge of anomalous body calculated without rugged terrain relief influence (blue circle) and after calculation of this influence (red circle). The calculated SP moment (after Eq. (16a)) is $M_{\Delta U} = \frac{1}{2} 440\,\text{mV} \cdot 90\,\text{m} = 19800\,\text{mV} \cdot \text{m}$. Employing Eq. (17) gives us some decreased value: 14600 mV·m. It is a sufficiently high value of SP moment (for a thin bed model). However, such giant SP anomalies of ore origin are rarely observed. The direction of self-potential vector was calculated by the use of Eq. (15). Position of this vector agrees well with the dipping of this pyrite-polymetallic body (Figure 8).

5.2.6. Uchambo ore field (Georgia)

Figure 9 depicts the position of the HCC center (characteristic point, tangent and areal methods were applied), which evidently fixes the edge of a flat-lying orebody in the Uchambo polymetallic deposit (southern Georgia). The SP moment calculated using Eqs. (16b) and (17) is $M_{\Delta U} = 13480\,\text{mV} \cdot \text{m}^2$. The complex form of ore-body obviously did not allow determining an exact position of self-potential vector.

5.2.7. Potentsialnoe polymetallic deposit (Rudnyi Altai, Russia)

Here three different interpreting models were utilized (thin bed, HCC and thick bed) (Figure 10). All three applied models are suitable ones. The calculated SP moment (for HCC model) is (after employing Eqs. (16b) and (17)) $M_{\Delta U} = 21890\,\text{mV} \cdot \text{m}^2$. The calculated position of polarization vector (HCC) coincides with the dipping of the polymetallic body (Figure 10).

5.2.8. Canyon Makhtesh Ramon (Negev Desert, southern Israel)

The Makhtesh Ramon erosional–tectonic depression (canyon), 40 km long and approximately 8 km wide, is situated in the Negev Desert (southern Israel), 65 km

493 southwest of the Dead Sea. On the basis of integrated geological-geophysical
494 investigations in this area were detected several tens of mictodiamonds (most largest
495 sample is 1.35 mm) and a lot of mineral-satellites of diamond (Eppelbaum et al., 2006).
496 Many geological-geophysical indicators testify that at least a part of the indigenous
497 sources (kimberlites or lamproites) of the aforementioned minerals can occur in
498 subsurface in this area. Compiled SP map (Figure 11a) displays presence of some
499 anomalous zones. Quantitative analysis of SP anomaly has been carried out along
500 profile A – B (Figure 11b) crossing one of the mentioned zones. Results of the
501 performed interpretation indicate that the anomalous inclined body (having a
502 geometrical form close to thin bed model) occurs at the depth of 40 m that agrees with
503 the preliminary available geophysical data.

504 **5.3. Archaeological sites**

505 SP measurements are not frequently applied for searching and localization of
506 archaeological targets (e.g., Wynn and Sherwood, 1984; Mauriello et al., 1998;
507 Eppelbaum et al., 2003a, b; Drahor, 2004; Drahor et al., 2006; Di Maio et al., 2010;
508 Shevnin et al., 2014; Tsokas et al., 2014; De Giorgi and Leucci, 2017, 2019).
509 Obviously, absence of reliable methodologies for quantitative analysis of SP
510 anomalies, weak SP anomalies and different kinds of noise impedes a wide
511 employment of self-potential method in archaeological prospection.

512 The territory of Israel contains more than 35,000 discovered archaeological sites
513 of different age and origin. For SP observations several typical archaeological sites
514 located in different areas of the country were selected (Eppelbaum et al., 2003b, 2004).
515 All SP measurements were performed using microVoltmeter with high input
516 impedance and distinctive non-polarizable electrodes (Cu in $CuSO_4$ solution). The

517 interpretation results obtained earlier at these sites were revised and generalized (the
518 unified methodologies were employed).

519 *5.3.1. Roman site of Banias (northern continuation) (northern Israel)*

520 The remains of the city of Banias are located in northern Israel, at the foot of Mt.
521 Hermon. Banias was the principal city of the Golan and Batanaea regions in the Roman
522 period and occupied an area of more than 250 acres (Reich, 1992; Meyers, 1996). Here
523 different ancient remains of Roman and other historical periods were found. The area
524 of the present study is located several km north of the well-investigated Banias site. In
525 the nearest vicinity of the area of geophysical examination (SP and magnetic surveys),
526 the remains of ancient Roman cemetery and aqueduct (Hartal, 1997) were discovered.
527 Mineralogical and geochemical analyses of the excavated Roman chambers indicated
528 that these objects were composed from the special type of hot worked limestone.

529 SP observations were carried out by the grid of 1 x 1 m. Compiled SP map
530 (Figure 12) nicely indicates two anomalies. Interpretation profiles I – I and II – II cross
531 centers of these anomalies (Figure 13). Upper edges of the recognized anomalous
532 targets occur at the depth of 1.1 – 1.3 meters. Presence of these anomalous sources was
533 confirmed by a comprehensive magnetic data analysis. Angle φ_p for anomaly I consists
534 of 75°, but it is calculated from the opposite side (due to inversion of parameters d_3
535 and d_4). SP moment for the anomaly I (thin bed) is
536 $M_{\Delta U} = \frac{1}{2} 16.5\,\text{mV} \cdot 1.2\,\text{m} = 9.9\,\text{mV} \cdot \text{m}$. Interestingly that this SP moment is almost
537 1,500 times smaller than the same parameter calculated for the giant SP anomaly in
538 the Filizchai deposit, Azerbaijan (see Figure 8). For anomaly II, taking into account
539 that parameters d_3 and d_4 are practically equal ($\theta \approx 0$), value of polarization angle φ_p

is close to 90°. SP moment for anomaly II (HCC) is $M_{\Delta U} = \frac{2.79\text{m}^2 \cdot 18\text{mV}}{2.6 \cdot \cos 15^\circ} \cong 20\,\text{mV} \cdot \text{m}^2$.

5.3.2. Nabatean site of Halutza (southern Israel)

The Halutza site is located 20 km southwest of the city of Be'er-Sheva (southern Israel). It was the central city of southern Palestine in the Roman and Byzantine periods and was founded as a way-station for Nabatean (7^{th}–2^{nd} centuries BC) traders traveling between Petra (Jordan) and Gaza. This site was occupied mainly throughout the Byzantine period (4^{th}–7^{th} centuries AD) (Kenyon, 1979; Kempinski and Reich, 1992).

At this site self-potential and magnetic measurements were carried out in a 20 x 10 m area with a 1 x 1 m grid (Eppelbaum et al., 2003b). The buried targets (ancient Roman limestone constructions) have produced negative anomalies in both geophysical potential fields. Results of the quantitative examination (here interpretation models of thin bed were utilized) are practically identical (Figure 14A, B). Amplitude of SP anomaly reached 40 mV and is the largest from the anomalies considered in this site. Depth of both these anomalous targets is about 0.85 m. The calculated moments for the magnetic and self-potential anomalies, are following: $M_{\Delta T} = 3.61\,\text{nT} \cdot \text{m}$ and $M_{\Delta U} = 20\text{mV} \cdot \text{m}$. φ_p angle for SP anomaly is calculated from the opposite side and consists of 70° (Figure 14B). It may be concluded that the recognized anomalous target approximated by thin bed in the SP method has not vertical dipping, but coinciding with the φ_p angle. The obtained quantitative parameters of ancient constructions agree with the results of archaeological excavations performed in the vicinity of this site.

5.3.3. Christian site of Emmaus-Nikopolis (central Israel)

563 Christian archaeological site Emmaus-Nikopolis is well known in the ancient and
564 Biblical history. The site is situated roughly halfway between Jerusalem and Tel Aviv
565 (central Israel). The Crusaders rebuilt it on a smaller scale in the 12th century (Meyers,
566 1996). Nikopolis is displayed in almost all Christian Pilgrim texts from the 4th century
567 onward; in majority of archaeological sources this site is named as Emmaus-Nikopolis.
568 Many scientists note that this site is characterized by multilayer sequence (e.g.,
569 Kempinski and Reich, 1992).

570 SP measurements in this site were performed by the grid of 1 x 1.5 m. In the
571 complied SP map (Figure 15), one local anomaly was selected for quantitative analysis
572 (Profile A – B in Figure 15). The determined depth of the target upper edge is about
573 1.5 m (depth of the HCC center is about 2.1 m) (Figure 16). Angle φ_p here is 85^o and
574 is calculated from the opposite side. Self-potential moment of this anomaly is 4.5
575 mV·m^2. Fragments of some glass vessels discovered in this burial cave allowed to
576 attributing it to the Byzantine period. Interestingly to note that magnetic field
577 examination allowed recognizing the same cave by the integrated effect from a few
578 tens of small magnetic anomalies produced by the glass vessel (made from the fired
579 clay).

580 **5.4. Environmental geophysics**

581 Other SP application is revealing some dangerous environmental phenomena (karst
582 cavities, faults, rockslides) (e.g., Ogilvi and Bogoslovsky, 1979; Corwin, 1990, 1996;
583 Quarto and Schiavone, 1996; Gurk and Bosch, 2001; Vichabian and Morgan, 2002;
584 Lapenna et al., 2003; Jardani et al., 2006a, 2006b; Eppelbaum, 2007; Jardani et al.,
585 2007; Rozycki et al., 2007; Gibert and Sailhac, 2008; Srigutomo et al., 2010; Tripathi
586 and Frayar, 2016; Chen et al., 2018; Gusev et al., 2018; Oliveti and Cardarelli, 2019).

587 *5.4.1. Buried cavities in dolomitic limestone (southern Italy)*

588 Several impressive examples of SP application for detection of underground cavities
589 in southern Italy were displayed in Quarto and Schiavone (1996). Let us will consider
590 one of these field cases, where the buried karst cavity exists in dolomitic limestones
591 (Figure 17). The cavity is horizontally extended and over it a significant SP anomaly
592 (up to 100 mV) was observed. Quantitative examination along profile A – B crossing
593 a center of this anomaly has been performed (Figure 18). For interpretation models of
594 thin bed (upper edge) and center of HCC were obtained depths of 6.0 and 9.5 meters,
595 respectively. Self-potential vector is oriented near-vertically. Self-potential moment of
596 anomaly from this cave is about $3300\,\mathrm{mV}\cdot\mathrm{m}^2$.

597 *5.4.1. Cavities in the Djuanda Forest Park (Bandung, Indonesia)*

598 Next example displays results of SP and electric resistivity observations carried out
599 above cavities (built during the WW II in early 1940s) at the Djuanda Forest Park,
600 Bandung, Indonesia. Fascinatingly that resistivity section (Figure 19B) nicely shows
601 two bright anomalies whereas SP graph (Figure 19A) indicates significant anomaly
602 (amplitude is more than 20 mV) over cave II, whereas anomaly over cave I is only
603 emerging (its amplitude is about 2 mV). Obviously, this fact is associated with the
604 hydrogeological peculiarities of the subsurface geological section. Quantitative
605 analysis of SP over cave II gave satisfactory results generally coinciding with the
606 results of resistivity section. Calculated self-potential moment here is
607 $M_{\Delta U} = 52\,\mathrm{mV}\cdot\mathrm{m}$.

608 *5.4.2. Subvertical fissure zone (Russia)*

609 Figure 20 displays SP and resistivity graphs over the subvertical fissured zone. SP
610 quantitative examination showed significant disagreement between the results of
611 interpretation and available geological section. However, it is entertainingly that
612 performed quantitative analysis of the resistivity curve ρa (presented in the upper part

613 of Figure 20) by the use of similar methodology (theoretical possibilities of such
614 analysis were reported in Eppelbaum (2007) and evaluated in Eppelbaum (2019), gave
615 the similar results. Shevnin (2018) also indicated a good correlation between the SP
616 and resistivity methods. Quantitative analysis of SP and resistivity curves gave about
617 the same results. Obviously, it can be explained by some erosion of the upper part of
618 anomalous body (fissured zone) and corresponding changes in its physical properties
619 (possibly appearing to be close to physical properties of the host media). Nevertheless,
620 orientation of the self-potential vector coincides with the fissured zone dipping. Value
621 of self-potential moment is estimated as $M_{\Delta U} = 23\,\mathrm{mV}\cdot\mathrm{m}$.

622 **5.5. Technogenic geophysics**

623 Let us designate technogenic geophysics as geophysical studies applied to detection or
624 determination of certain parameters of hidden modern industrial objects**.** The SP
625 method fits well in such studies.

626 Onojasun and Takum (2015) have been successfully applied SP investigations
627 for localization of an underground concreate water pipeline at the Kwinana industrial
628 area of Southern Perth (Western Australia). In a second example, comprehensive
629 examination of SP imaging over metallic contamination plume has been performed in
630 Cui et al. (2017). The authors have concluded that SP method can be successfully used
631 to monitor the underground metallic contaminants.

632 It was established that examination of SP anomalies is significant for localization
633 of corrosion in buried oil, gas and water pipes (e.g., Corwin, 1996; Castermant et al.,
634 2008; Ekine and Emujakporve, 2010; Rittgers et al., 2013; Oliveti and Cardarelli,
635 2019).

636 *5.5.1. Underground metallic water-pipe (southern Russia)*

637 Fomenko (2010) presented a case of a typical SP field distribution over the buried
638 metallic water-pipe (Figure 21). This anomaly has been interpreted by the use of
639 tangent and characteristic point methods. The obtained position of the HCC center
640 agrees (with some assumption) with a center of the hidden water-pipe. The calculate
641 self-potential moment $M_{\Delta U} = 79.8\,\mathrm{mV}\cdot\mathrm{m}^2$.

642 **5.6. Generalization of the calculated self-potential moments**

643 The calculated self-potential moments for the variety of investigated targets are
644 compiled in Table 5.

645 **Table 5.** Comparison of self-potential moments calculated from different anomalous
646 targets (considered in sections 5.2 – 5.5)

Object	Location	Approximation model	Value of self-potential moment $M_{\Delta U}$
I. ***Ore geophysics***			
Sariyer sulphide-pyrite deposit	near Istanbul, Turkey	HCC	$31800\,\mathrm{mV}\cdot\mathrm{m}^2$
Polymetallic deposit	Russia	Thin bed	$181\,\mathrm{mV}\cdot\mathrm{m}$
Katsdag polymetallic deposit	Southern Greater Caucasus, Azerbaijan	Thin bed	$3450\,\mathrm{mV}\cdot\mathrm{m}$
Filizchai polymetallic deposit (Azerbaijan)	Southern Greater Caucasus, Azerbaijan	Thin bed	$14600\ \mathrm{mV}\cdot\mathrm{m}$
Uchambo ore field	Lesser Caucasus, Georgia	HCC	$13480\,\mathrm{mV}\cdot\mathrm{m}^2$
Potentsialnoe polymetallic deposit	Rudnyi Altai, Russia	Thin bed, thick bed, HCC	$21890\,\mathrm{mV}\cdot\mathrm{m}^2$
II. ***Archaeogeophysics***			
Banias (anomaly I)	northern Israel	Thin bed	$9.9\,\mathrm{mV}\cdot\mathrm{m}$
Banias (anomaly II)	"—"	HCC	$20\,\mathrm{mV}\cdot\mathrm{m}^2$
Halutza	southern Israel	Thin bed	$20\,\mathrm{mV}\cdot\mathrm{m}$
Emmaus-Nikopolis	central Israel	HCC	$4.5\ \mathrm{mV}\cdot\mathrm{m}^2$
III. ***Environmental geophysics***			
Underground cave	southern Italy	HCC	$3300\,\mathrm{mV}\cdot\mathrm{m}^2$
Underground cave	Bandung, Indonesia	Thin bed	$52\ \mathrm{mV}\cdot\mathrm{m}$

Fissured zone	Russia	Thin bed	$23\,\mathrm{mV}\cdot\mathrm{m}$
IV. ***Technogenic geophysics***			
Underground metallic water-pipe	Southern Russia	HCC	$79.8\,\mathrm{mV}\cdot\mathrm{m}^2$

Values of self-potential momentpresented in Table 5 demonstrate a wide range $M_{\Delta U}$ of the calculated parameter. $M_{\Delta U}$ values can be divided in three groups: (1) comparatively large values corresponding to comparatively big ore bodies, (2) middle values relating to targets studying in environmental and technogenic geophysics, and (3) relatively small values reflecting archaeological targets. However, even smallest $M_{\Delta U}$ value calculated, for instance, for the ancient cave in the site of Emmaus-Nikopolis has independent importance.

CONCLUSIONS

Self-potential method is one of the oldest and simultaneously non-expensive geophysical methods. One of its main preferences is that the presence of water in subsurface does not limit this method capabilities. The various disturbances complicated SP observations under different physical-geological environments are analyzed. The available interpretation methodologies are briefly discussed. The proved common aspects between the magnetic and self-potential fields enable to apply for interpretation of SP anomalies the modern interpreting procedures developed for complicated environments in magnetic prospecting (oblique magnetization (polarization), rugged topography and an unknown level of the normal field). Explanation of these procedures is presented in detail. These interpretation procedures applied for SP anomalies enable to obtain reliably geometric parameters of buried anomalous targets occurring in complex physical-geological environments. The

669 suggested calculation of direction of electric self-polarization vector allows in many
670 cases to estimate dipping of anomalous objects. It is proposed to apply in SP method
671 calculation of self-potential moment which can be used for classification of observed
672 SP anomalies. Testing these procedures in mining, environmental, archaeological and
673 technogenic geophysics in various regions of the world indicates an effectiveness of
674 these methodologies.
675

676 **ACKNOWLEDGEMENTS**

677 The author would like to thank two anonymous reviewers, who thoroughly reviewed
678 the manuscript, and their critical comments and valuable suggestions were very helpful
679 in preparing this paper.
680

References

Abdelrahman, E.M., El-Araby, T.M., Ammar, A.A. and Hassanein, H.I., 1997. A least-squares approach to shape determination from selfpotential anomalies. *Pure and Applied Geophysics*, **150**, 121-128.

Abdelrahman, E.M., Ammar, A.A., Hassanein, H.I. and Hafez, M.A., 1998. Derivative analysis of SP anomalies. *Geophysics*, **63**, 890-897.

Abdelrahman, E.M. and Sharafeldin, S.M., 1997. A least squares approach to depth determination from residual self-potential anomalies caused by horizontal cylinders and spheres. *Geophysics*, **62**, 44-48.

Agarwal, B.N.P. and Srivastava, S., 2009. Analyses of self-potential anomalies by conventional and extended Euler deconvolution techniques. *Computers and Geosciences,* **35,** 2231-2238.

Akgün, M., 2001. Estimation of some bodies parameters from the self potential method using Hilbert transform. *Jour. of the Balkan Geophysical Society*, **4**, No. 2, 29-44.

Al-Garni, M.A., 2017. Interpretation of spontaneous potential anomalies from some simple geometrically shaped bodies using neural network inversion. *Acta Geophysica*, **58**, No. 1, 143-162.

Alizadeh, A.M., Guliyev, I.S., Kadirov, F.A. and Eppelbaum, L.V., 2017. Geosciences in Azerbaijan. Volume **II**: *Economic Minerals and Applied Geophysics*. Springer. Heidelberg – N.Y.

Babu, R.H.V. and Rao, A.D., 1988. Inversion of self-potential anomalies in mineral exploration. *Computers & Geosciences*, **14**, No. 3, 377-387.

Banerjee, B. and Pal, B.P., 1990. Frequency domain interpretation of Self-Potential anomalies. *Gerlands Beitrage zur Geophysik*, **99**, No. 6, 531-538.

Bhattacharya, B.B., Shalivakhan, J.A. and Bera, A., 2007. Three-dimensional probability tomography of self-potential anomalies of graphite and sulphide mineralization in Orissa and Rajasthan, India. *First Break*, **5**, 223-230.

Biswas, A., 2018. Inversion of amplitude from the 2-D analytic signal of self-potential anomalies. *In*: (KS Essa, Ed.), *Minerals*, IntechOpen, 13-45.

Biswas, A. and Sharma, S.P., 2016. Integrated geophysical studies to elicit the structure associated with uranium mineralization around South Purulia shear zone, India: A review. *Ore Geology Reviews*, **72**, 1307-1326.

Bukhnikashvili, A.V., Kebuladze, V.V., Tabagua, G.G., Dzhashi, G.G., Gugunava, G.E., Tatishvili, O.V. and Gogua, R.A., 1974. *Geophysical Exploration of Adjar Group of Copper-Polymetallic Deposits*. Metsniereba, Tbilisi (in Russian).

Castermant, J., Mendonça, C., Revil, A., Trolard, F., Bourrie, G. and Linde, N., 2008. Redox potential distribution inferred from self-potential measurements associated with the corrosion of a burden metallic body. *Geophysical Prospecting*, **56**, No. 2, 269-282.

Chen, Y., Qin, X., Huang, Q., Gan, F., Han, K., Zheng, Z. and Meng, Y., 2018. Anomalous spontaneous electrical potential characteristics of epikarst in the Longrui Depression, Southern Guangxi Province, China. *Environmental Earth Sciences*, **77**, 659, 1-9.

Corry, C.E., 1985. Spontaneous polarization associated with porphyry sulfide mineralization. *Geophysics*, **50**, No. 6, 1020-1034.

726 Corwin, R.F., 1990. Application of the self-potential method for engineering and
727 environmental investigations. *SAGEEP Proceedings*, Tulsa, OK, USA, 107-121.

728 Corwin, R.F., 1996. The self-potential method for environmental and engineering
729 application. In: (Ward, S.H., Ed.), *Geotechnical and Environmental Geophysics*,
730 vol. **1**, Society of Exploration Geophysicists, Tulsa, 127-145.

731 Cowan, D.R., Allchurch, P.D. and Omnes, G., 1975. An integrated geo-electrical survey
732 on the Nangaroo copper-zinc prospect, near Leonora, Western Australia.
733 *Geoexploration*, **13**, 77-98.

734 Cui, Y., Zhu, X., Wei, W., Liu, J. and Tong, T., 2017. Dynamic imaging of metallic
735 contamination plume based on self-potential data. *Trans. Nonferrous Met. Soc.*
736 *China*, **27**, 1822-1830.

737 De Giorgi, L. and Leucci, G., 2017. The archaeological site of Sagalassos (Turkey):
738 exploring the mysteries of the invisible layers using geophysical methods.
739 *Exploration Geophysics*, **49**, 751-761.

740 De Giorgi, L. and Leucci, G., 2019. Passive and active electric methods: New frontiers
741 of application. In: (Eds. R. Persico, S. Piro and N. Linford) *Innovation in Near-*
742 *Surface Geophysics*, 1-21.

743 Di Maio, R., Fedi, M., Lamanna, M., Grimaldi, M. and Pappaladro, U., 2010. The
744 Contribution of Geophysical Prospecting in the Reconstruction of the Buried
745 Ancient Environments of the House of Marcus Fabius Rufus (Pompeii, Italy).
746 *Archaeological Prospection*, **17**, 259-269.

747 Di Maio, R., Piegari, E., Rani, P. and Avella, A., 2016. Self-Potential data inversion
748 through the integration of spectral analysis and tomographic approaches.
749 *Geophysical Jour. International*, **206**, 1204-1220.

750 Dmitriev, A.N., 2012. Direct and inverse SP modeling on the basis of exact model of
751 self-potential field nature. *Geology and Geophysics*, **53**, No. 6, 797-812.

752 Drahor, M.G., 2004. Application of the self-potential method to archaeological
753 prospection: some case histories. *Archaeological Prospection*, **11**, 77-105.

754 Drahor, M.G., Akyol, A.L. and Dilaver, N., 2006. An application of the self-potential
755 (SP) method in archaeogeophysical prospection. *Archaeological Prospection*, **3,**
756 No. 3, 141-158.

757 El-Araby, H.M., 2004. A new method for complete quantitative interpretation of self-
758 potential anomalies. *Journal of Applied Geophysics*, **55**, 211-224.

759 Ekine, A.S. and Emujakporue, G.O., 2010. Investigation of corrosion of buried oil
760 pipeline by the electrical geophysical methods. *Jour. of Appl. Sci. Environ.*
761 *Manage*., **14**(1), 63-65.

762 Eppelbaum, L.V., 2007. Revealing of subterranean karst using modern analysis of
763 potential and quasi-potential fields. *Proceedings of the 2007 SAGEEP Conference*,
764 **20**, Denver, USA, 797-810.

765 Eppelbaum, L.V., 2015. Quantitative interpretation of magnetic anomalies from bodies
766 approximated by thick bed models in complex environments. *Environmental Earth*
767 *Sciences*, **74**, 5971-5988.

768 Eppelbaum, L.V., 2019a. *Geophysical Potential Fields: Geological and Environmental*
769 *Applications*. Elsevier. Amsterdam – N.Y.

770 Eppelbaum, L.V., 2019b. Advanced system of self-potential field analysis in ore
771 deposits of the South Caucasus. *Proceedings of the National Azerbaijan Academy*
772 *of Sciences*, No. 2, 21-35.

773 Eppelbaum, L., Ben-Avraham, Z. and Itkis, S., 2003a. Ancient Roman remains in Israel
774 provide a challenge for physical-archaeological modeling techniques. *First Break*,
775 **21**, No. 2, 51-61.

776 Eppelbaum, L.V., Ben-Avraham, Z. and Itkis, S.E., 2003b. Integrated geophysical
777 investigations at the Halutza archaeological site. *Proceed. of the **64** EAGE Conf.*,
778 Florence, Italy, P151, 1-4.

779 Eppelbaum, L.V. and Khesin, B.E., 2012. *Geophysical Studies in the Caucasus*.
780 Springer, Heidelberg – N.Y.

781 Eppelbaum, L.V., Khesin, B.E. and Itkis, S.E., 2001. Prompt magnetic investigations of
782 archaeological remains in areas of infrastructure development: Israeli experience.
783 *Archaeological Prospection*, **8**, No. 3, 163-185.

784 Eppelbaum, L.V., Khesin, B.E., Itkis, S.E. and Ben-Avraham, Z., 2004. Advanced
785 analysis of self-potential data in ore deposits and archaeological sites. *Proceed. of*
786 *the 10th European Meeting of Environmental and Engineering Geophysics*,
787 Utrecht, The Netherlands, 1-4.

788 Eppelbaum, L.V. and Mishne, A.R., 2011. Unmanned Airborne Magnetic and VLF
789 investigations: Effective Geophysical Methodology of the Near Future. *Positioning*,
790 **2**, No. 3, 112-133.

791 Eppelbaum, L.V., Vaksman, V.L., Kouznetsov, S.V., Sazonova, L.M., Smirnov, S.A.,
792 Surkov, A.V., Bezlepkin, B., Katz, Y., Korotaeva, N.N., and Belovitskaya, G.,
793 2006. Discovering of microdiamonds and minerals-satellites in Canyon Makhtesh
794 Ramon (Negev desert, Israel). *Doklady Earth Sciences* (*Springer*), **407**, No. 2, 202-
795 204.

796 Ernstson, K. and Scherer, V., 1986. Self-potential variations with time and their relation
797 to hydrogeologic and meteorological parameters. *Geophysics*, **51**, No. 10, 1967-
798 1977.

799 Erofeev, L.Ya., Orekhov, A.N. and Erofeeva, G.V., 2017. Natural electric fields in
800 Siberian gold deposits: structure, origin, and relationship with gold orebodies.
801 *Geology and Geophysics*, **58**, 984-989.

802 Essa, K., Mehanee, S. and Smith, P.D., 2008. A new inversion algorithm for estimating
803 the best fitting parameters of some geometrically simple body to measured self-
804 potential anomalies. *Exploration Geophysics*, **39**, 155-163.

805 Fitterman, D.V., 1979. Calculation of self-potential anomalies near vertical contacts.
806 *Geophysics*, **44**, No. 2, 195-205.

807 Fomenko, N.E., 2010. *Ecological Geophysics*. South State University, Rostov-on-Don,
808 Russia (in Russian).

809 Fox, R.W., 1830. On the electromagnetic properties of metallicferous veins in the mines
810 of Cornwall. *Royal Society*, London, *Philosophical Transactions*, 399-414.

811 Fedi, M. and Abbas, M., 2013. A fast interpretation of self-potential data using the depth
812 from extreme points method. *Geophysics*, **78**, E107–E116.

813 Giannakis, I., Tsourlos, P., Papazachos, C., Vargemezis, G., Giannopoulos, A.,
814 Papadopoulos, N., Tosti, F. and Alani, A., 2019. A hybrid optimization scheme for

self-potential measurements due to multiple sheet-like bodies in arbitrary 2D resistivity distributions. *Geophysical Prospecting*, **67**, 1948-1964.

Gibert, D. and Sailhac, P., 2008. Comment on ‘‘Self-potential signals associated with preferential groundwater flow pathways in sinkholes’’ by A. Jardani, J. P. Dupont, and A. Revil, J. of Geophys. Res., 113, B03210. *Jour of Geoph. Research*, **113**, B03210, 1-4.

Gibert, D. and Pessel, M., 2001. Identification of sources of potential fields with the continuous wavelet transform: application to SP profiles. *Geophysical Research Letters*, **28**, 1863-1866.

Gobashy, M., Abdelazeem. M., Abdrabou, M. and Khalil, M.H., 2019. Estimating model parameters from self-potential anomaly of 2D inclined sheet using whale optimization algorithm: Applications to mineral exploration and tracing shear zones. *Natural Resources Research*, https://doi.org/10.1007/s11053-019-09526-0, 1-21.

Göktürkler, G. and Balkaya, Ç., 2012. Inversion of self-potential anomalies caused by simple-geometry bodies using global optimization algorithms. *Journal of Geophysics and Engineering*, **10**, 498-507.

Goldie, M., 2002. Self-potentials associated with the Yanacocha high-sulfidation gold deposit in Peru. *Geophysics*, **67**, 684-689.

Gurk, M. and Bosch, F. 2001. Cave detection using the Self-Potential-Surface (SPS) technique on a karstic terrain in the Jura mountains (Switzerland), In (Eds. A. Hördt und J. B. Stoll), Trans. of the 'Kolloquium Elektromagnetische Tiefenforschung', Burg Ludwigstein, 2001, 283-291.

Gusev, A.P., Kaleichik, P.A., Fedorsky, M.S. and Shavrin, I.A., 2018. Dynamics of self-potential field as indicator of dangerous rock-slide areas in industrial landscape (on example of Belarus). *Bull. of Perm University* (Russia), **17**, No. 2, 120-127 (in Russian).

Hartal, M., 1997. Banias, The Aqeduct. *Excavations and Surveys in Israel*, **16**, 5-8.

Hristenko, L.A. and Stepanov, Yu.I., 2012. Transformation of SP observations for solving engineering-geological problems. *Mining Information-Analytical Bull*., No, 5, 169-173 (in Russian).

Jardani, A., Dupont, J. and Revil, A., 2006a. Self-potential signals associated with preferential groundwater flow pathways in sinkholes. *Journal of Geophysical Research*, **111**, B09204, 1-13.

Jardani, A. and Revil, A., 2009. Stochastic joint inversion of temperature and self-potential data. *Geophysical Jour. International*, **179,** 640-654.

Jardani, A., Revil, A., Bolève, A. and Dupont, J. P., 2008. Three-dimensional inversion of self-potential data used to constrain the pattern of groundwater flow in geothermal fields. *Journal of Geophysical Research*, **113**, B09204.

Jardani, A., Revil, A. and Dupont, J., 2006b. Self-potential tomography applied to the determination of cavities. *Geophysical Research Letters*, **23**, L13401, 1-4.

Jardani, A., Revil, A., Santos, F., Fauchard, C. and Dupont, J., 2007. Detection of preferential infiltration pathways in sinkholes using joint inversion of self-potential and EM-34 conductivity data. *Geophysical Prospecting*, **55**, No. 5, 749-760.

Kempinski, A. and Reich, R. (Eds.), 1992. *The Architecture of Ancient Israel*. Israel Exploration Society, Jerusalem, Israel.

Kenyon, K.M., 1979. *Archaeology in the Holy Land*. Norton, USA.

Khesin, B.E., Alexeyev, V.V. and Eppelbaum, L.V., 1996. *Interpretation of Geophysical Fields in Complicated Environments*. Kluwer Academic Publishers (Springer), Ser.: Modern Approaches in Geophysics, Boston – Dordrecht – London.

Kilty, K.T., 1984. On the origin and interpretation of self-potential anomalies. *Geophysical Prospecting*, **32**, No.1, 51-62.

Lapenna, V., Lorenzo, P., Perrone, A., Piscitelli, S., Sdao, F. and Rizzo, E., 2003. High-resolution geoelectrical tomographies in the study of Giarrossa landslide (southern Italy). *Bull Eng. Geol. Environ*., **62**, 259-268.

Lile, O.B., 1996. Self potential anomaly over a sulphide conductor tested for use as a current source. *Journal of Applied Geophysics*, **36**, No. 2-3, 97-104.

Logn, O. and Bolviken, B., 1974. Self potentials at the Joma pyrite deposit, Norway. *Geoexploration*, **12**, 11-28.

Mendonça, C.A., 2008. Forward and inverse self-potential modeling in mineral exploration. *Geophysics*, **73**, No. 1, F33-F43.

Mauriello, P., Monna, D. and Patella, D., 1998. 3D geoelectric tomography and archaeological applications. *Geophysical Prospecting*, **46**, 543-570.

Meyers, E.M. (Ed.), 1996. *The Oxford Encyclopedia of Archaeology in the Near East*. 5 Vols., Oxford University Press, Oxford.

Murty, B.V. and Haricharan P., 1984. A simple approach toward interpretation SP anomaly due to 2-D sheet model of short dipole length. *Geophysical Research Bulletin*, **22**, No. 4, 213-218.

Nayak, P.N., 1981. Electromechanical potential in surveys for sulphide. *Geoexploration*, **18**, 311-320.

Ogilvy, A.A. and Bogoslovsky, V.A., 1979. The possibilities of geophysical methods applied for investigating the impact of man on the geological medium. *Geophysical Prospecting*, **27**, 775-789.

Oliveti, I. and Cardarelli, E., 2019. Self-Potential data inversion for environmental and hydrogeological investigations. *Pure and Applied Geophysics*, **176**, No. 8, 3607-3628.

Onojasun, O.E. and Takum, E., 2015. Geophysical investigation using self-potential techniques: A case of locating underground water pipeline at Kwinana industrial area, Perth. *African Journal of Geo-Science Research*, **3**, No. 4, 19-23.

Parasnis, D.S., 1986. *Principles of Applied Geophysics*, 4th ed., revised and supplemented. Chapman & Hall, London.

Patella, D., 1997. Introduction to ground surface self-potential tomography. *Geophysical Prospecting*, **45**, 653-681.

Perrier, F. and Morat, P., 2000. Characterization of electrical faily variations induced by capillary flow in the non-saturated zone. *Pure and Applied Geophysics*, **157**, 785-810.

Perrier, F. and Pant, S.R., 2005. Noise reduction in long-term self-potential monitoring with travelling electrode referencing. *Pure and Applied Geophysics*, **162**, 165-179.

Petrovsky, A., 1928. The problem of a hidden polarized sphere. *Philosophical Magazine*, **5**, Series 7, 914-933.

905 Rao, D.A. and Babu**,** H.V., 1983. Quantitative interpretation of self-potential anomalies
906 due to two-dimensional inclined sheets. *Geophysics*, **48**, No. 2, 1659-1664.

907 Rao, D.A. and Babu, H.V. and Sivakumar, G.D.J., 1982. A Fourier transform method
908 for the interpretation of SP anomalies due to two-dimensional inclined sheets of
909 finite depth extent. *Pure and Applied Geophysics*, **120**, 365-374.

910 Rao, K., Jain, S. and Biswas, A., 2020. Global optimization for delineation of self-
911 potential anomaly of a 2D inclined plate. *Natural Resources Research*, 1-15,
912 https://doi.org/10.1007/s11053-020-09713-4

913 Rao, S.V.S. and Mohan, N.L., 1984. Spectral interpretation of self-potential anomaly
914 due to an inclined sheet. *Current Science*, **53** (No. 9): 474-477.

915 Reich, R., 1992. *Architecture of Ancient Israel*. Israel Exploration Society, Jerusalem.

916 Revil, A. and Jardani, A., 2013. *The Self-Potential Method: Theory and Applications in*
917 *Environmental Geosciences*. Cambridge Univ. Press, Cambridge, UK.

918 Rittgers, J.B., Revil, A., Karaoulis, M., Mooney, M.A., Slater, L.D. and Atekwana, E.A.,
919 2013. Self-potential signals generated by the corrosion of buried metallic objects
920 with application to contaminant plumes. *Geophysics*, **78**, No 5, EN65-EN82.

921 Rozycki, A., Fonticiella, J.M.R. and Cuadra, A., 2006. Detection and evaluation of
922 horizontal fractures in Earth dams using self-potential method. *Engineering*
923 *Geology*, **82**, 145-153.

924 Quarto, R. and Schiavone, D., 1996. Detection of cavities by the self-potential method.
925 *First Break*, **14**, No. 11, 419-430.

926 Safipour, R., Hölz, S., Halbach, J., Jegen, M., Petersen, S., and Swidinsky, A., 2017. A
927 self-potential 382 investigation of submarine massive sulfides, Palinuro Seamount,
928 Tyrrhenian Sea. *Geophysics*, **383,** 82(6), A51-A56.

929 Sailhac, P. and Marquis, G., 2001. Analytic potentials for the forward and inverse
930 modeling of SP anomalies caused by subsurface fluid flow. *Geophysical Research*
931 *Lett*., **28**, No. 9, 1851-1854.

932 Sato, M. and Mooney, H.M., 1960. The electrochemical mechanism of sulfide self-
933 potentials. *Geophysics*, **25**, 226-249.

934 Semenov, A.S., 1980. *Electric Prospecting by Self-Potential Method*. 4st ed., revised and
935 supplemented. Nedra, Leningrad (in Russian).

936 Semenov, M.V., 1975. *Principles of Prospecting and Investigating Pyrite-Polymetallic*
937 *Ore Fields by Geophysical Methods*. Nedra, Leningrad (in Russian).

938 Sengupta, S.N., Bose, R.N. and Mitra, S.K., 1969. Geophysical investigations for copper
939 ores in the Singhana-Gotpo area, Khetri copper belt, Rajasthan (India).
940 *Geoexpoloration*, **7**, 73-82.

941 Shevnin, V.A., 2018. Identification of self-potential anomalies of a diffusion-absorption
942 origin. *Moscow Univ. Geology Bulletin,* **73***,* No. 3, 306-311.

943 Shevnin, V.A., Bobachev, A.A., Ivanova, S.V. and Baranchuk, K.I., 2014. Joint analysis
944 of self potential and electrical resistivity tomography data for studying
945 Alexandrovsky settlement. *Trans. of the 20th Meeting of Environmental and*
946 *Engineering Geophysics*. Athens, Greece, Mo PA2 04, 1-5.

947 Sindirgi, P., Pamukçu, O. and Özyalin, S., 2008. Application of normalized full gradient
948 method to self potential (SP) data. *Pure and Applied Geophysics*, **165**, 409-427.

949 Sindrigi, P and Özyalin, S., 2019. Estimating the location of a causative body from a
950 self-potential anomaly using 2D and 3D normalized full gradient and Euler
951 deconvolution. *Turkish Journal of Earth Sciences*, **28**, 640-659.

952 Skianis, G.A., Papadopoulos, T.D. and Vaiopoulos, D.A., 1991. 1-D and 2-D spatial
953 frequency analysis of SP field anomalies produced by a polarized sphere. *Pure and*
954 *Applied Geophysics*, **137**, 251-260.

955 Skianis, G., Papadopoulos, T., Vaiopoulos, D.A. and Nikolaou, S., 1995. A new method
956 of quantitative interpretation of SP anomalies produced by a polarized inclined
957 sheet. *Geophysical Prospecting*, **43**, 677-691.

958 Srigutomo, W., Arkanuddin, M.R., Pratomo, P.M., Novana, E.C. and Agustina, R.D.,
959 2010. Application of qualitative and quantitative analyses of self potential anomaly
960 in caves detection in Djuanda Forest Park, Bandung. *Amer. Inst. of Physics Proc*.,
961 **1325**, No. 164, 164-167.

962 Srivastava, S. and Agarwal, B.N.P., 2009. Interpretation of self-potential anomalies by
963 enhanced local wave number technique. *Journal of Applied Geophysics*, **68**, 259-
964 268.

965 Stern, W., 1945. Relation between spontaneous polarization curves and depth, size, and
966 dip of ore bodies. *Trans. Am. Inst. Min., Metallurg*., Petr. Eng., **164**, 189-196.

967 Sungkono, 2020. Robust interpretation of single and multiple self-potential anomalies
968 via flower pollination algorithm. *Arabian Journal of Geosciences*, **13** (100), 1-15.

969 Telford, W.M., Geldart, L.P. and Sheriff, R.E., 1990. *Applied Geophysics*, 2nd edition.
970 Cambridge University Press, Cambridge.

971 Tlas, M. and Asfahani, J., 2013. An approach for interpretation of self-potential
972 anomalies due to simple geometrical structures using Fair function minimization.
973 *Pure and Applied Geophysics*, **170**, 895-905.

974 Tripathi, G.N. and Frayar, A.E., 2016. Integrated surface geophysical approach to locate
975 a karst conduit: a case study from Royal Spring Basin, Kentucky, USA. *Jour. of*
976 *Nepal Geological Society*, **51**, 27-37.

977 Tsokas, G.N., Tourlos, P.I., Kim, J.-H., Papazachos, C.B., Vargemezis, G. and
978 Bogiatzis, P., 2014. Assessing the condition of the rock mass over the tunnel of
979 Eupalinus in Samos (Greece) using both conventional geophysical methods and
980 surface to tunnel electrical resistivity tomography. *Archaeological Prospection*, **21**,
981 277-291.

982 Vichabian, Y. and Morgan, F.D., 2002. Self-potentials in cave detection. *The Leading*
983 *Edge*, **21**, 866-871.

984 Wang, J-H. and Geng, Yu., 2015. Terrain correction in the gradient calculation of
985 spontaneous potential data. *Chinese Jour. of Geophysics*, **58**, No. 6, 654-664.

986 Wynn, J.C. and Sherwood, S.I., 1984. The self-potential (SP) method: an inexpensive
987 reconnaissance and archaeological mapping tool. *Journal of Field Archaeology*, **11**,
988 195-204.

989 Yüngül, S., 1954. Spontaneous-potential survey of a copper deposit at Sariyer, Turkey.
990 *Geophysics*, **19**, No. 3, 455-458.

991 Zaborovsky, A.I., 1963. *Electric Prospecting*. Gostoptekhizdat, Moscow (in Russian).

992 Zhdanov, M.S. and Keller, G.V., 1994. *The Geoelecrical Methods in Geophysical*
993 *Exploration*. Elsevier, Amsterdam.

994 Zhu, Z., Shen, J., Tao, C., Deng, X., Wu, T., Nie, Z., Wang, W and Su, Z., 2020.
995 Autonomous underwater vehicle based marine multi-component self-potential
996 method: observation scheme and navigational correction. *Geoscientific*
997 *Instrumentation Methods and Data Systems*, 1-25, doi.org/10.5194/gi-2020-24

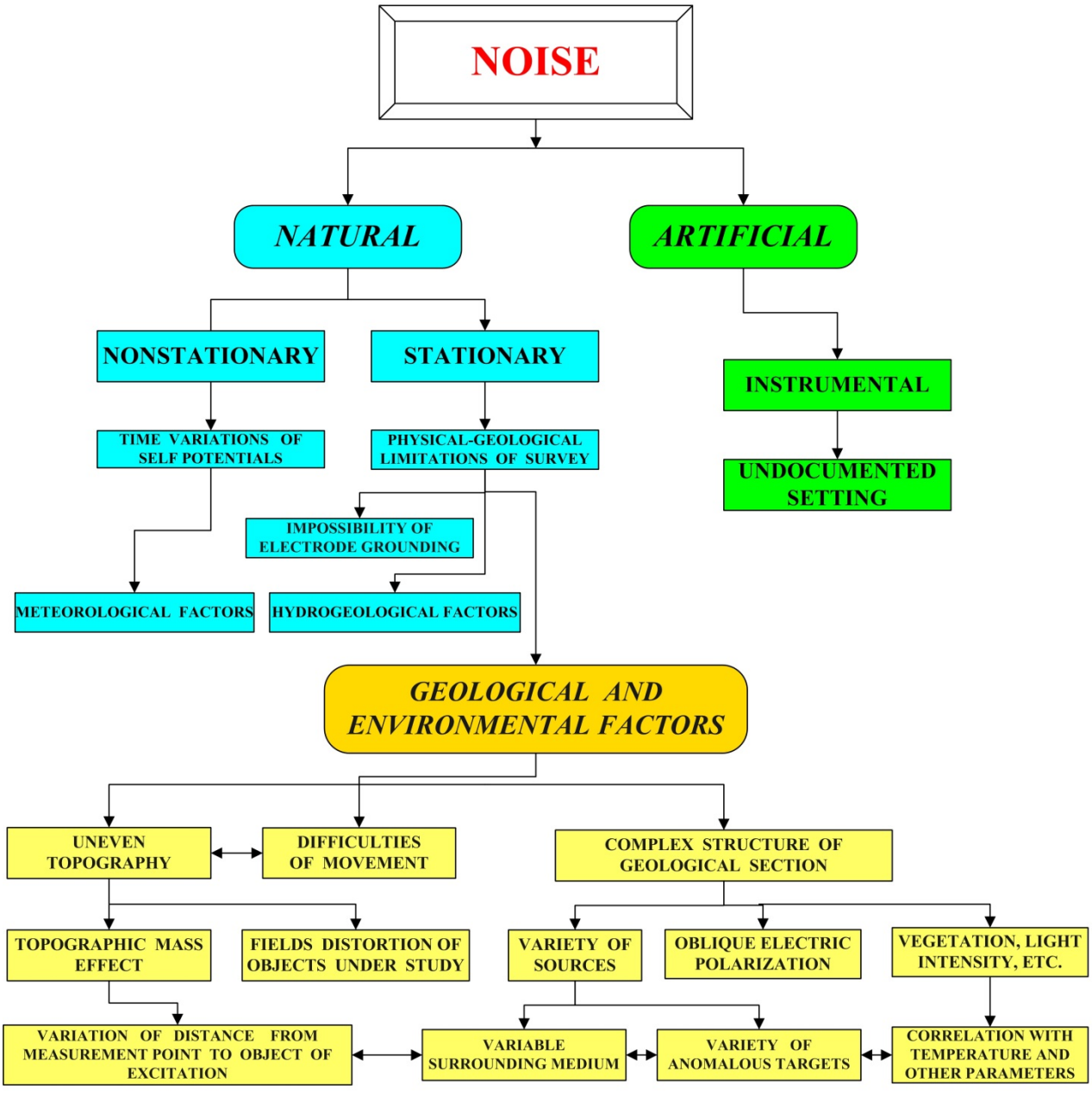

998

999 **Figure 1**. General scheme of disturbances in SP method

1000

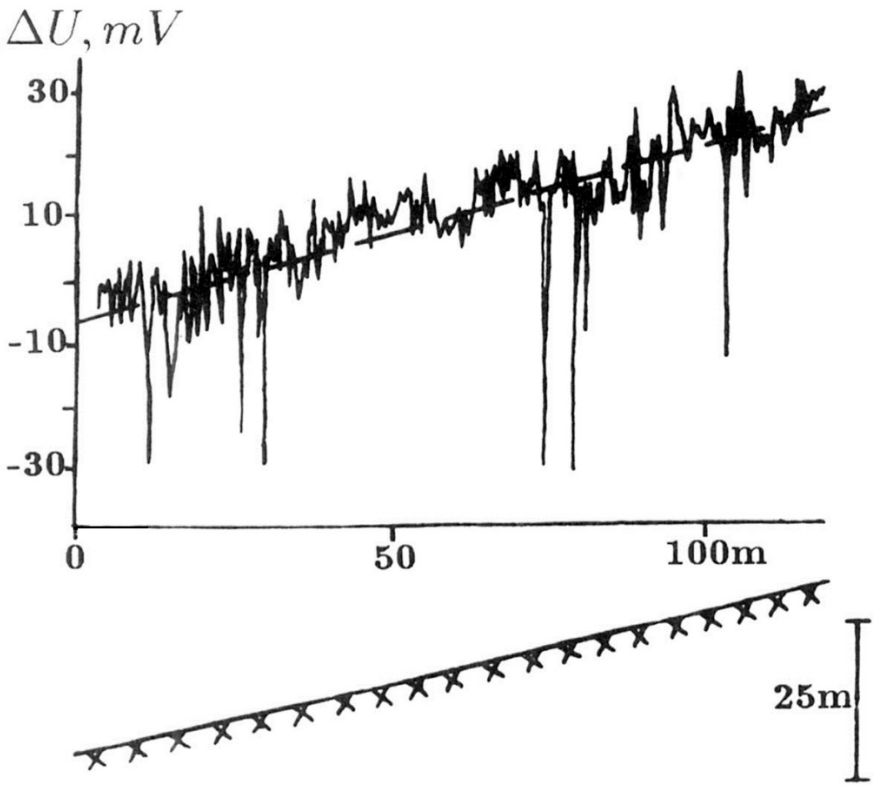

Figure 2. SP observations at inclined relief (after Ernstson and Schrerer (1986), with small modifications) (Middle Keuper of the Steigerwald highlands, 60 km east of Würzburg, Germany**)**

1005

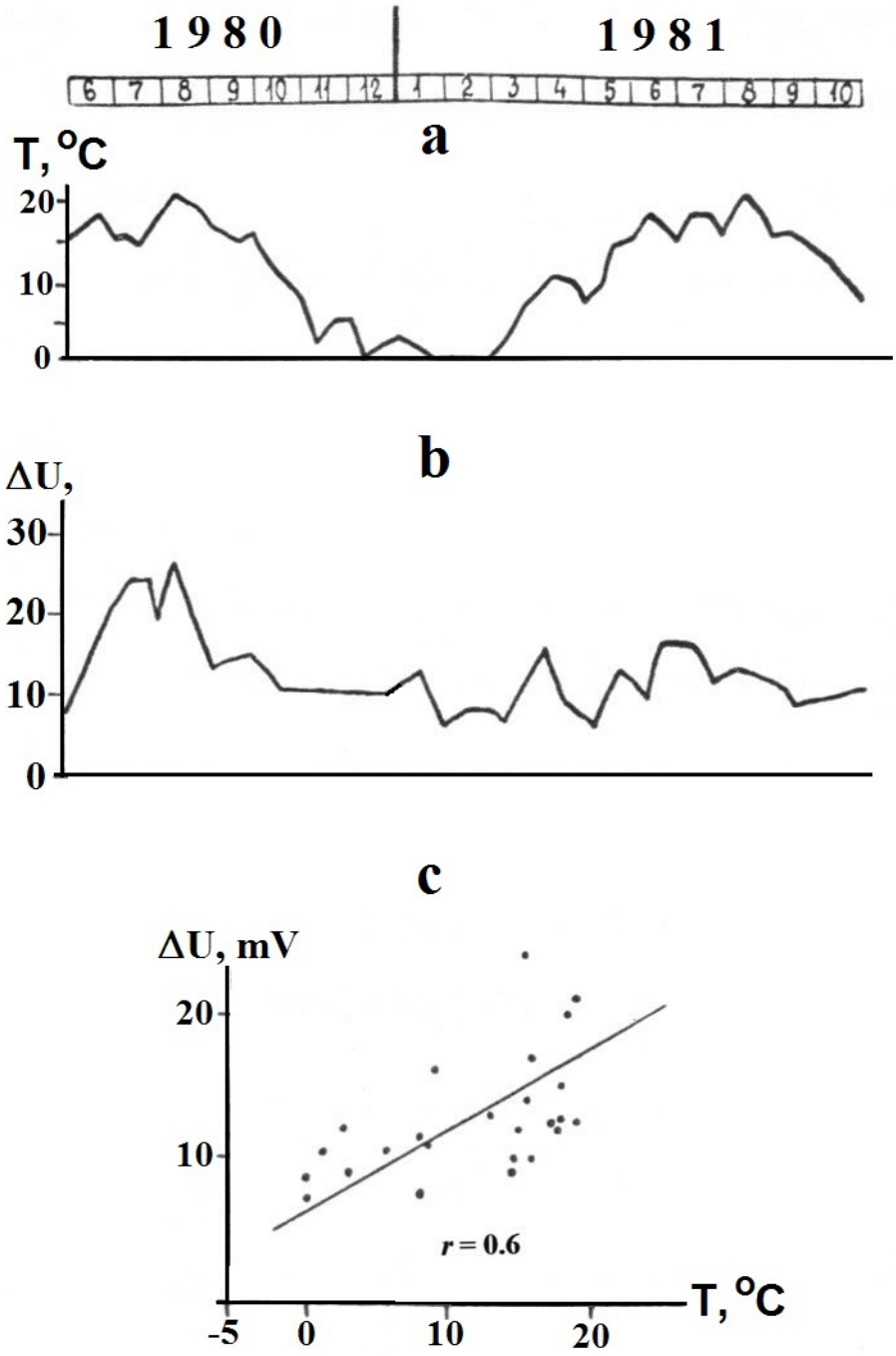

1006 **Figure 3**. A correlation between temperature and SP observations: **a** – temperature, **b**
1007 – SP intensity, **c** – correlation between these parameters (**a** and **b** – after Ernstson and
1008 Schrerer (1986)). SP observations were carried out in the Middle Keuper of the
1009 Steigerwald highlands 60 km east of Würzburg, Germany

1010

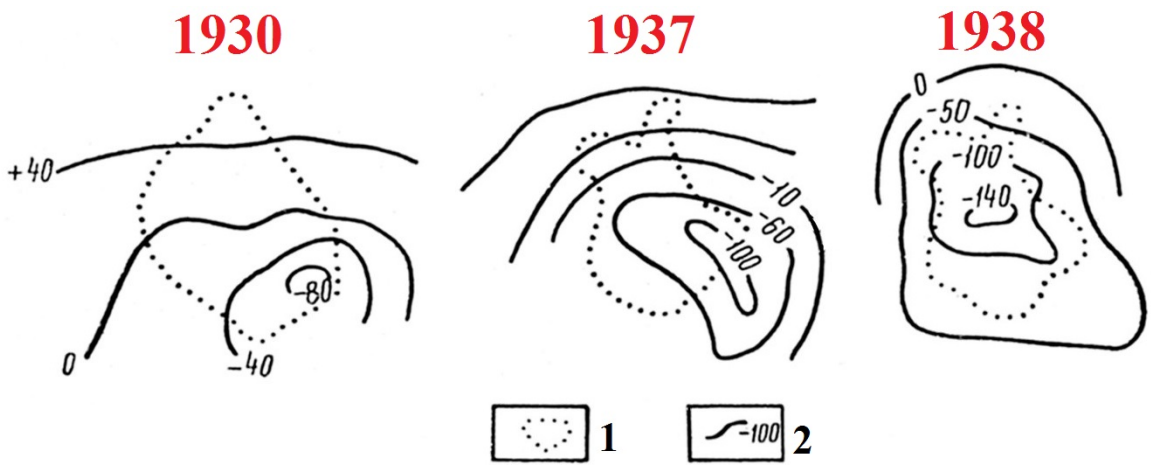

Figure 4. Displacement of self-potential isolines during exploitation of the new shaft of Chyragdere sulfur deposit (Lesser Caucasus) (after Eppelbaum and Khesin, 2012, with modifications).

(1) stock contour, (2) isolines of self-potential field (in milliVolts)

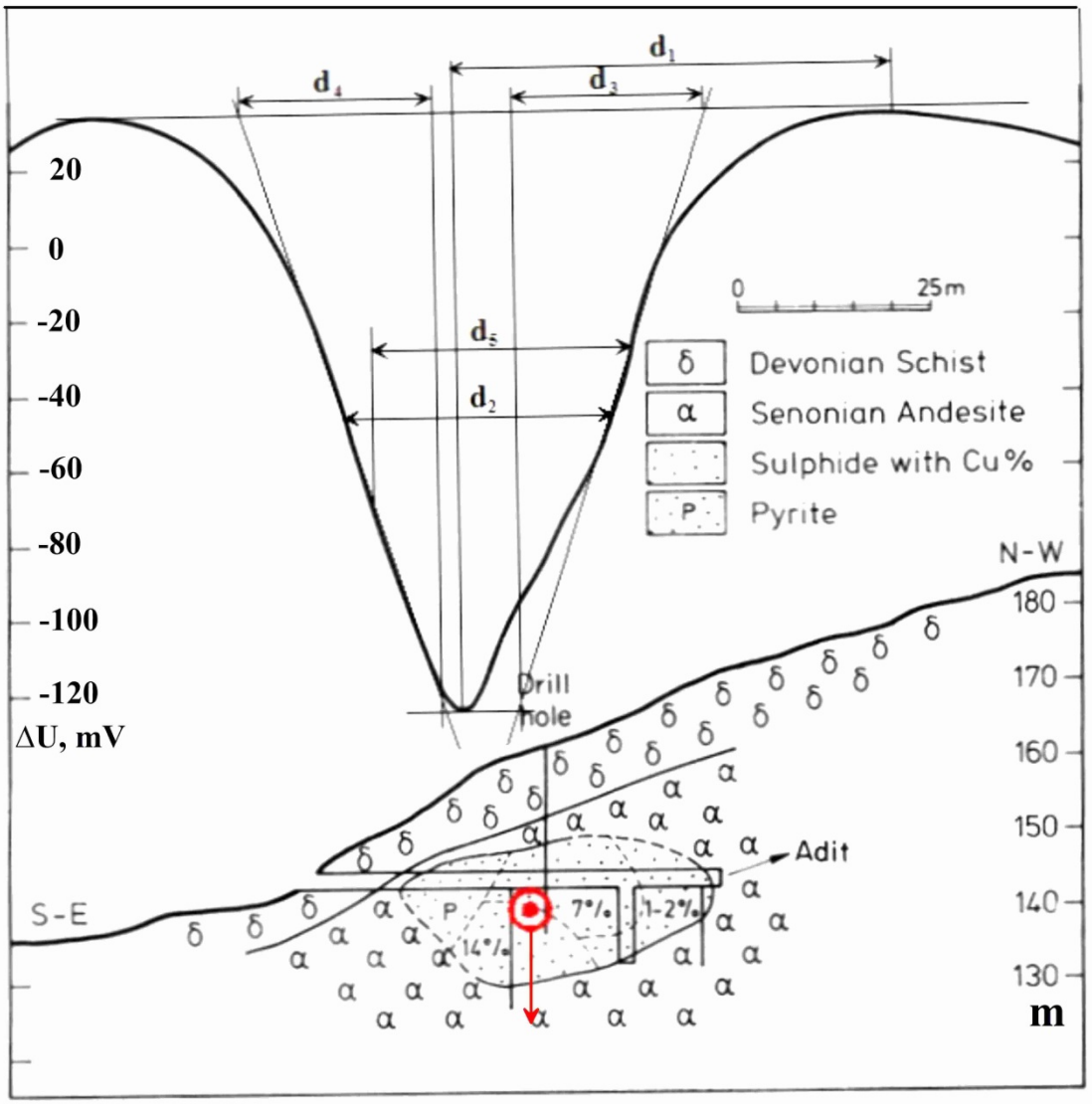

Figure 5. Quantitative interpretation of *SP* anomaly by the characteristic point and tangent methods in the Sariyer area, Turkey. The "⊙" symbol marks the obtained position of the ore body center (approximated by a HCC). Red arrow shows the direction of self-polarization vector. Observed SP curve and geological section are taken from Yüngül (1954)

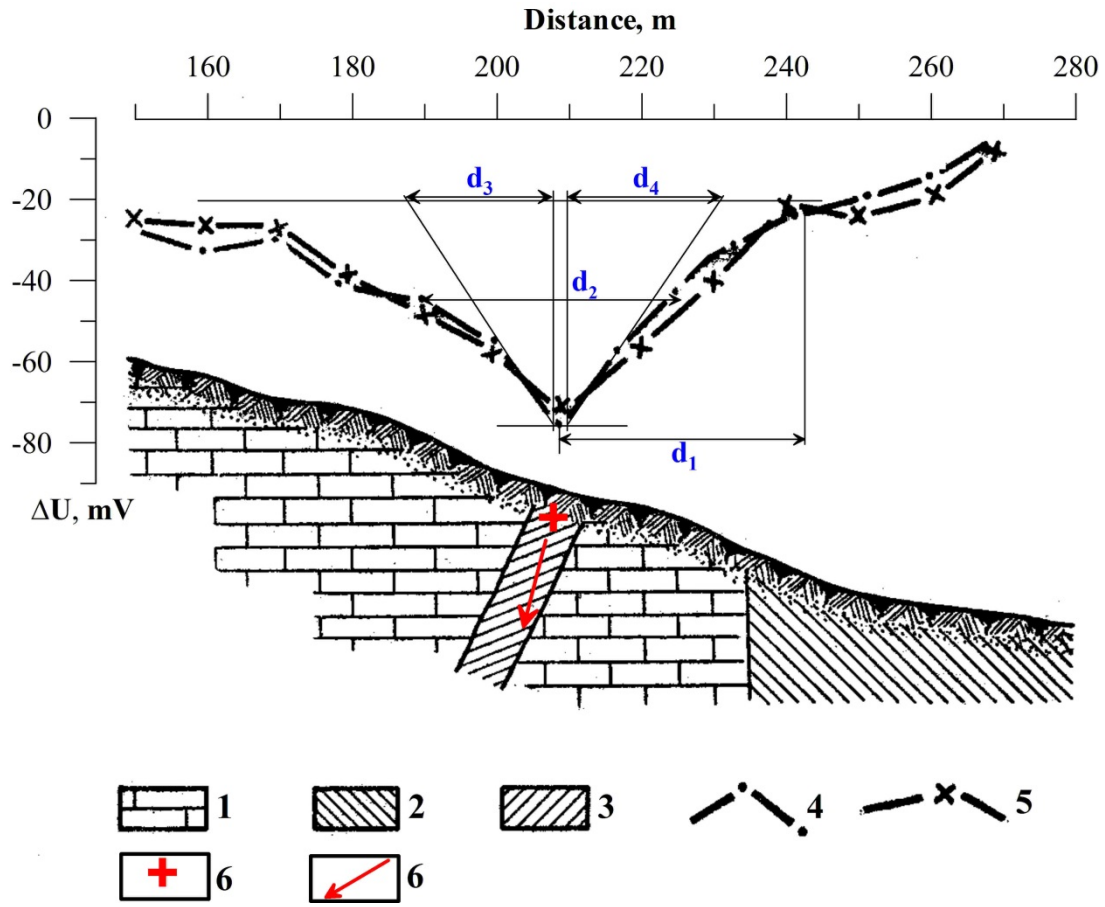

Figure 6. Quantitative interpretation of *SP* anomaly over polymetallic body (USSR). Observed SP curve and geological section are taken from Zaborovsky (1963)

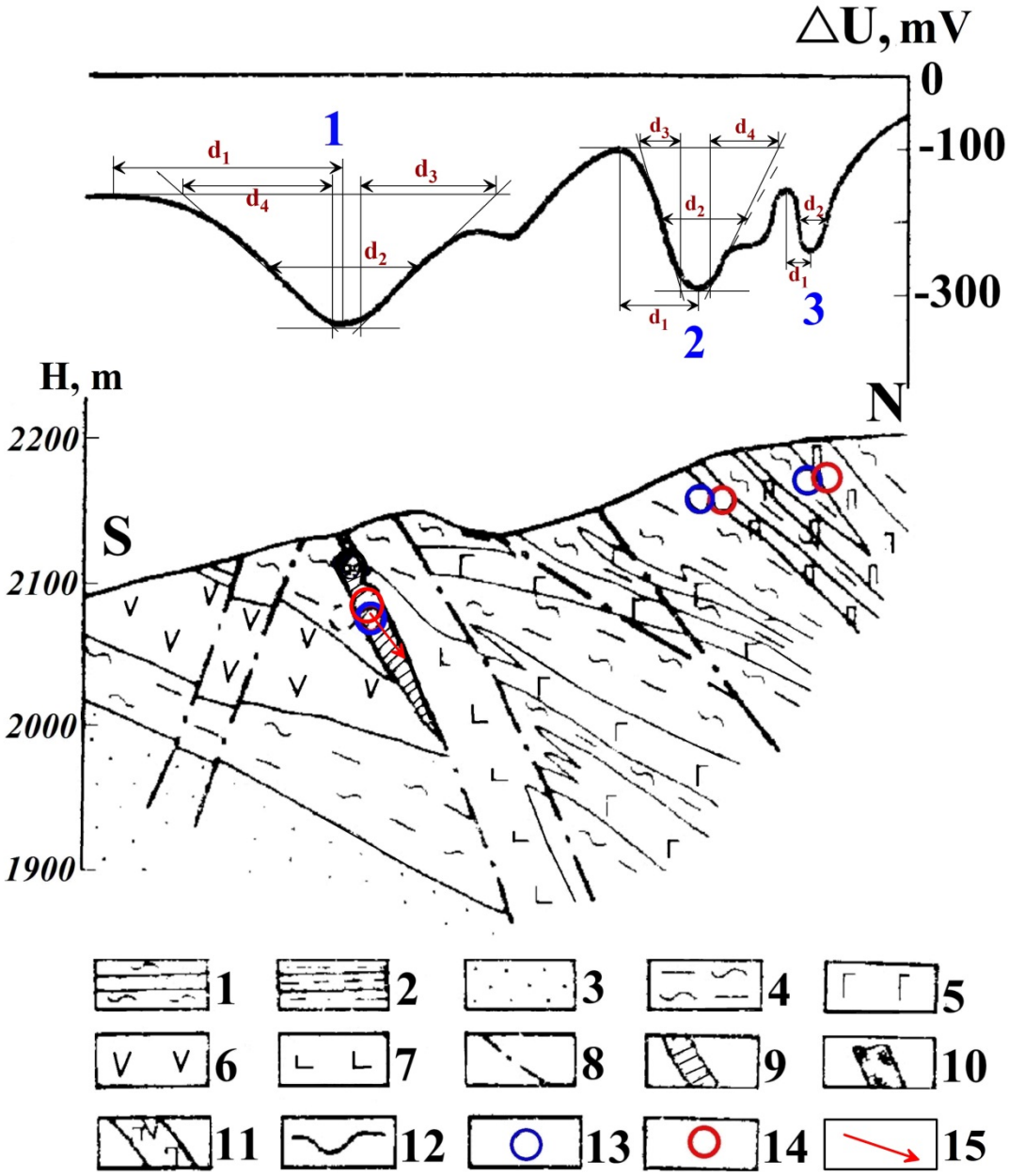

Figure 7. Results of quantitative interpretation of *SP* anomalies in the area of Katsdagh copper-polymetallic deposits on the southern slope of the Greater Caucasus (Azerbaijan).

(1) interbedding of sands and clay schists, (2) clay schists with the flysh packages, (3) clay sandstone; (4) sand-clay schists; (5) diabases, gabbro-diabases and diabasic porphyrites; (6) andesites and andesite-porphyrites; (7) dacitic porphyrites; (8) faults; (9) massive ore of pyrite-polymetallic composition; (10) oxidized ore; (11) zones of brecciation, crush and boudinage with lean pyrite-polymetallic ore; (12) *SP* curves; location of anomalous source: (13) without calculation of inclined relief influence,

(14) after introducing correction for terrain relief, (15) position of the self-potential vector

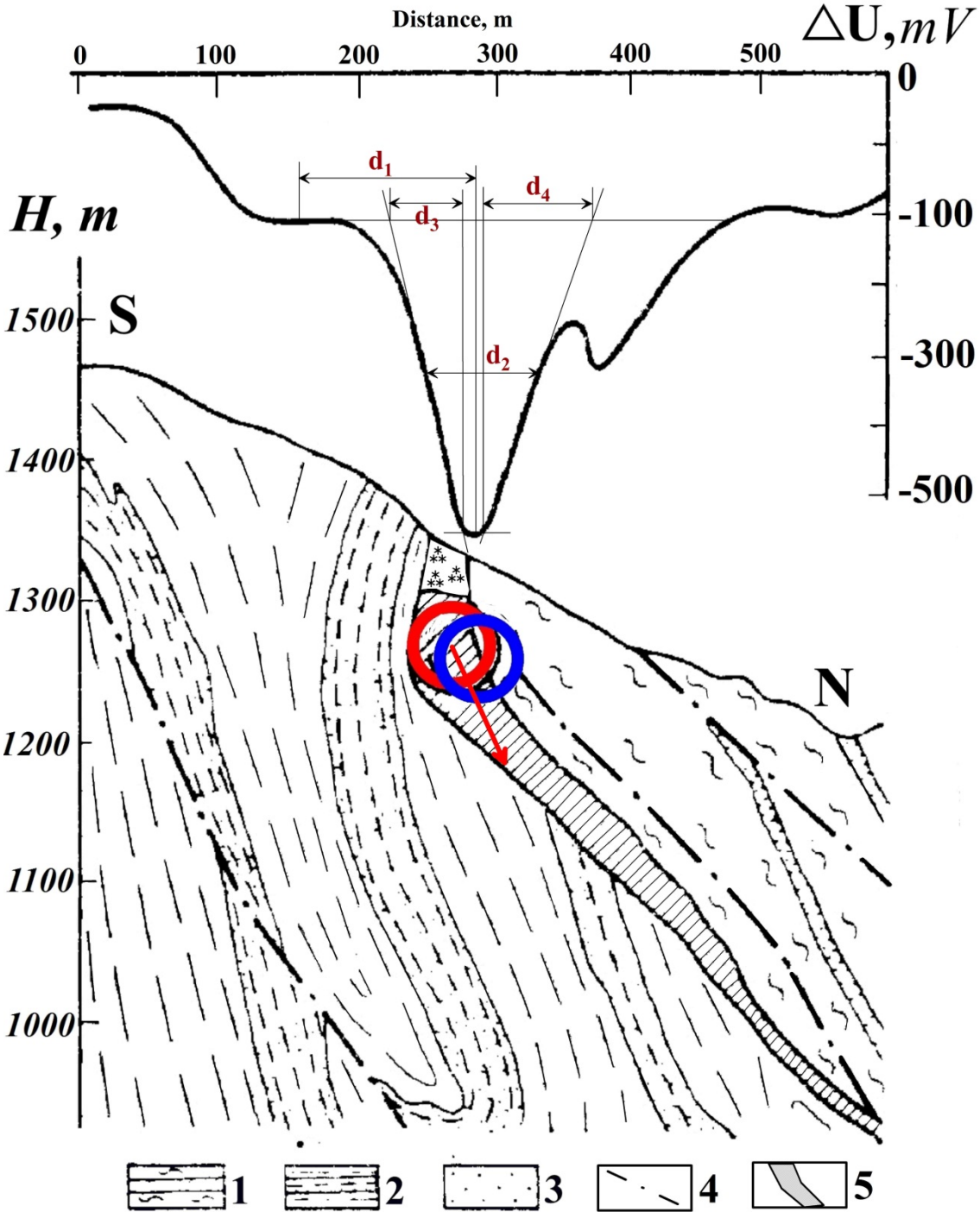

Figure 8. Results of quantitative interpretation of *SP* anomaly in the area of Filizchay copper-polymetallic deposit in the southern slope of the Greater Caucasus (Azerbaijan) (revised after Eppelbaum and Khesin (2012)).

(1) interbedding of sands and clay schists, (2) clay schists with the flysh packages, (3) clay sandstone, (4) faults; (5) massive ore of pyrite-polymetallic composition; (6)

oxidized ore; (7) *SP* curves, location of anomalous source: (8) without calculation of inclined relief influence, (9) after introducing correction for relief

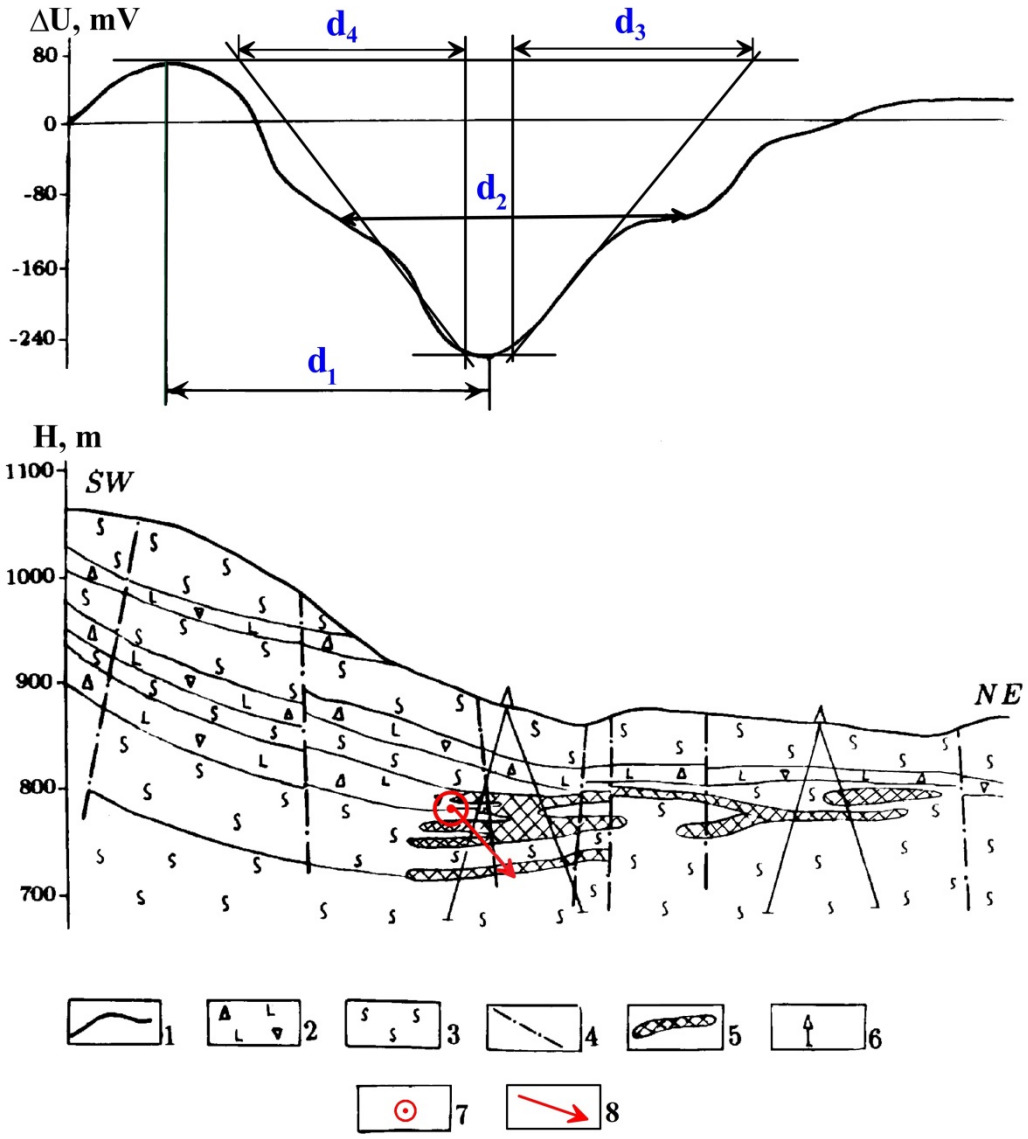

Figure 9. Interpretation of SP anomaly by the method of characteristic points in the area of the Uchambo ore field of the Adjar group of copper-polymetallic deposits (Georgia, Lesser Caucasus)

(1) SP observed values; (2) heteroclastic tuff breccia and their tuffs; (3) cover trachyandesite-basalts with pyroclastic interbeds; (4) disjunctive dislocations; (5) zones of increased mineralization; (6) drilled wells; (7) location of HCC center according to the interpretation results ((1-6) from Bukhnikashvili et al. (1974)

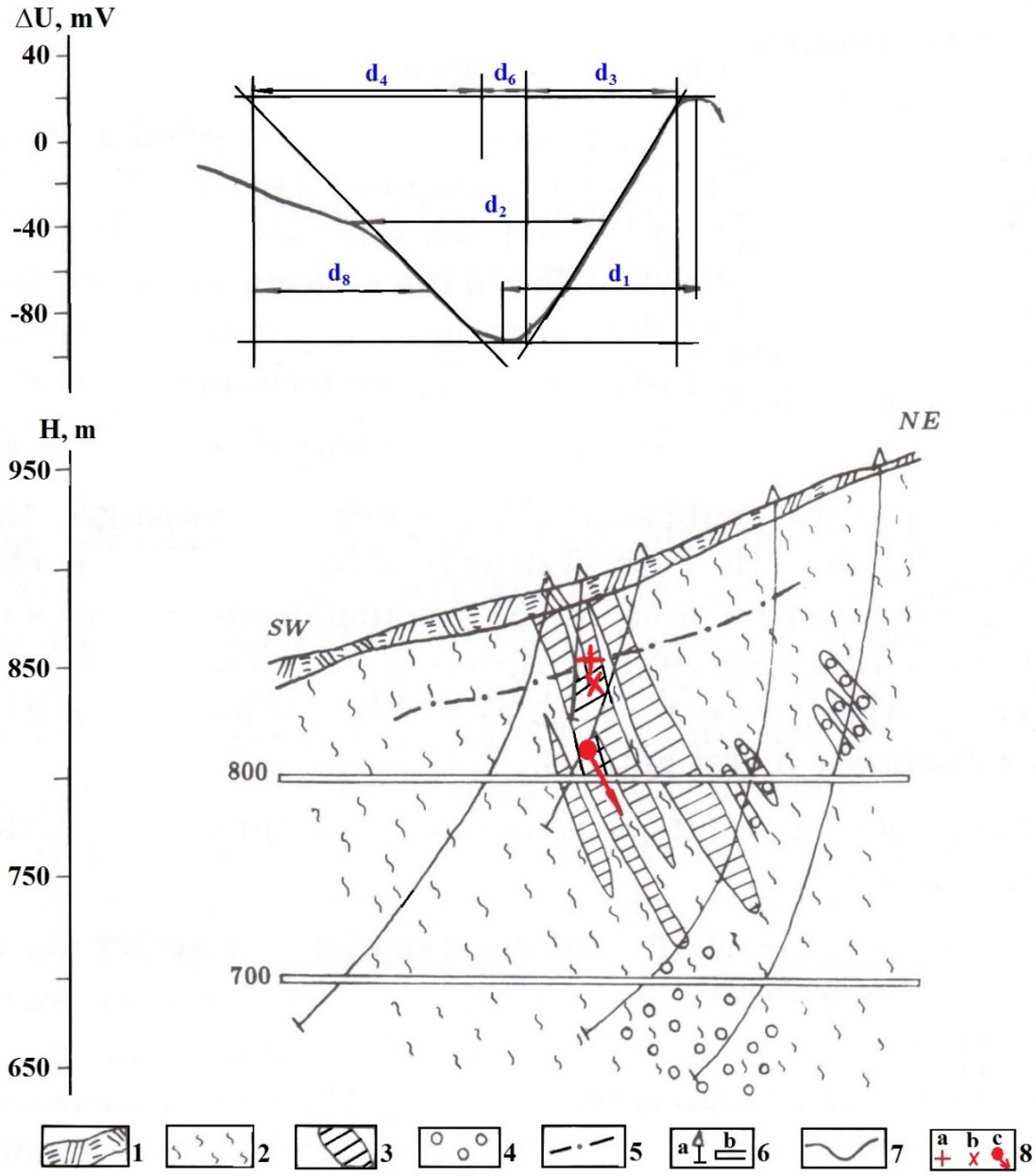

Figure 10. Interpretation by the developed techniques of SP anomaly in the area of deposit Potentsialnoe (Rudny Altai, Russia) (initial data from Semenov (1975))
(1) soil-vegetative layer; (2) alternation of lavas and tuffs of acid composition and chlorite-sericitic schists; (3) sulfide ores; (4) sulfide impregnation, pyritization; (5) level of ground waters; (6) drilling wells (a) and adits (b); (7) plot of SP; (8) interpretation results: (a) upper edge of the thin bed, (b) mid-point of the inclined thick bed's upper edge, (c) center of a horizontal circular cylinder (arrow indicates the direction of the polarization vector obtained by interpretation)

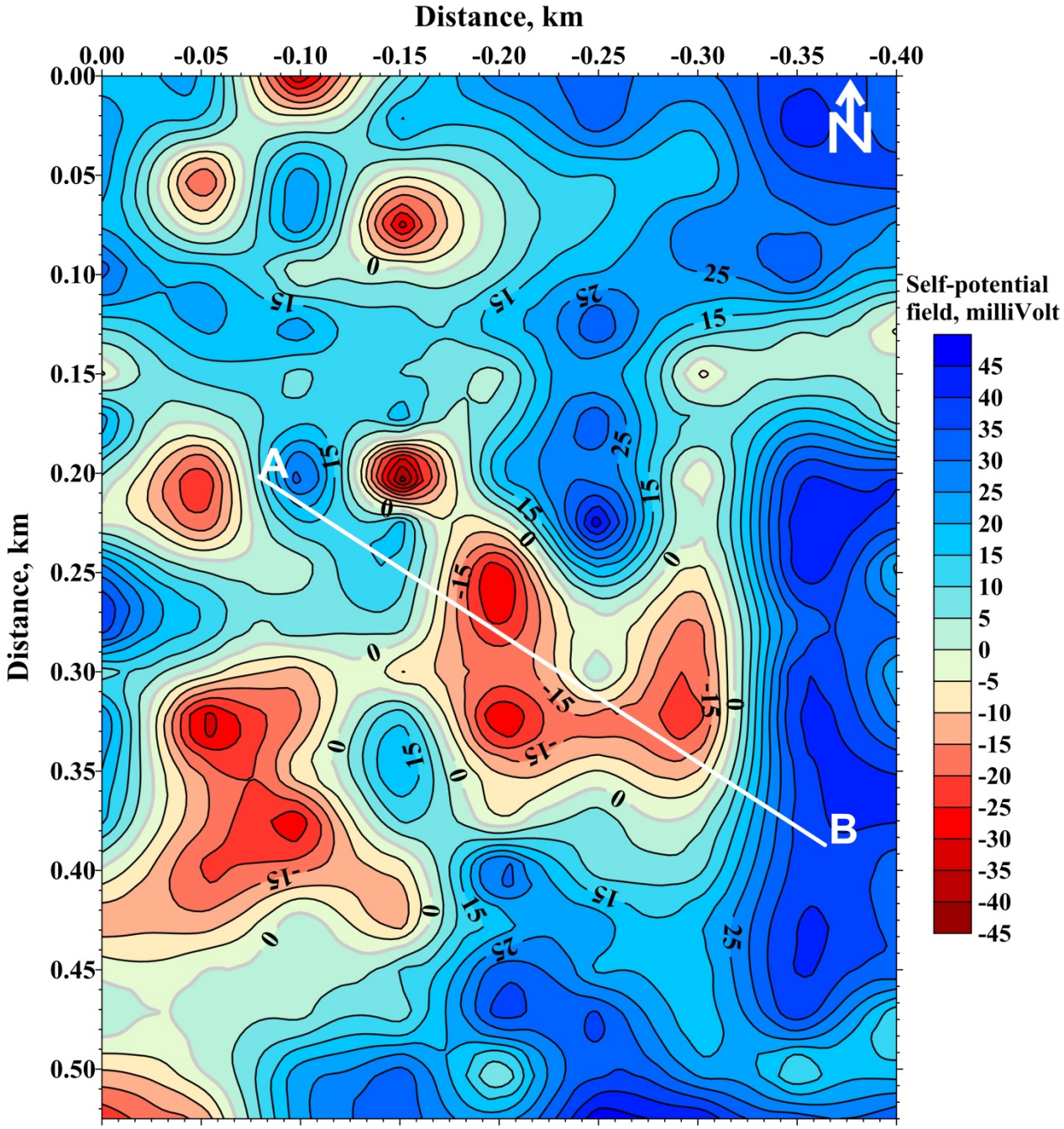

Figure 11a. SP map observed in the western Makhtesh Ramon (northern Negev desert)

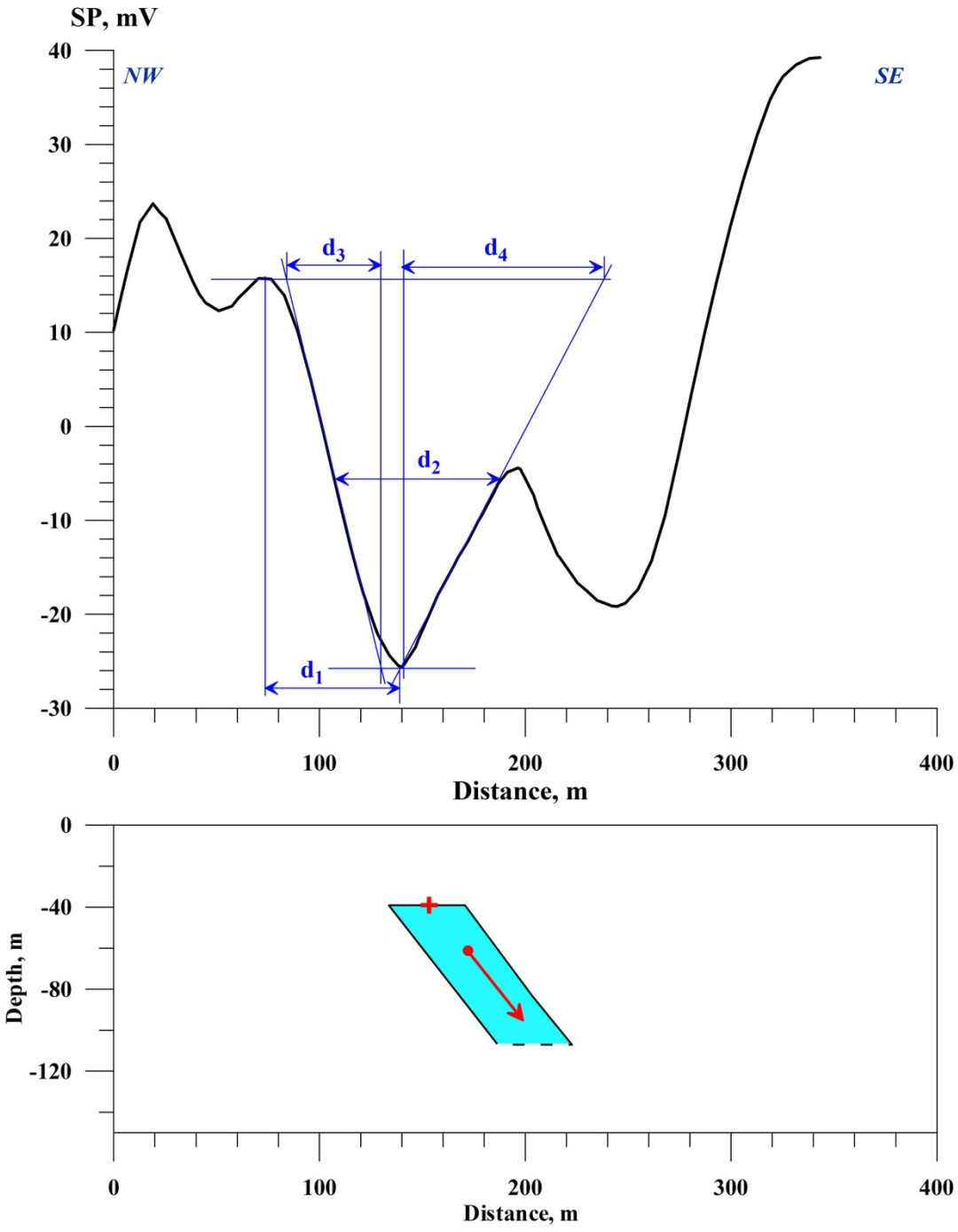

Figure 11b. Interpretation of SP anomaly along profile A – B, western Makhtesh Ramon (see Figure 11a)

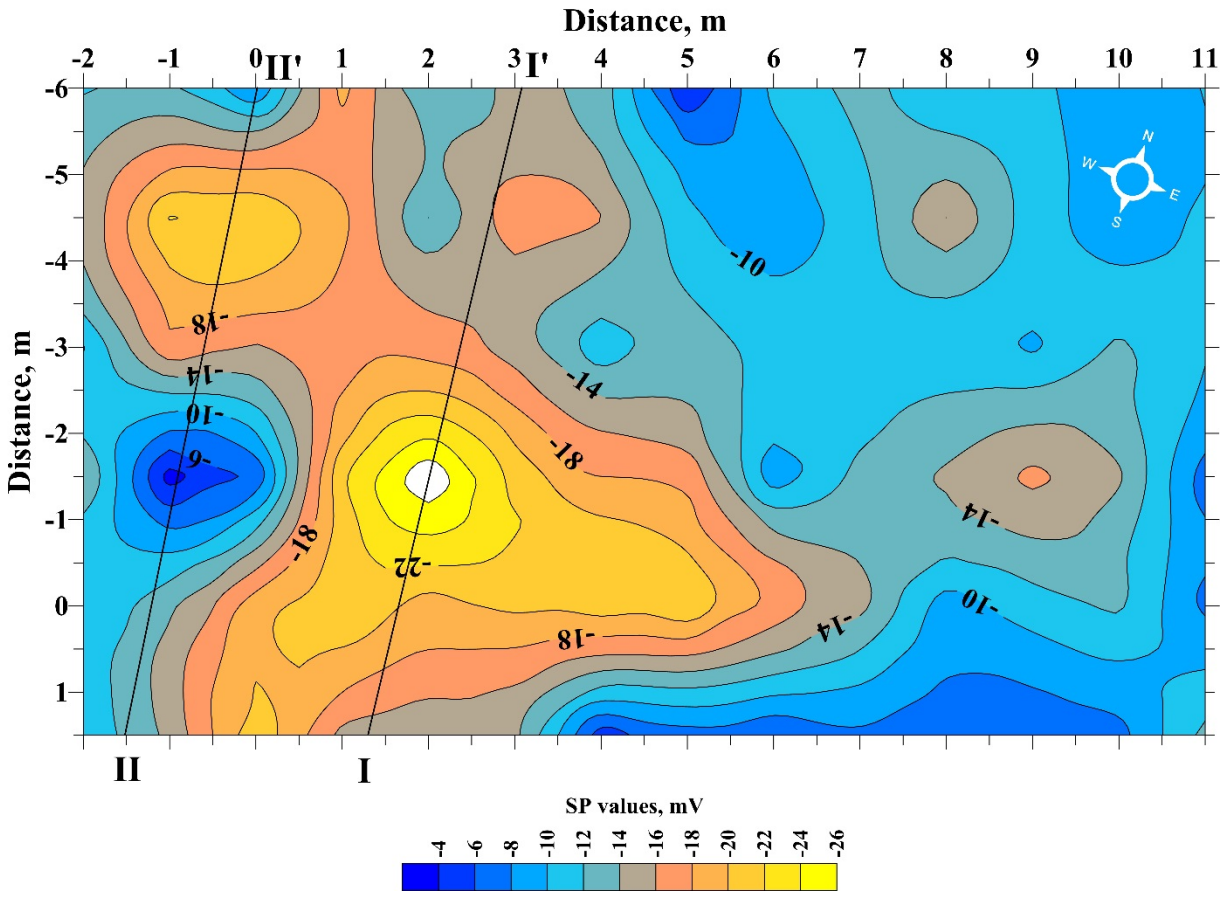

1081

1082 **Figure 12**. Self-potential map observed in the Banias site (northern Israel) and location

1083 of interpreting profiles I – I' and II – II'

1084

1085

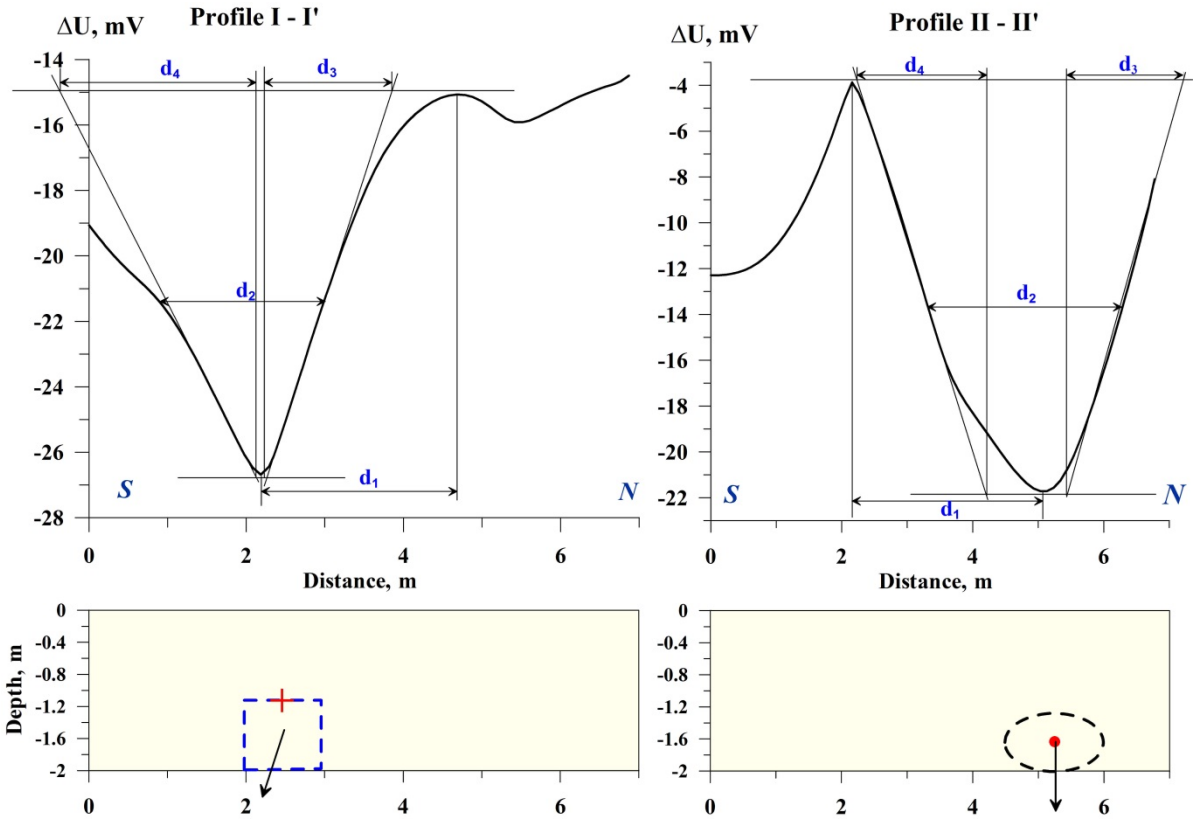

Figure 13. Quantitative analysis of anomalies I – I' and II – II' (see Figure 12) in the Banias site (northern Israel). Red cross indicates position of the center of upper edge, bold red point testifies position of HCC center, and the black arrows show direction of polarization angle ϕ_p

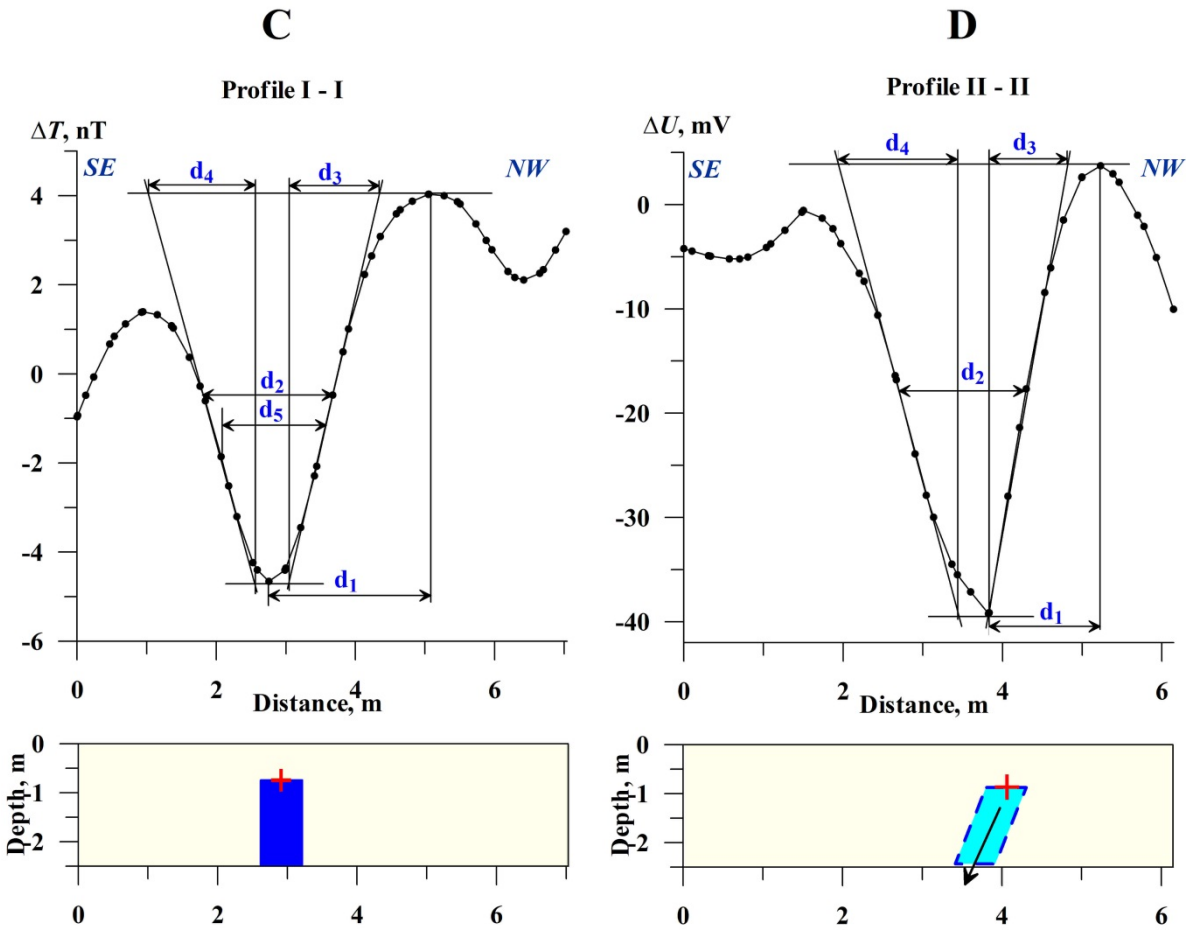

Figure 14. Quantitative analysis of magnetic (A) and self-potential (B) anomalies in the site of Halutza (southern Israel). Red cross in both models indicates position of the center of the upper edge, red arrow shows direction of polarization angle ϕ_p

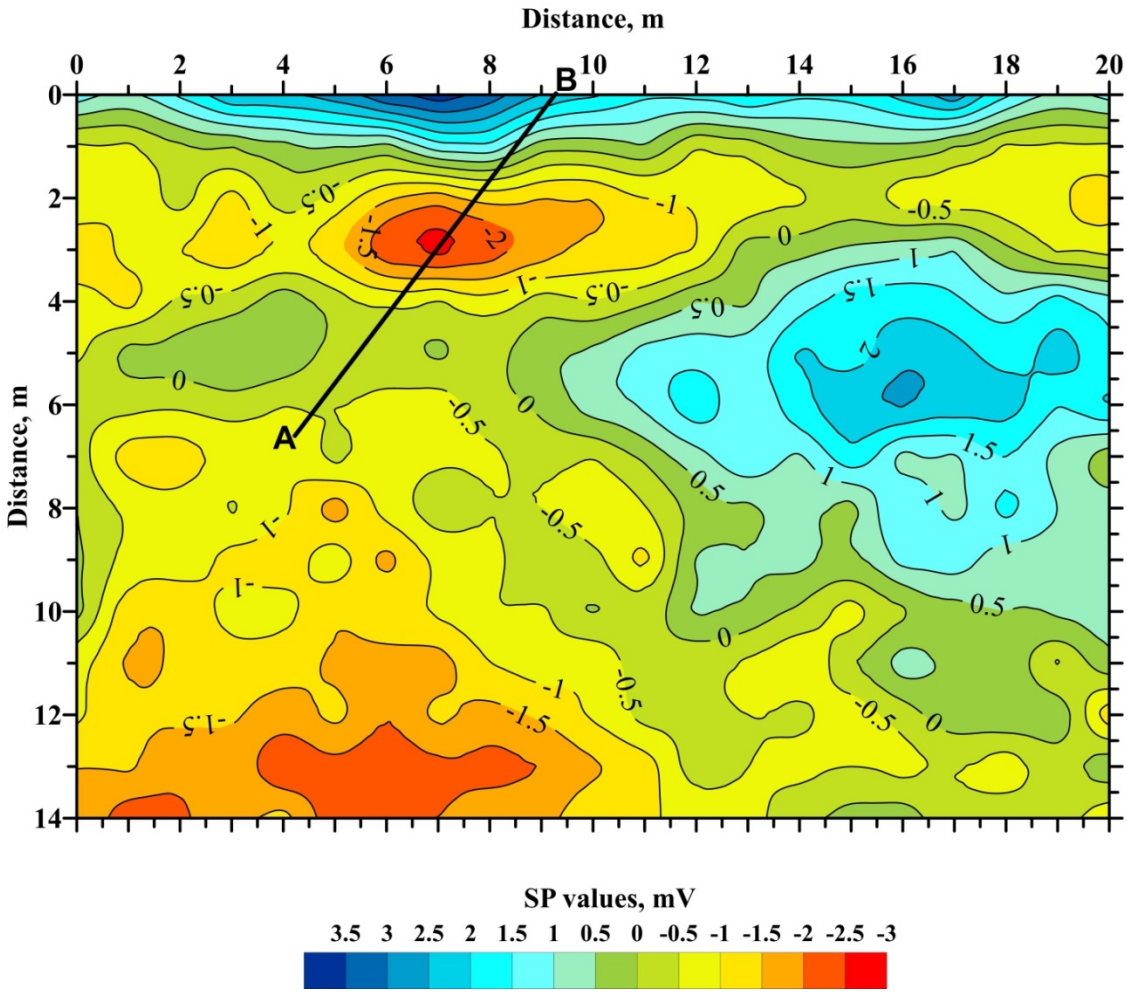

Figure 15. Self-potential map observed in the site of Emmaus-Nikopolis (central Israel)

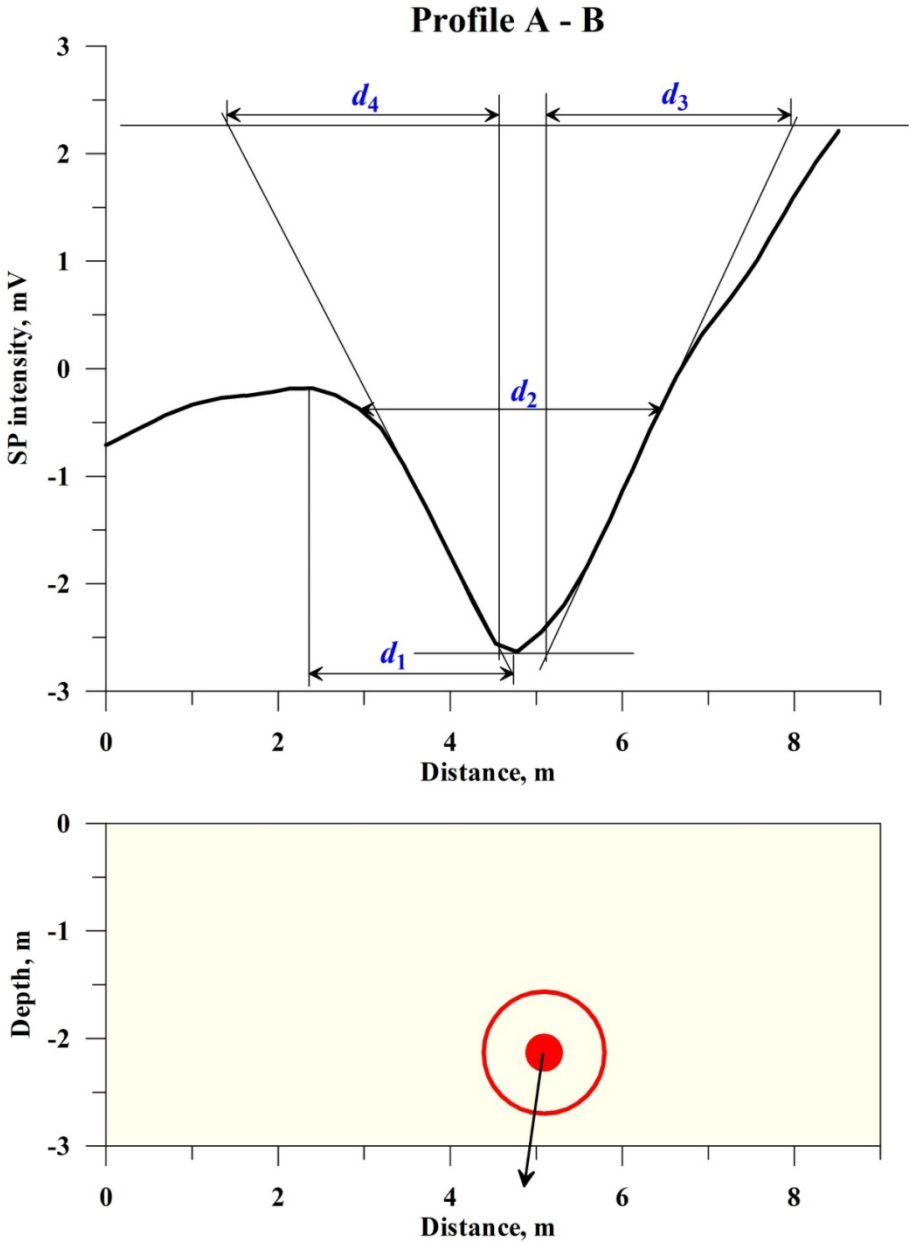

Figure 16. Quantitative analysis of self-potential anomaly along profile A – B in the site of Emmaus-Nikopolis (SP map is presented in Figure 15). Black arrow shows direction of polarization angle ϕ_p

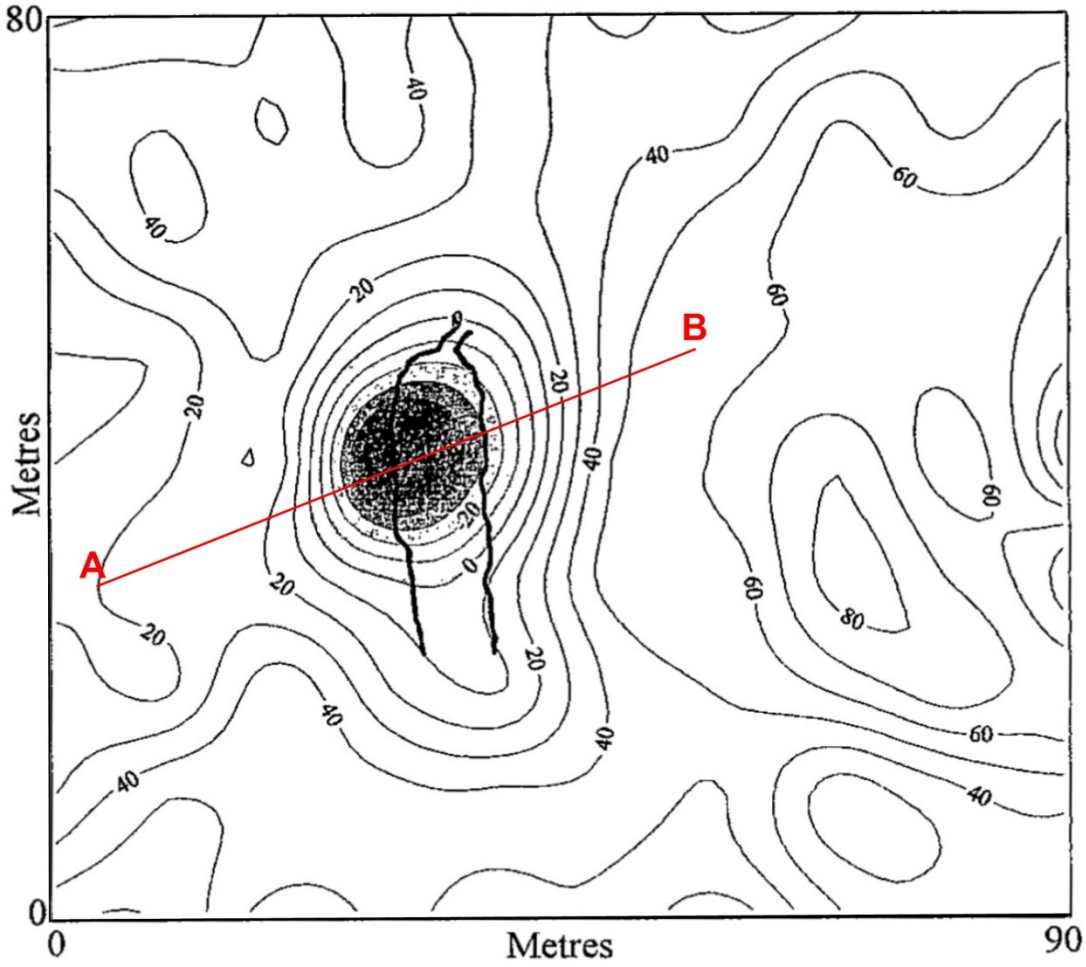

Figure 17. SP map over underground cave and position of interpreting profile A – B (SP map after Quarto and Schiavone (1996))

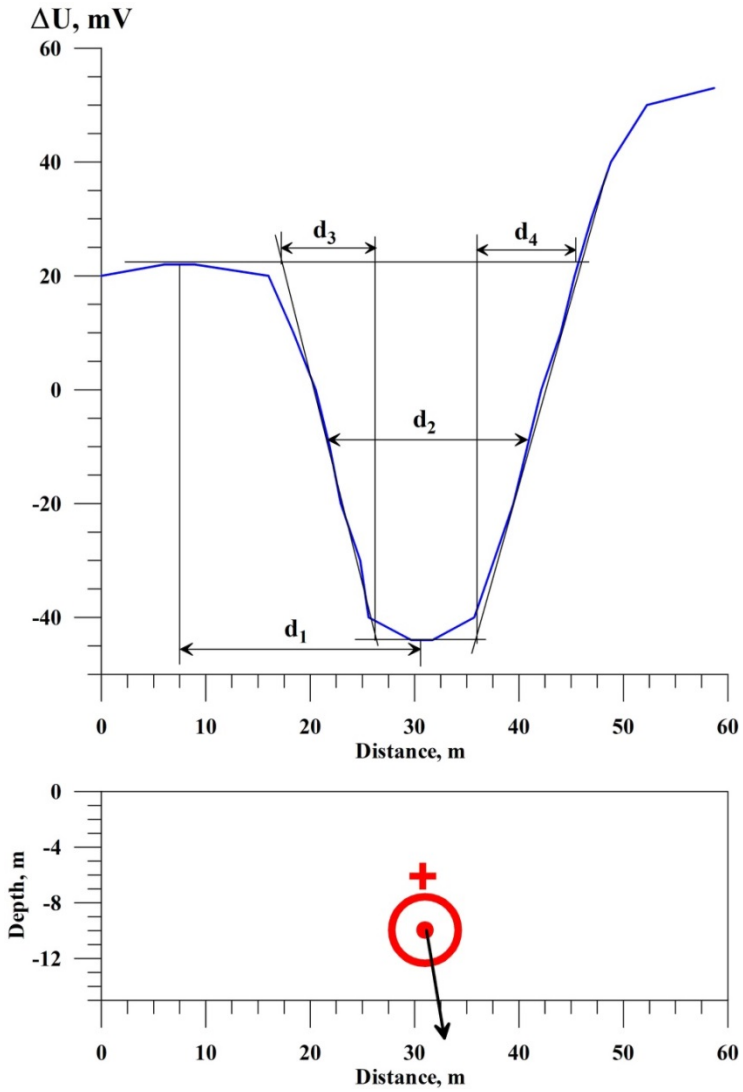

Figure 18. Quantitative analysis of SP anomaly along profile A – B (location of profile is shown in Figure 17). Red cross designates position of the middle of the thin bed upper edge, and circle – position of the center of the horizontal circular cylinder.

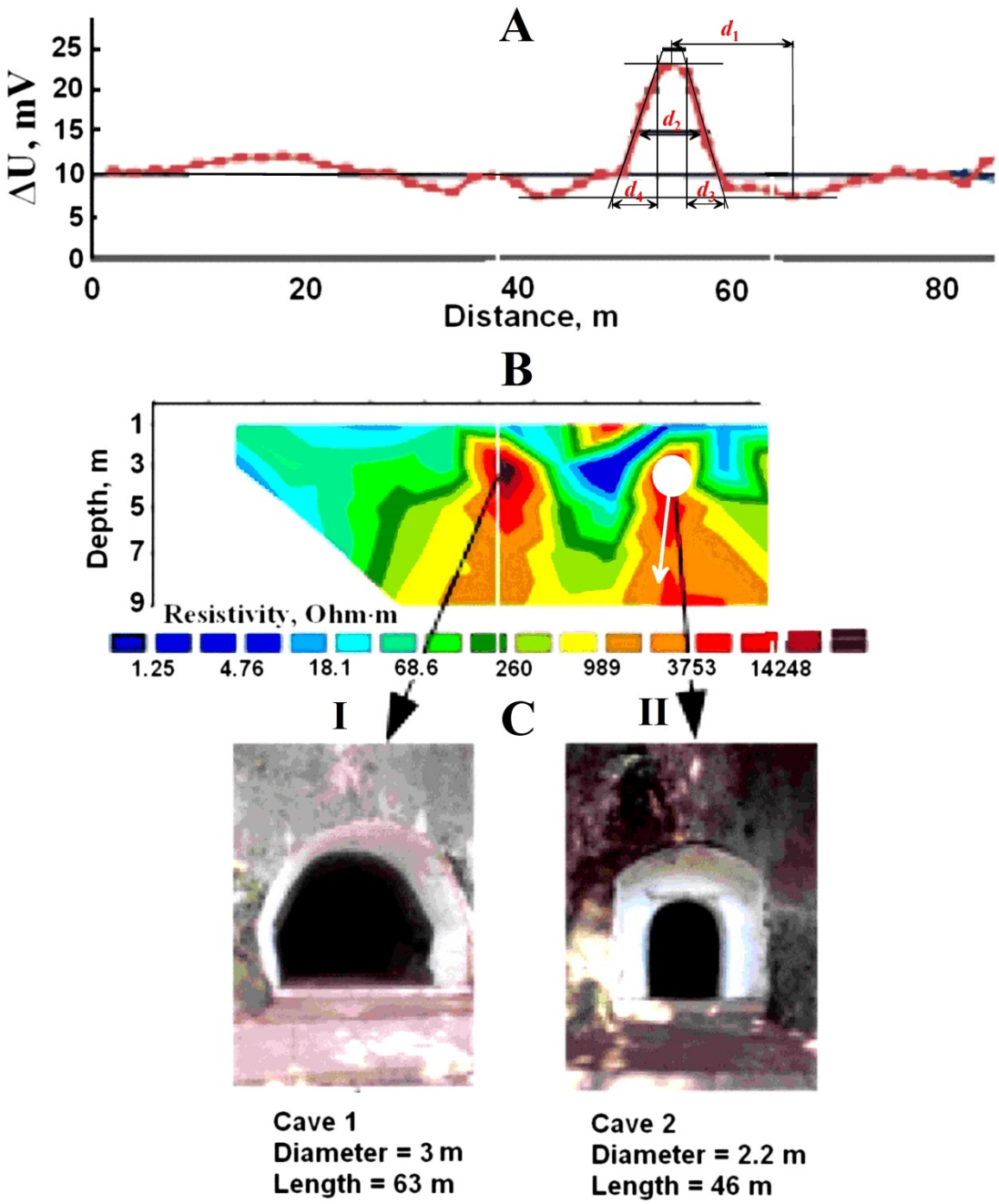

Figure 19. Quantitative analysis of SP anomaly over underground cave in the Djuanda Forest Park, Bandung (Indonesia). Initial data are taken from Srigumoto et al. (2010). White circle and arrow indicate the position of upper edge of cave II and its dipping (distribution of the highest resistivities)

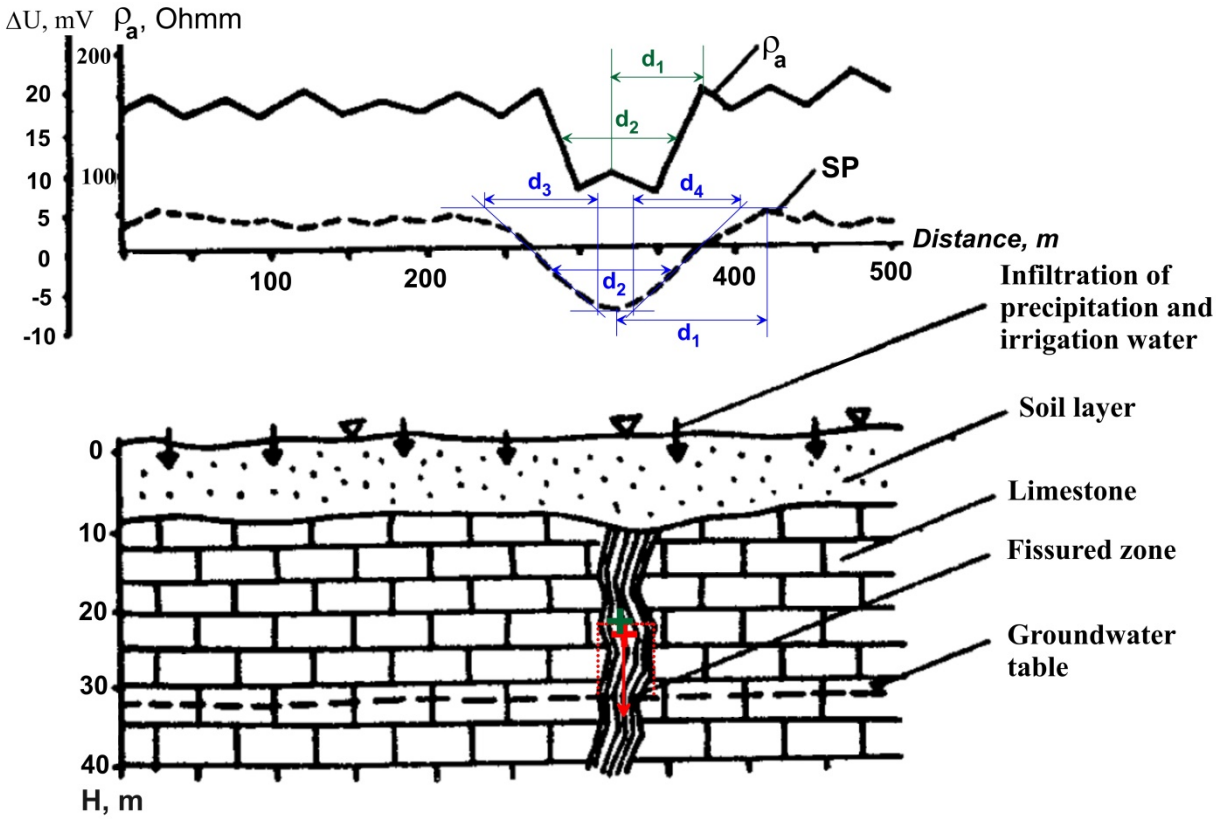

Figure 20. Interpretation of SP anomaly over the fissured zone (Russia) (resistivity and SP graphs and geological section are from Ogilvy and Bogoslovsky (1979)). Red and green crosses show the positions of the upper edge of the anomalous target determined from SP and resistivity curves, respectively. Red arrow indicates the position of self-potential vector

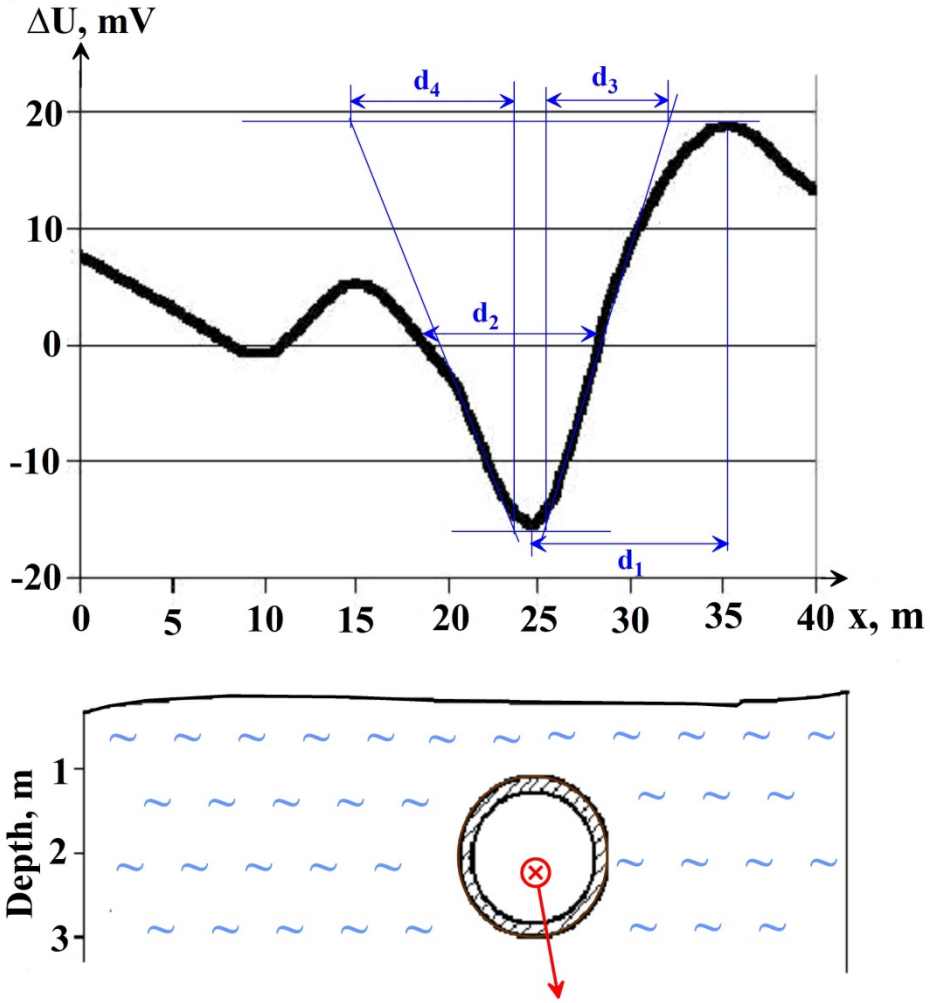

Figure 21. Quantitative examination of SP anomaly from the buried metallic pipe (southern Russia). Observed SP graph and environmental section are taken from Fomenko (2010). Red circle indicates determined position of the center of HCC, and arrow shows position of self-potential vector

Figures

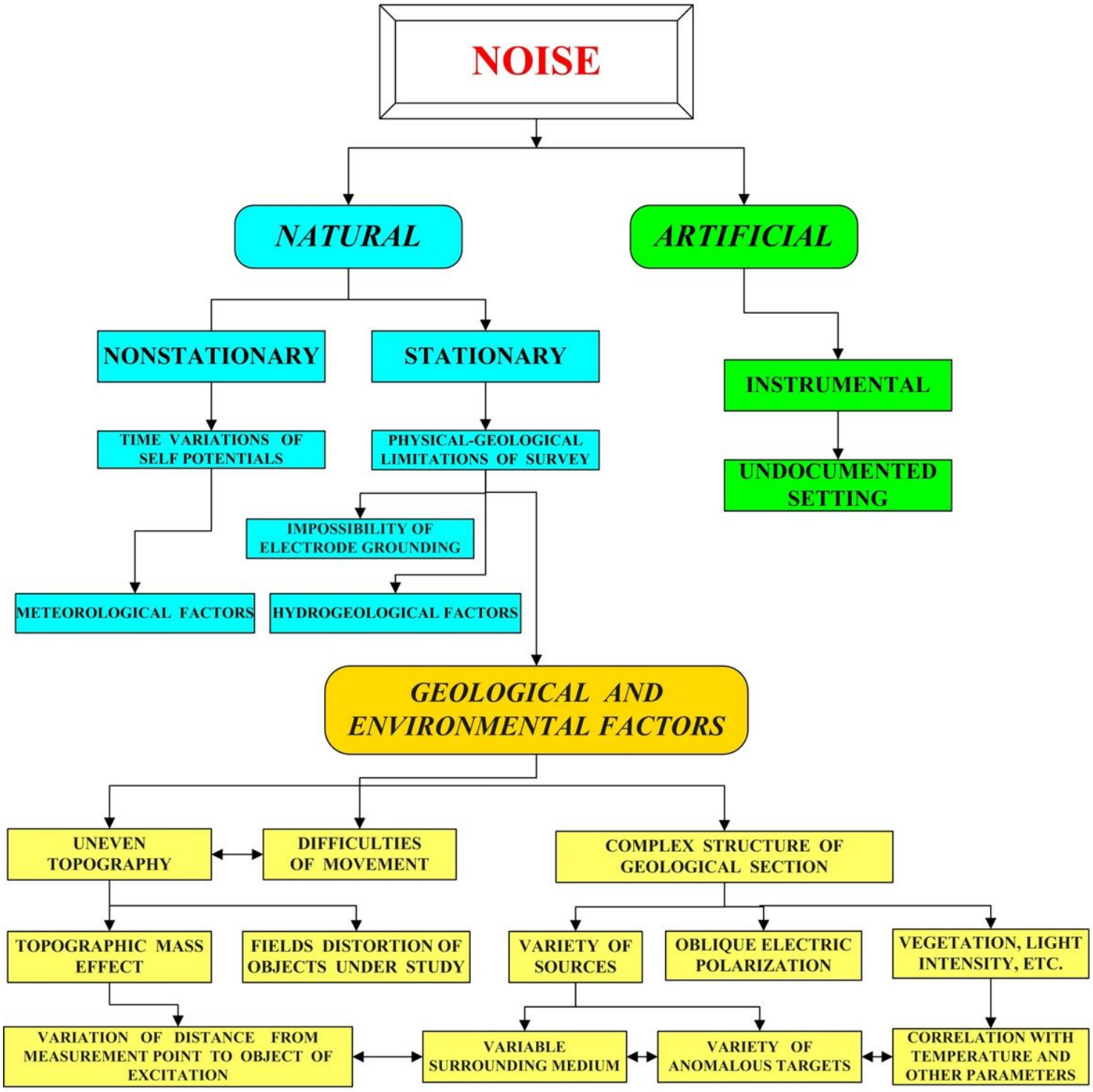

Figure 1

General scheme of disturbances in SP method

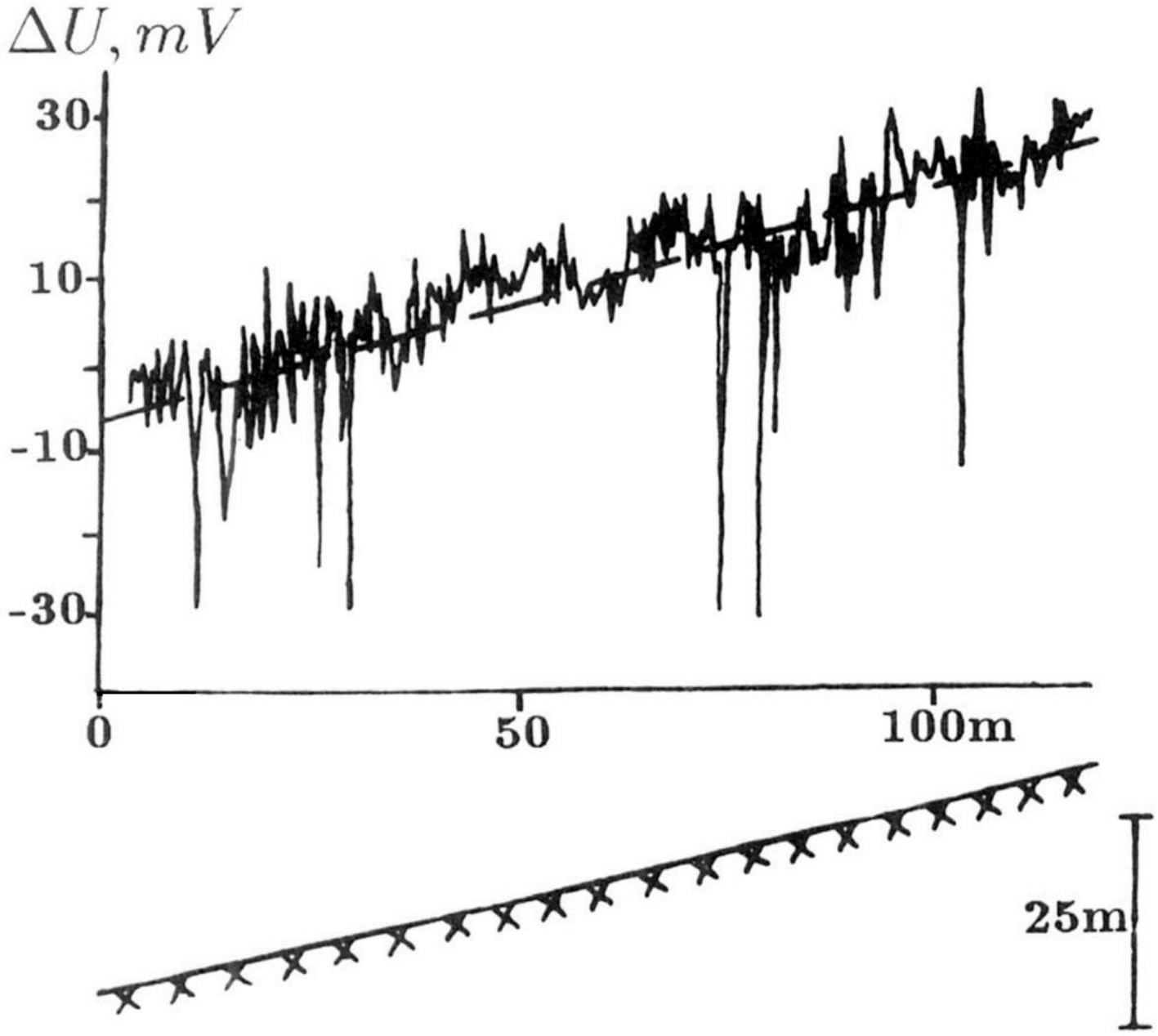

Figure 2

SP observations at inclined relief (after Ernstson and Schrerer (1986), with small modifications) (Middle Keuper of the Steigerwald highlands, 60 km east of Würzburg, Germany)

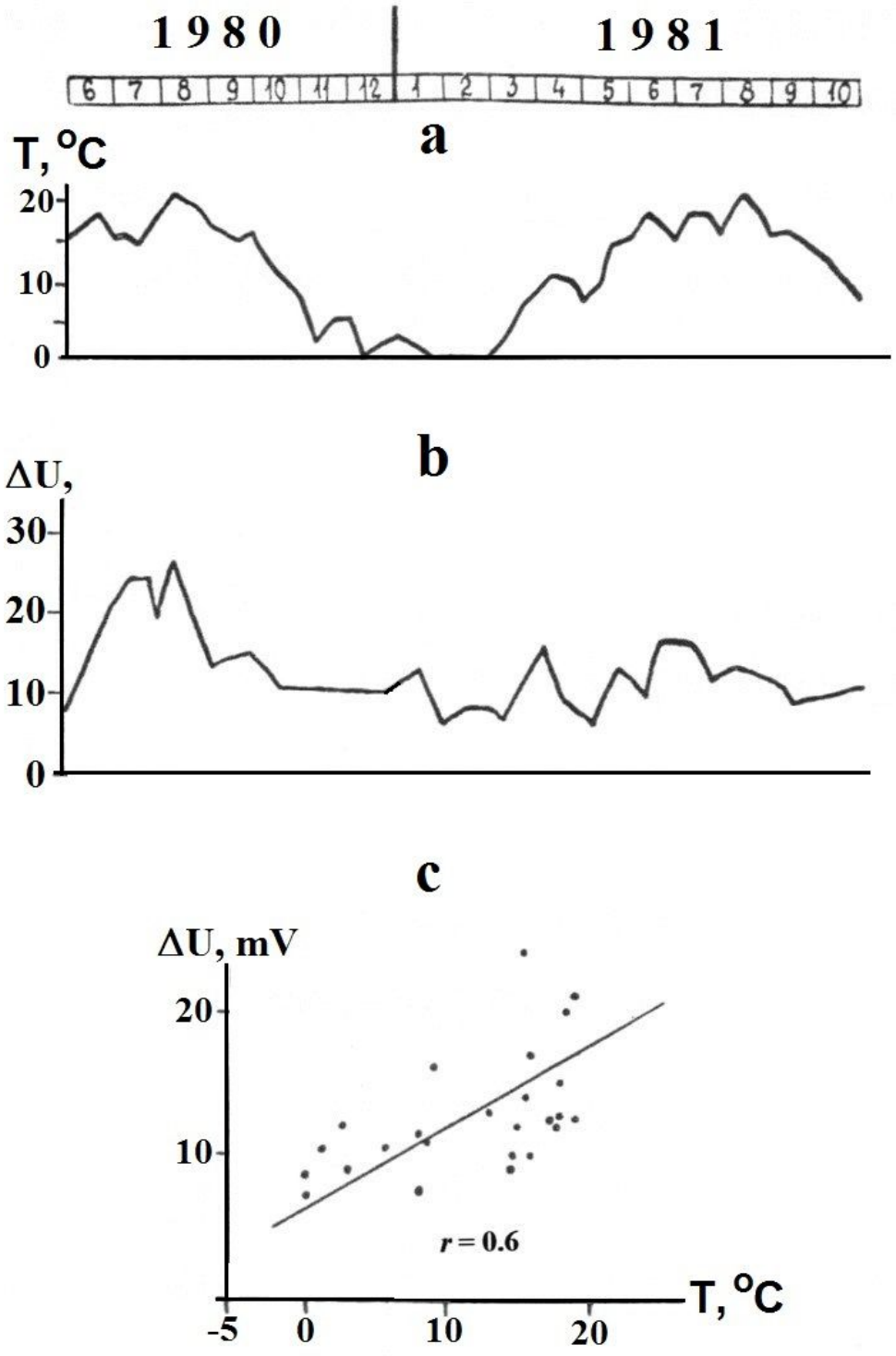

Figure 3

A correlation between temperature and SP observations: a – temperature, b – SP intensity, c – correlation between these parameters (a and b – after Ernstson and Schrerer (1986)). SP observations were carried out in the Middle Keuper of the Steigerwald highlands 60 km east of Würzburg, Germany

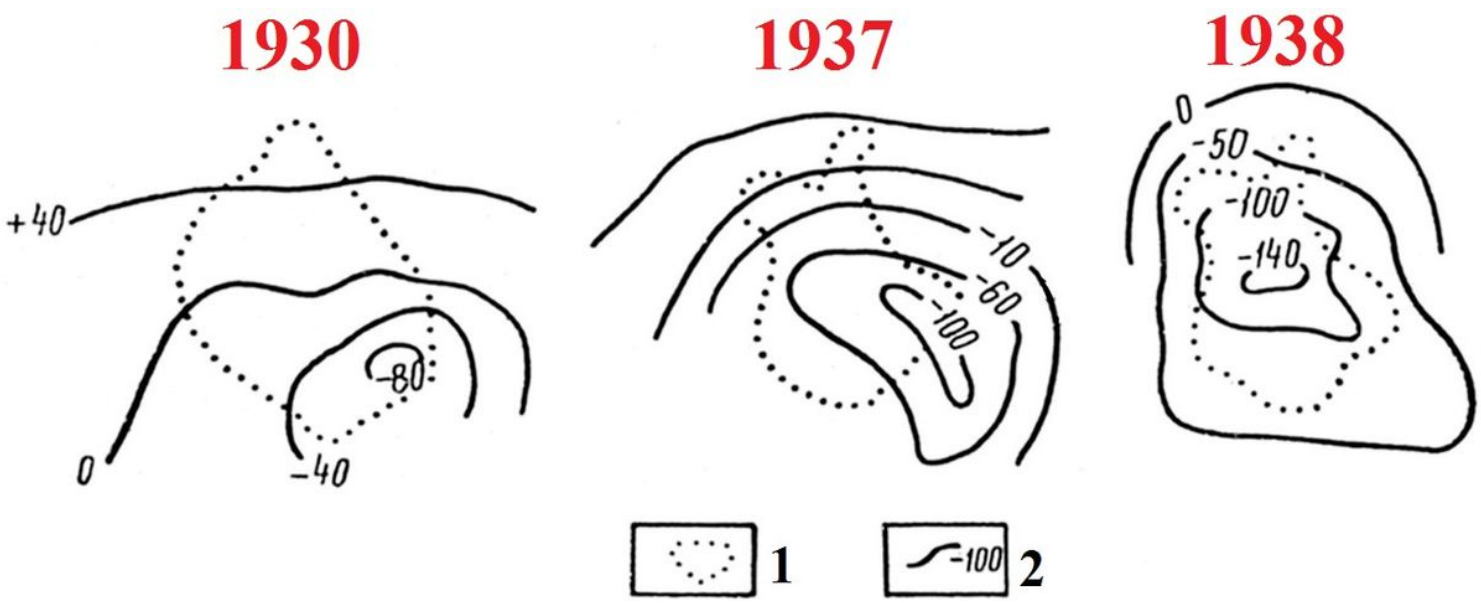

Figure 4

Displacement of self-potential isolines during exploitation of the new shaft of Chyragdere sulfur deposit (Lesser Caucasus) (after Eppelbaum and Khesin, 2012, with modifications). (1) stock contour, (2) isolines of self-potential field (in milliVolts)

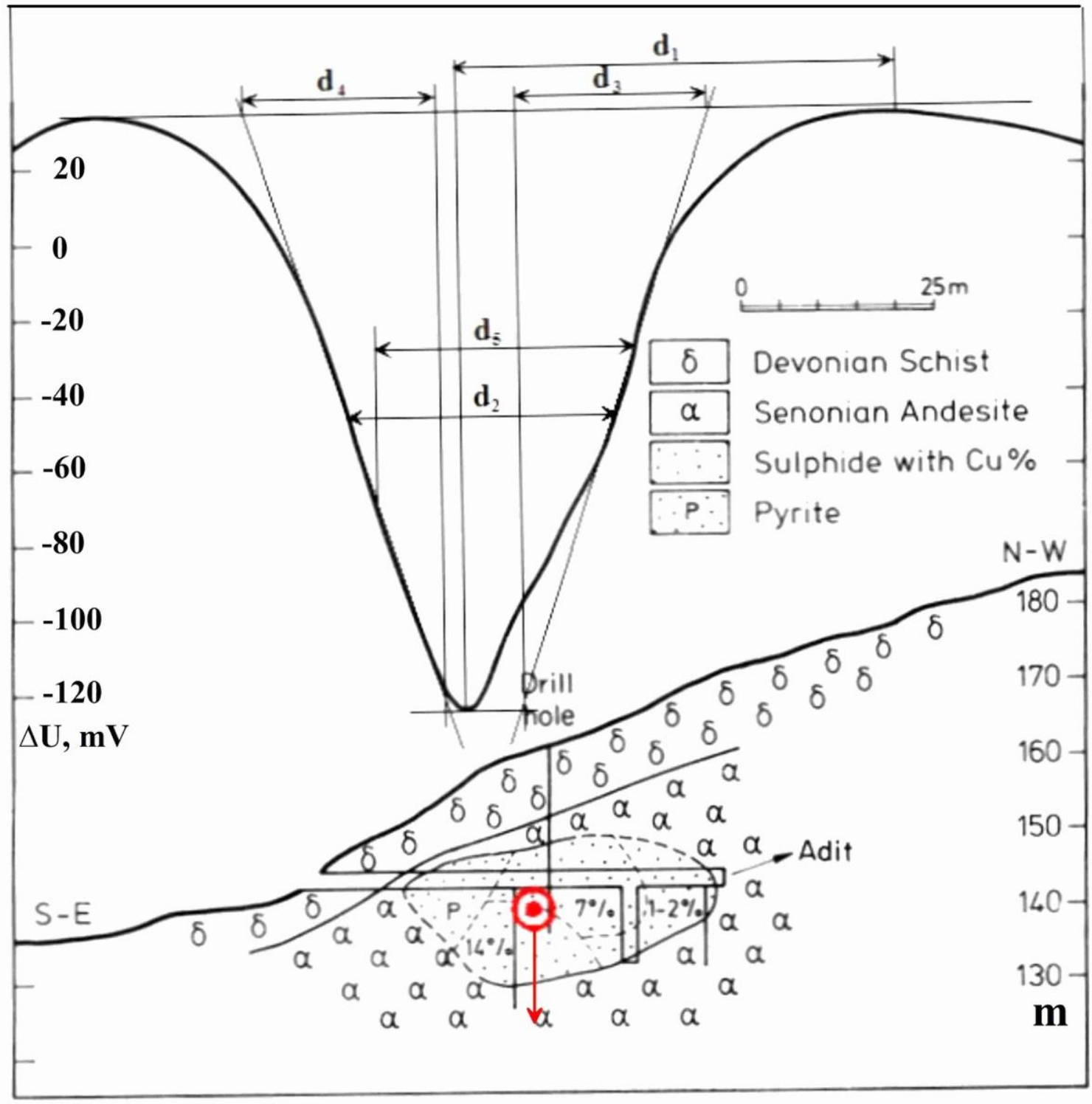

Figure 5

Quantitative interpretation of SP anomaly by the characteristic point and tangent methods in the Sariyer area, Turkey. The target symbol marks the obtained position of the ore body center (approximated by a HCC). Red arrow shows the direction of self-polarization vector. Observed SP curve and geological section are taken from Yüngül (1954)

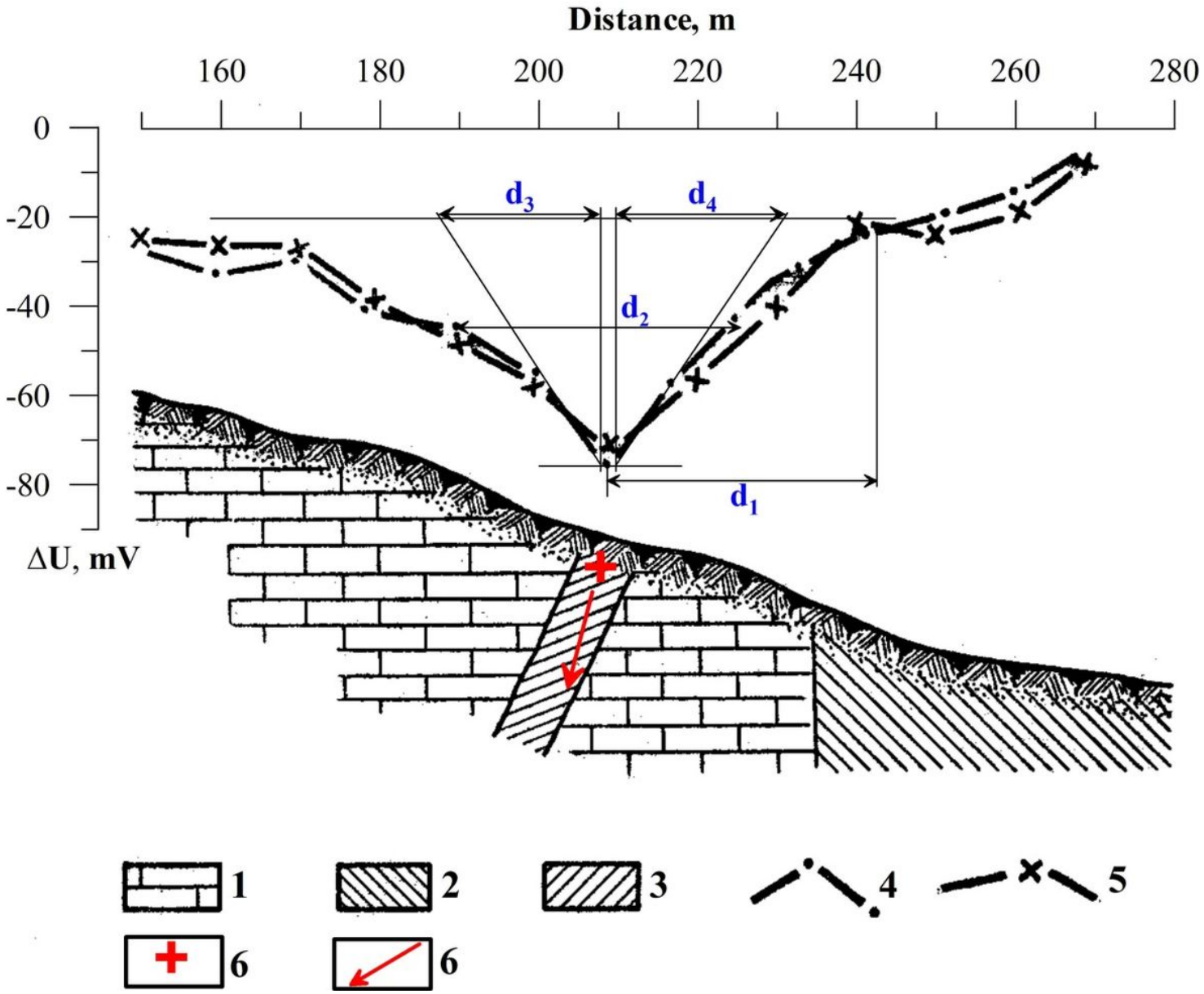

Figure 6

Quantitative interpretation of SP anomaly over polymetallic body (USSR). Observed SP curve and geological section are taken from Zaborovsky (1963)

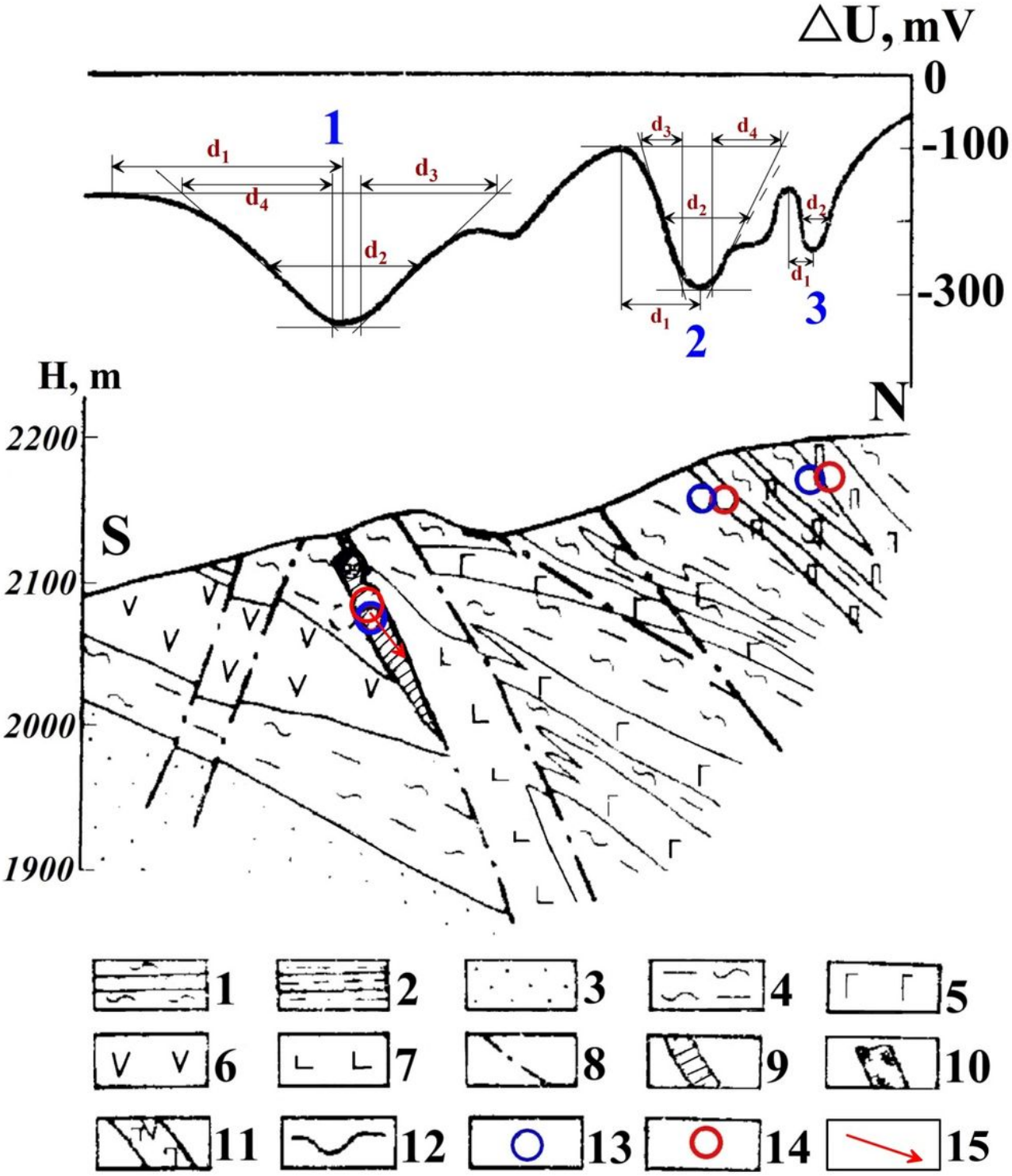

Figure 7

. Results of quantitative interpretation of SP anomalies in the area of Katsdagh copper-polymetallic deposits on the southern slope of the Greater Caucasus (Azerbaijan). (1) interbedding of sands and clay schists, (2) clay schists with the flysh packages, (3) clay sandstone; (4) sand-clay schists; (5) diabases, gabbro-diabases and diabasic porphyrites; (6) andesites and andesite-porphyrites; (7) dacitic porphyrites; (8) faults; (9) massive ore of pyrite-polymetallic composition; (10) oxidized ore; (11) zones of brecciation,

crush and boudinage with lean pyrite-polymetallic ore; (12) SP curves; location of anomalous source: (13) without calculation of inclined relief influence, (14) after introducing correction for terrain relief, (15) position of the self-potential vector

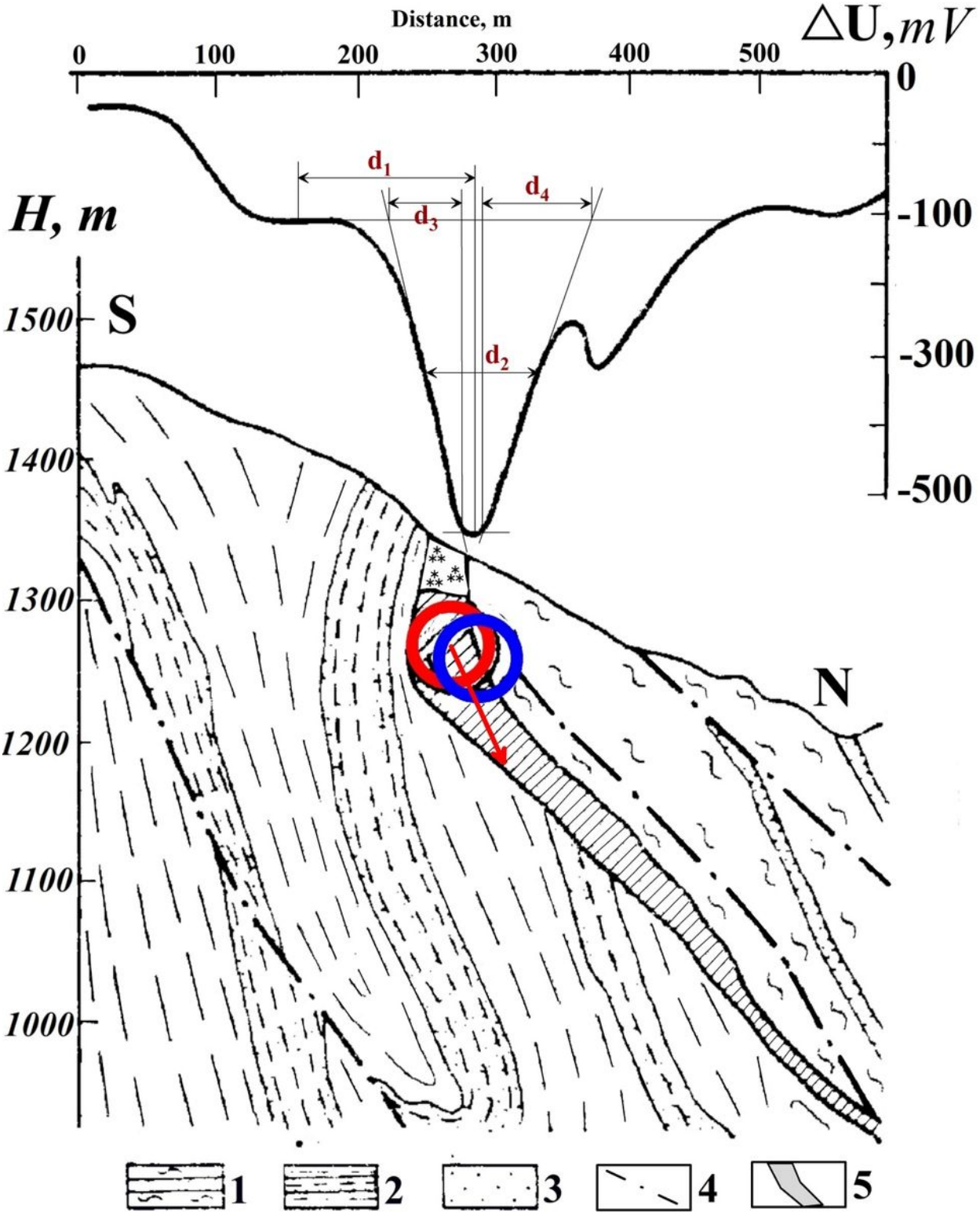

Figure 8

Results of quantitative interpretation of SP anomaly in the area of Filizchay copper-polymetallic deposit in the southern slope of the Greater Caucasus (Azerbaijan) (revised after Eppelbaum and Khesin (2012)).

(1) interbedding of sands and clay schists, (2) clay schists with the flysh packages, (3) clay sandstone, (4) faults; (5) massive ore of pyrite-polymetallic composition; (6) oxidized ore; (7) SP curves, location of anomalous source: (8) without calculation of inclined relief influence, (9) after introducing correction for relief

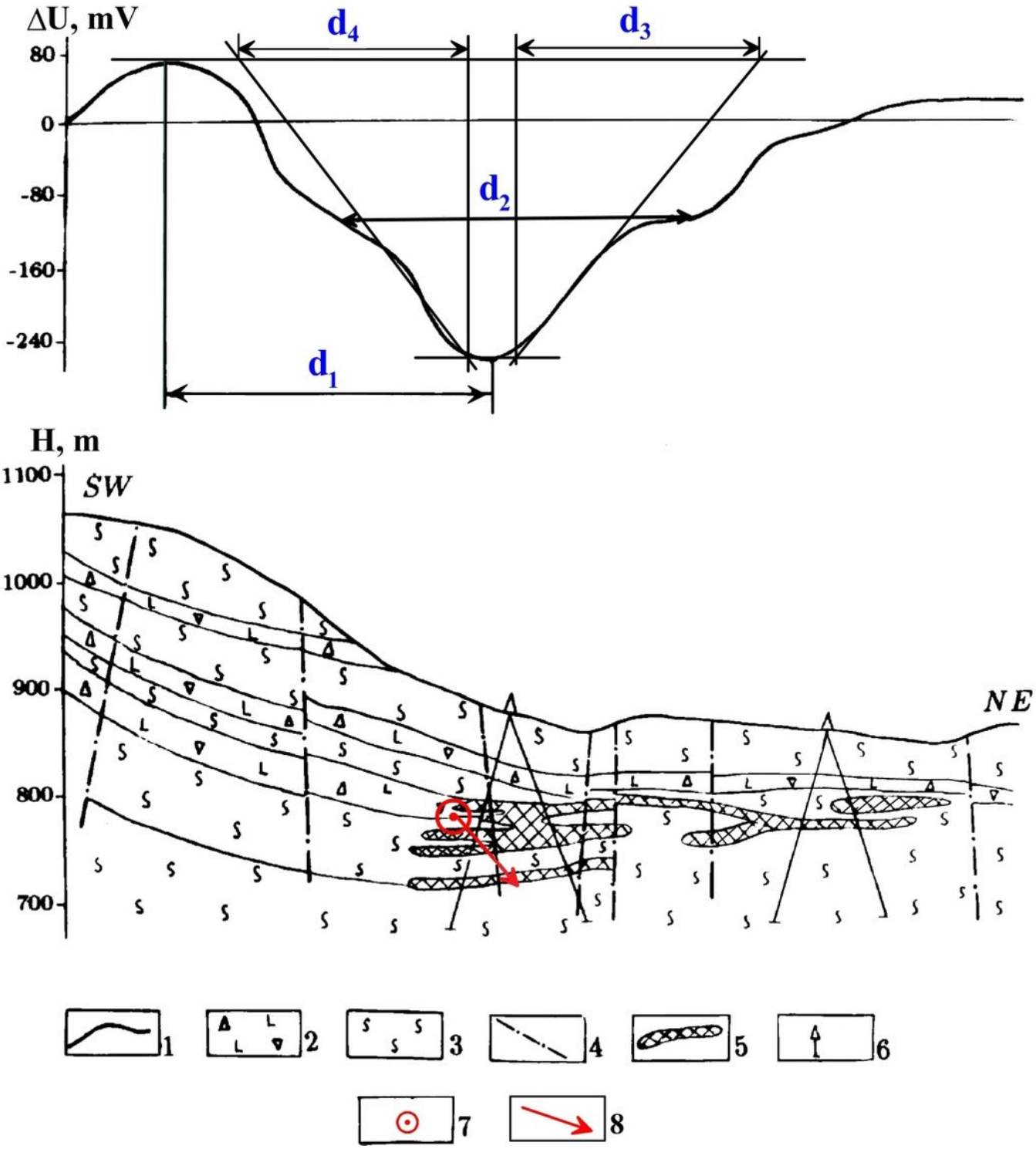

Figure 9

Interpretation of SP anomaly by the method of characteristic points in the area of the Uchambo ore field of the Adjar group of copper-polymetallic deposits (Georgia, Lesser Caucasus) (1) SP observed values; (2) heteroclastic tuff breccia and their tuffs; (3) cover trachyandesite-basalts with pyroclastic interbeds; (4) disjunctive dislocations; (5) zones of increased mineralization; (6) drilled wells; (7) location of HCC center according to the interpretation results ((1-6) from Bukhnikashvili et al. (1974)

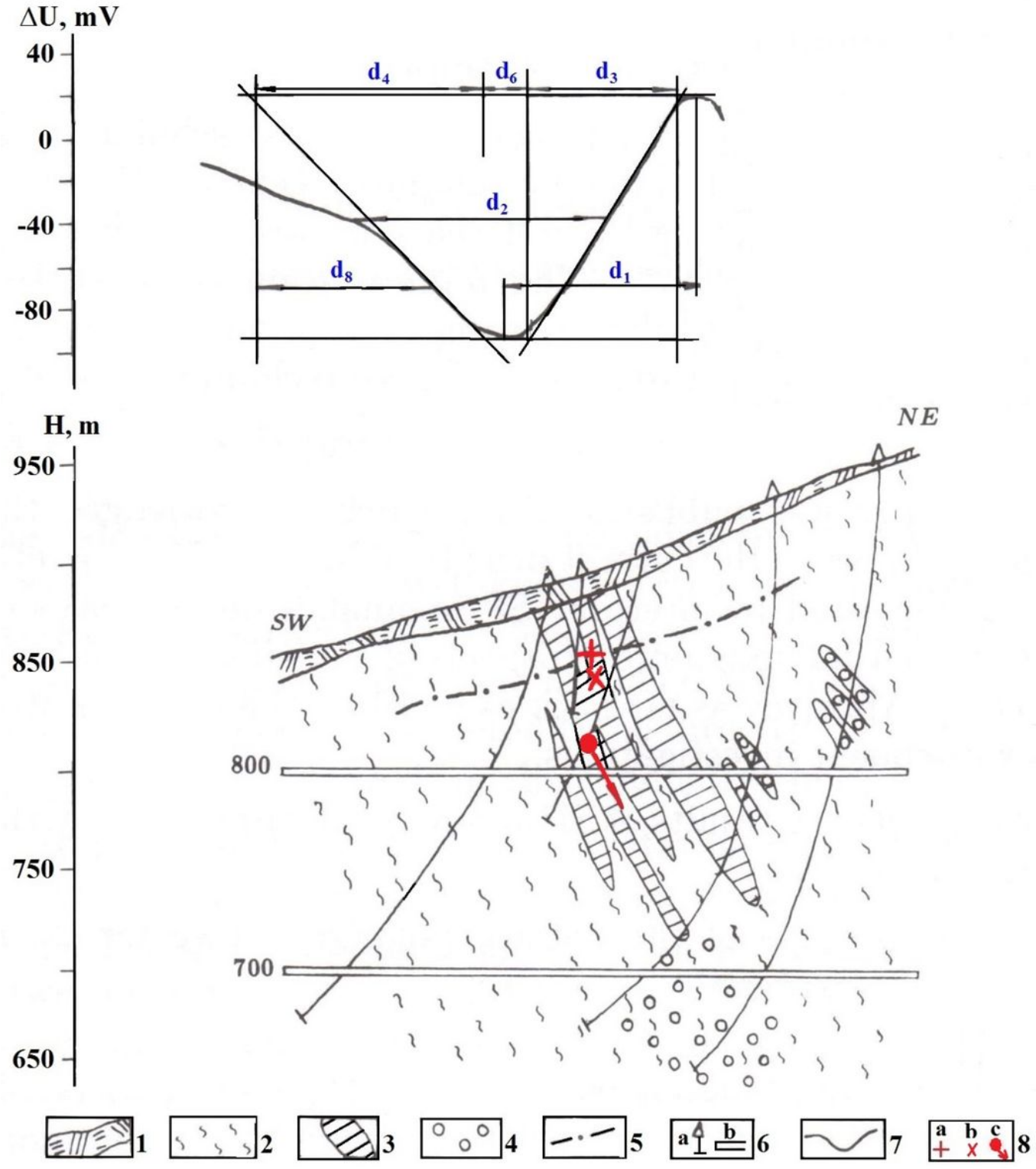

Figure 10

Interpretation by the developed techniques of SP anomaly in the area of deposit Potentsialnoe (Rudny Altai, Russia) (initial data from Semenov (1975)) (1) soil-vegetative layer; (2) alternation of lavas and tuffs of acid composition and chlorite-sericitic schists; (3) sulfide ores; (4) sulfide impregnation, pyritization; (5) level of ground waters; (6) drilling wells (a) and adits (b); (7) plot of SP; (8) interpretation results: (a) upper edge of the thin bed, (b) mid-point of the inclined thick bed's upper edge, (c) center of a horizontal circular cylinder (arrow indicates the direction of the polarization vector obtained by interpretation)

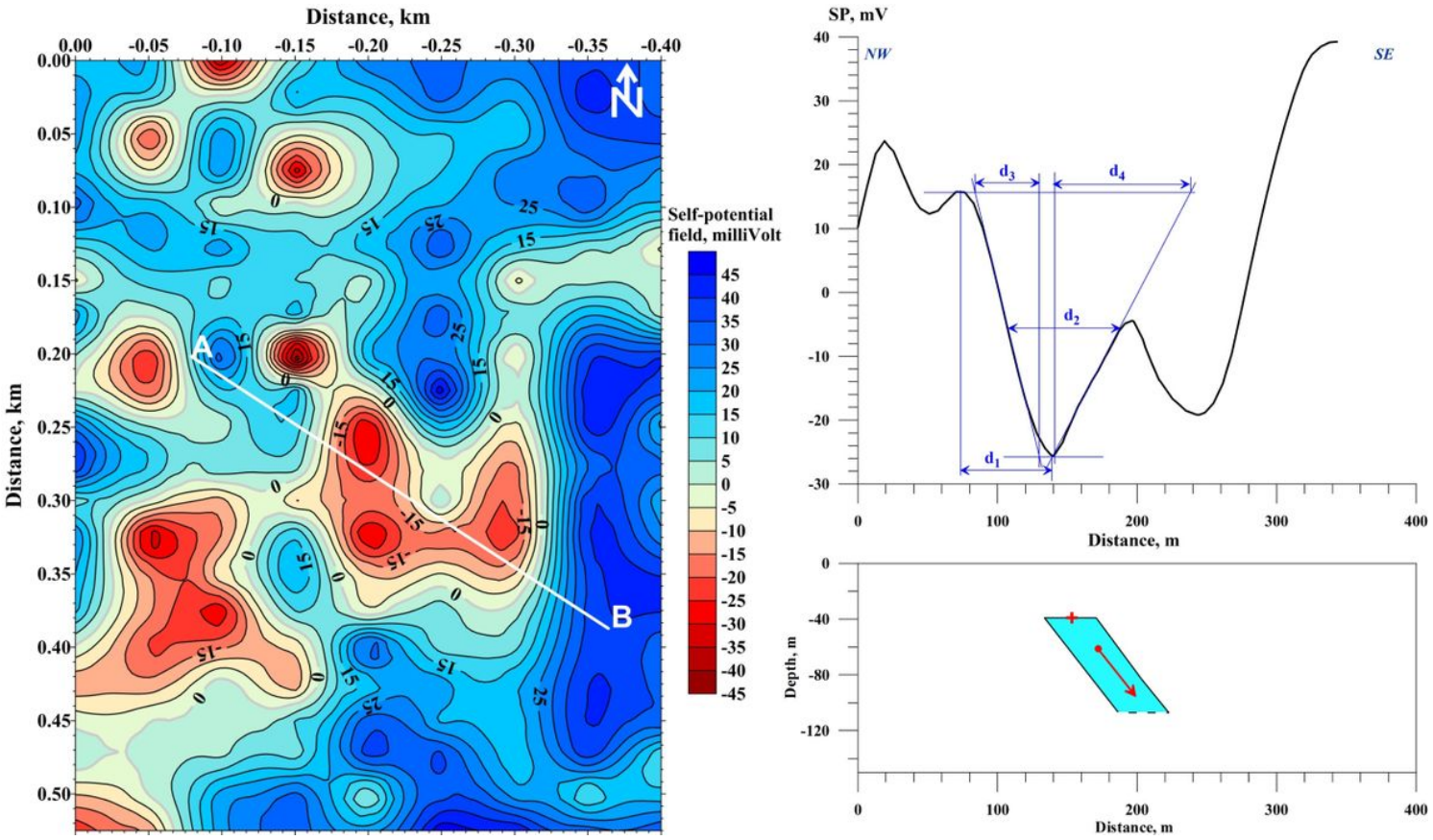

Figure 11

a: (left) SP map observed in the western Makhtesh Ramon (northern Negev desert) b: (right) Interpretation of SP anomaly along profile A – B, western Makhtesh Ramon (see Figure 11a)

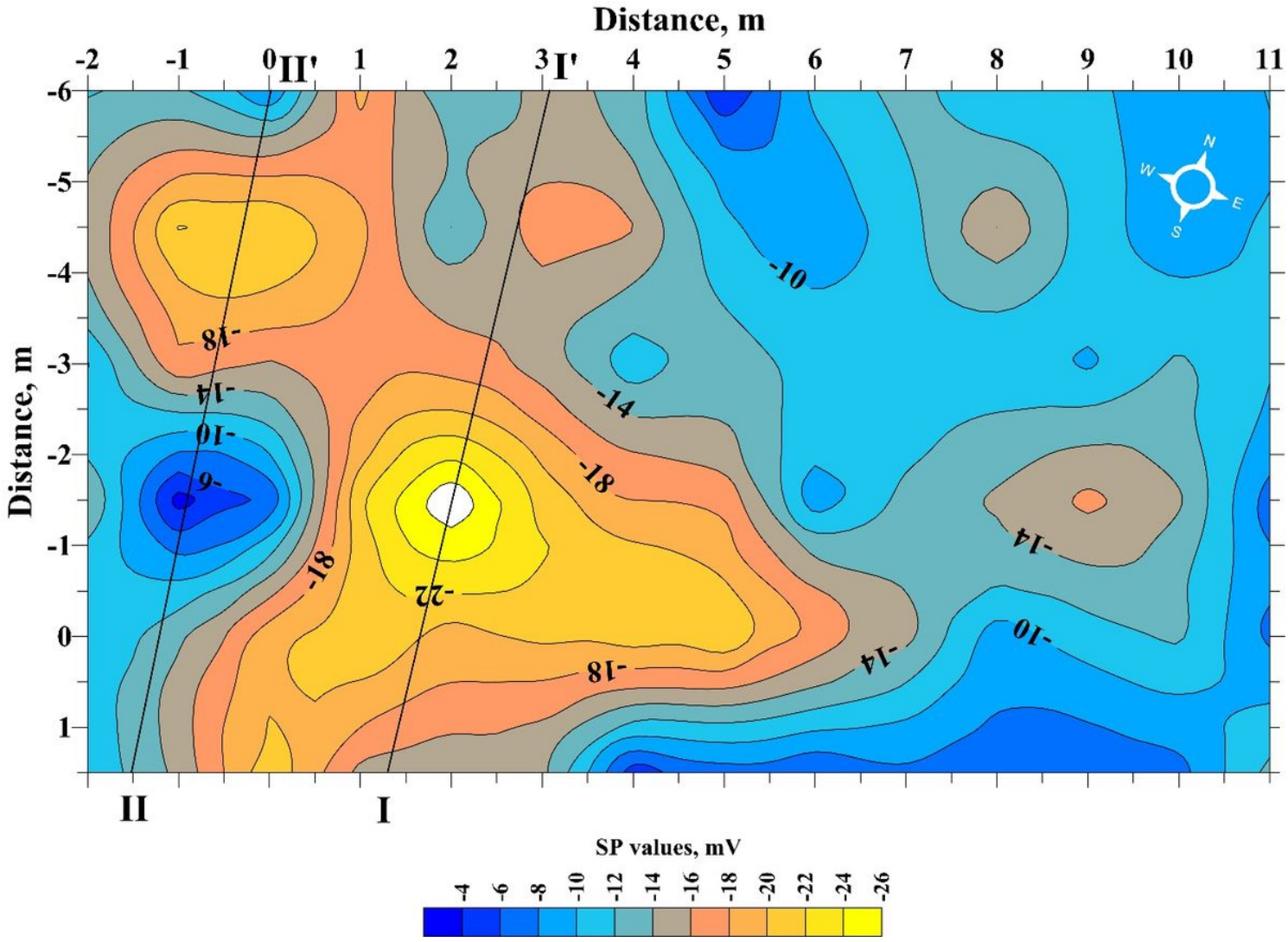

Figure 12

Self-potential map observed in the Banias site (northern Israel) and location of interpreting profiles I – I' and II – II'

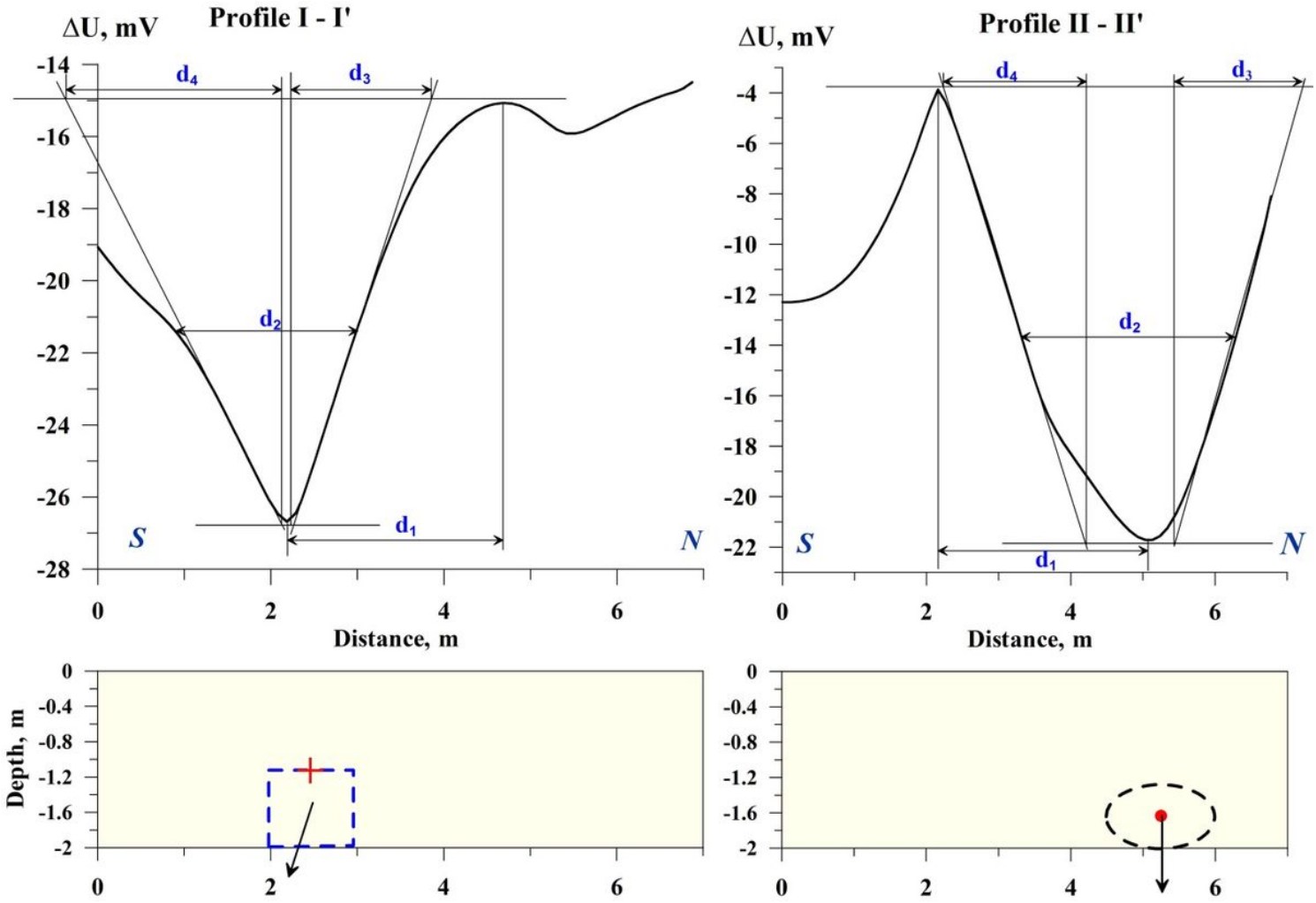

Figure 13

Quantitative analysis of anomalies I – I' and II – II' (see Figure 12) in the Banias site (northern Israel). Red cross indicates position of the center of upper edge, bold red point testifies position of HCC center, and the black arrows show direction of polarization angle Φp

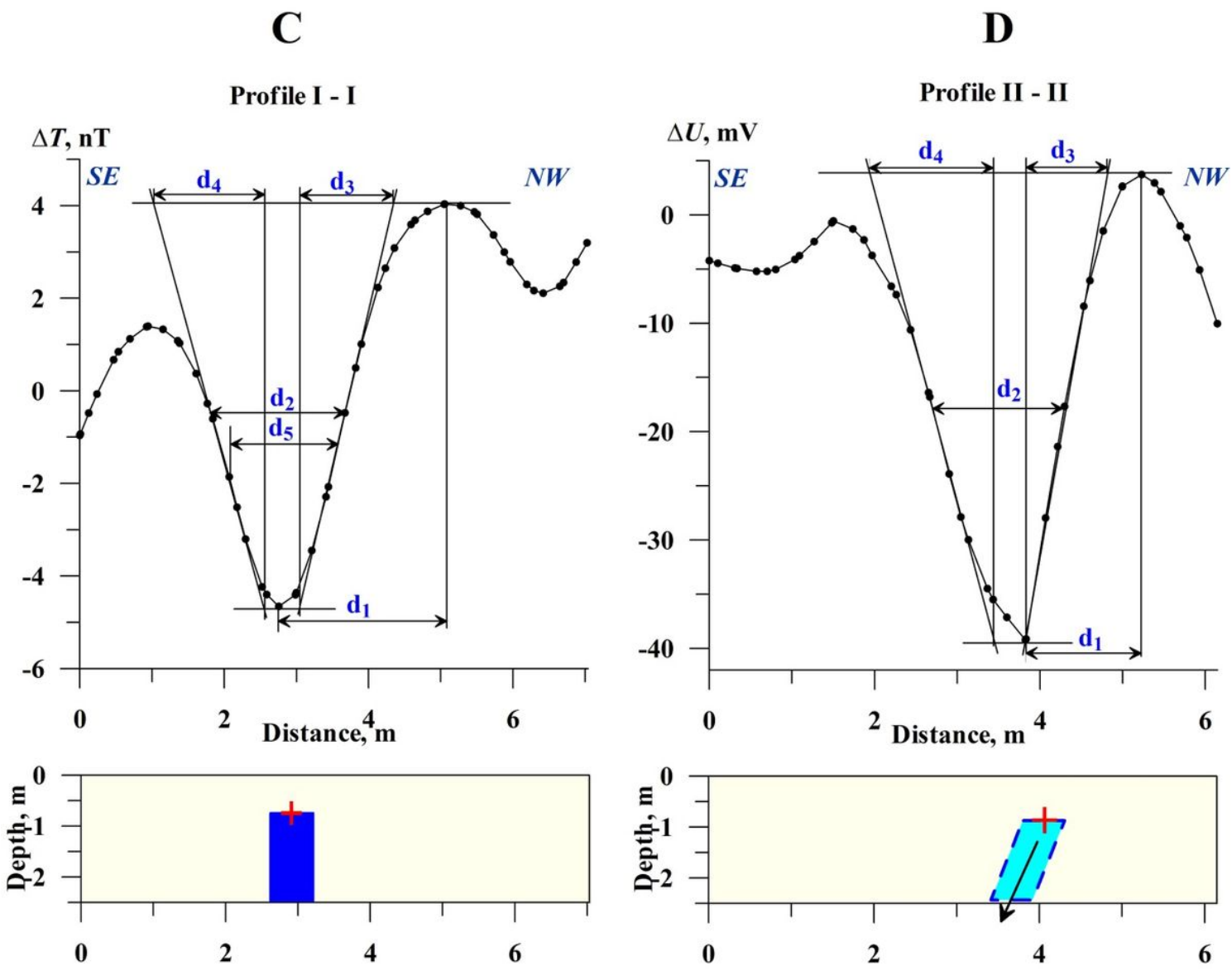

Figure 14

Quantitative analysis of magnetic (A) and self-potential (B) anomalies in the site of Halutza (southern Israel). Red cross in both models indicates position of the center of the upper edge, red arrow shows direction of polarization angle ΦP

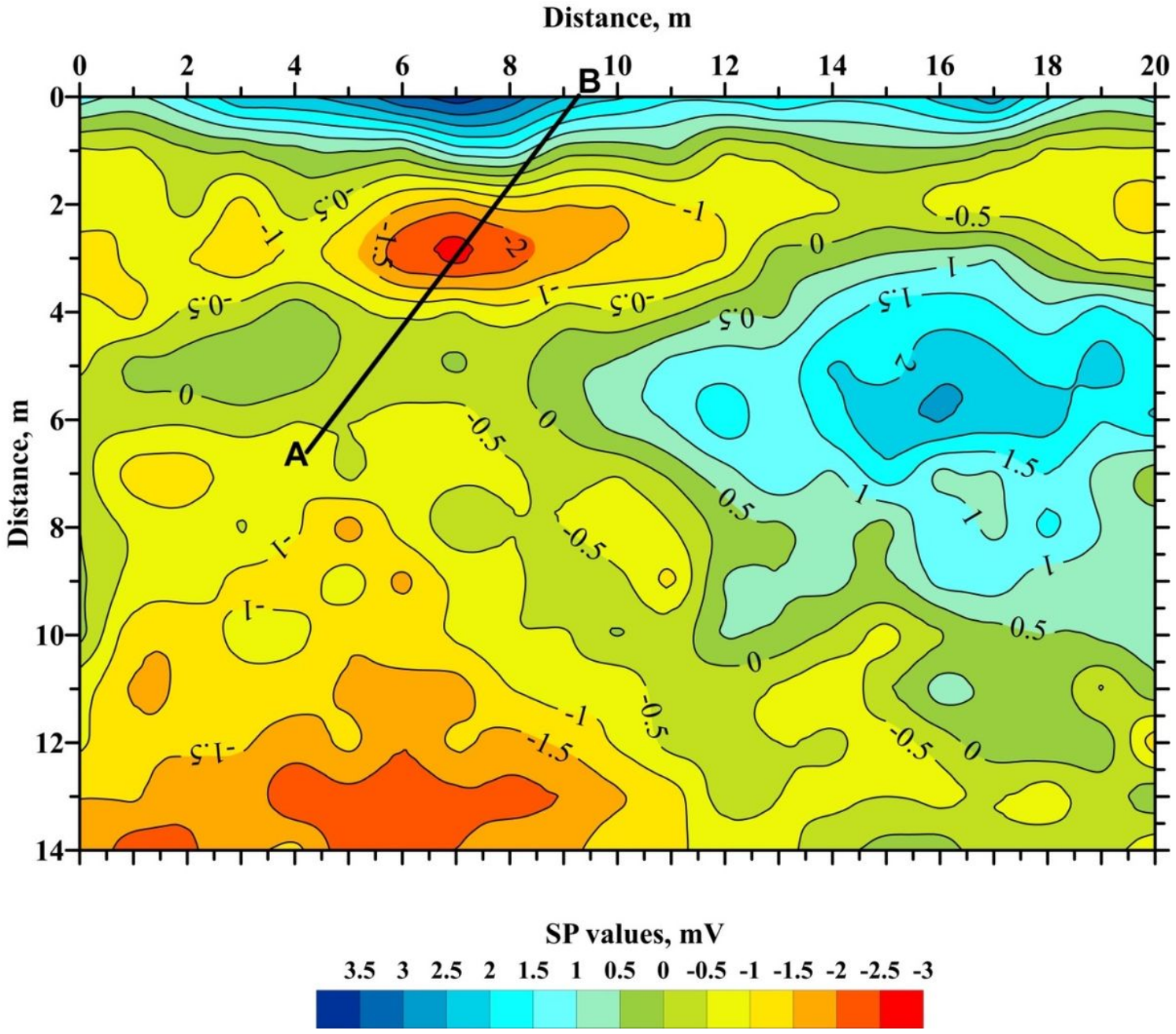

Figure 15

Self-potential map observed in the site of Emmaus-Nikopolis (central Israel)

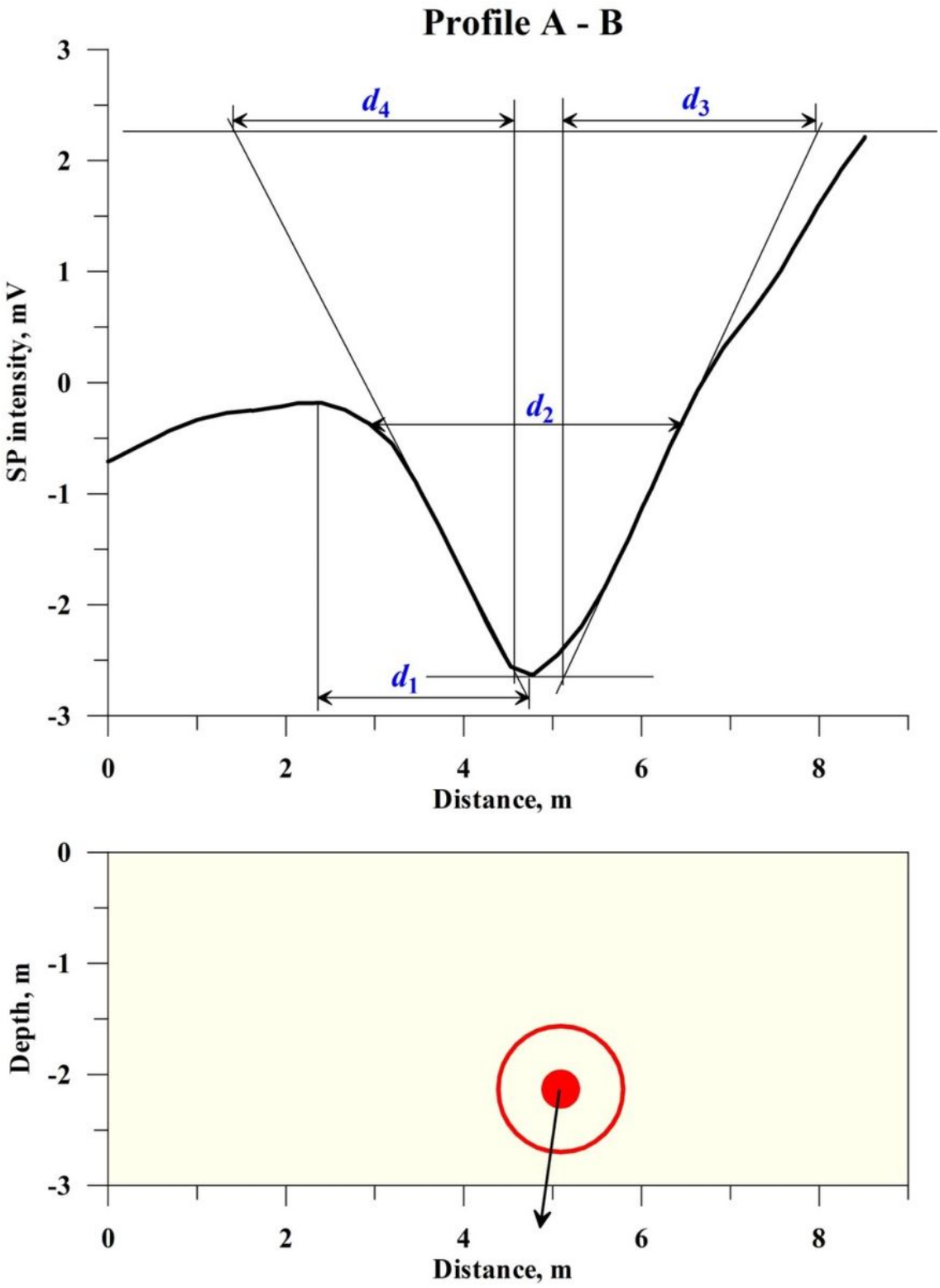

Figure 16

Quantitative analysis of self-potential anomaly along profile A – B in the site of Emmaus-Nikopolis (SP map is presented in Figure 15). Black arrow shows direction of polarization angle ΦP

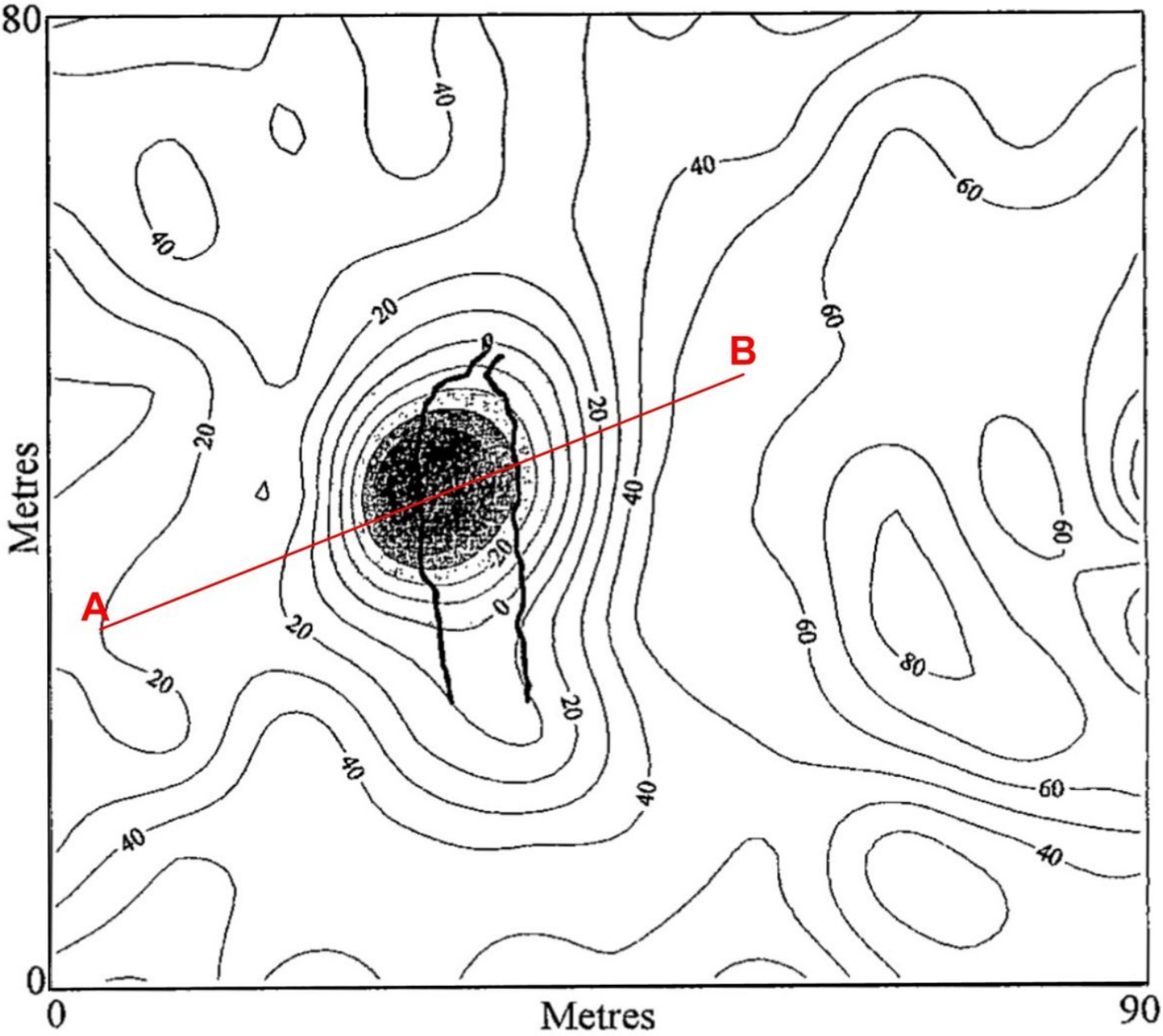

Figure 17

SP map over underground cave and position of interpreting profile A – B (SP map after Quarto and Schiavone (1996))

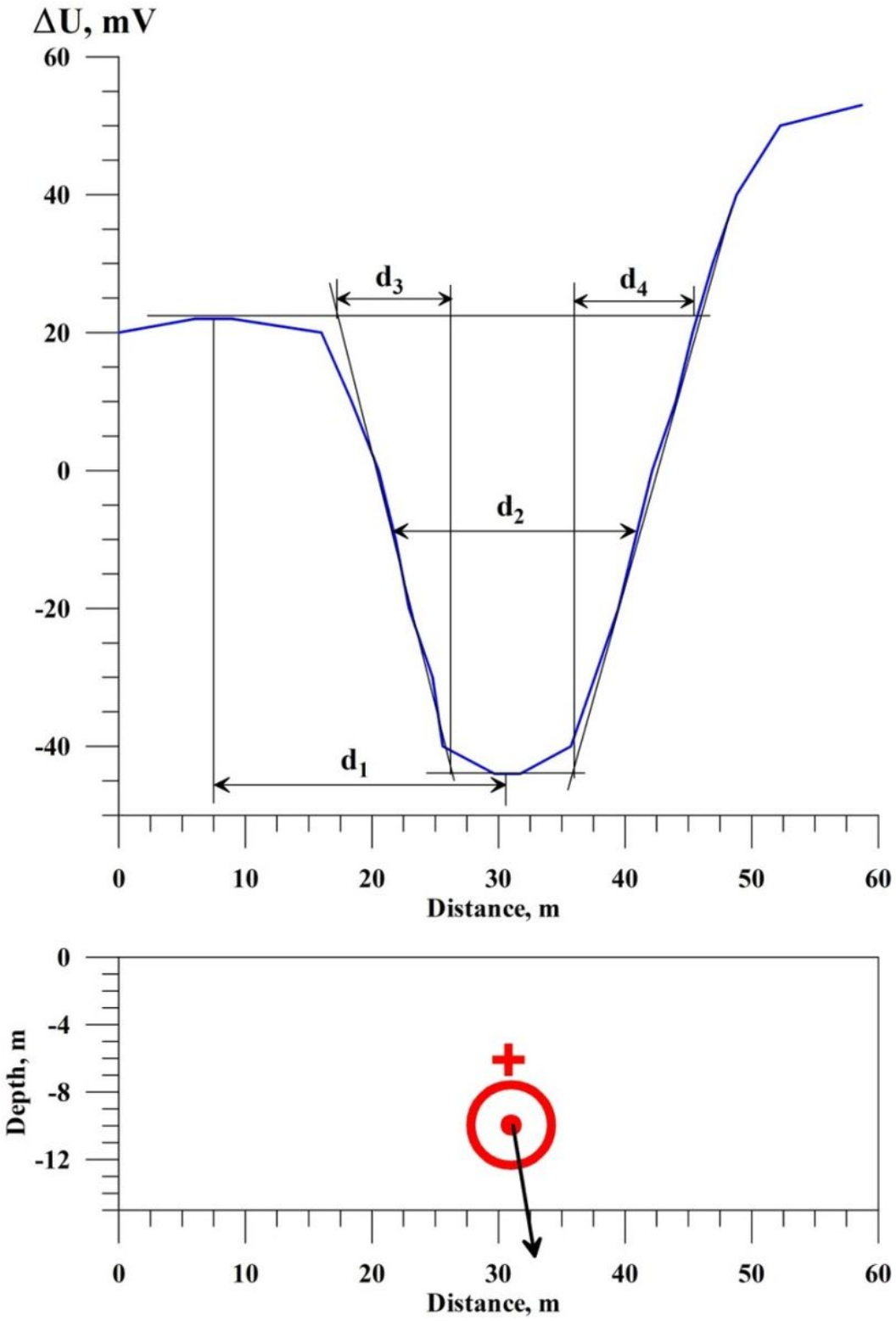

Figure 18

Quantitative analysis of SP anomaly along profile A – B (location of profile is shown in Figure 17). Red cross designates position of the middle of the thin bed upper edge, and circle – position of the center of the horizontal circular cylinder.

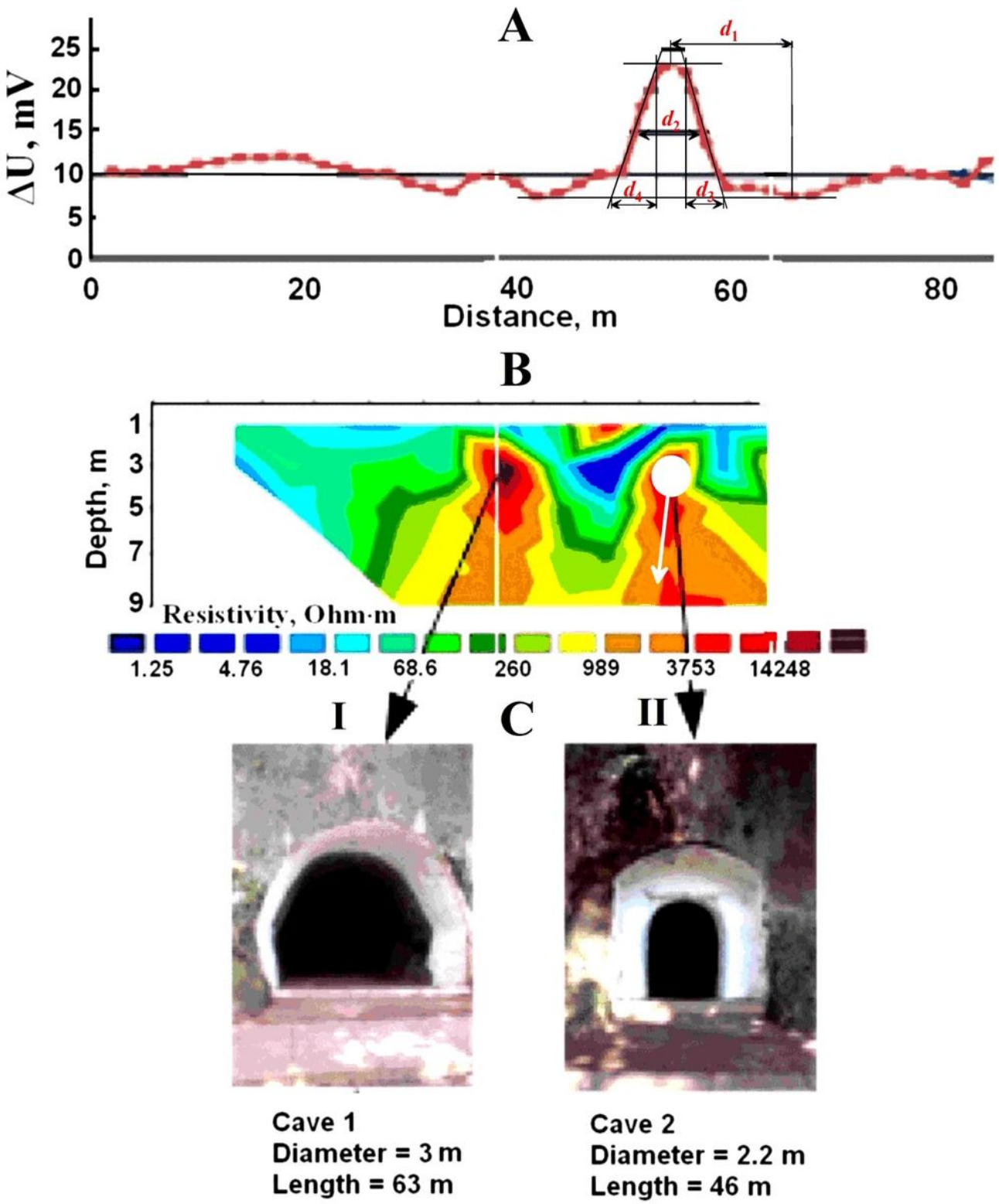

Figure 19

Quantitative analysis of SP anomaly over underground cave in the Djuanda Forest Park, Bandung (Indonesia). Initial data are taken from Srigumoto et al. (2010). White circle and arrow indicate the position of upper edge of cave II and its dipping (distribution of the highest resistivities)

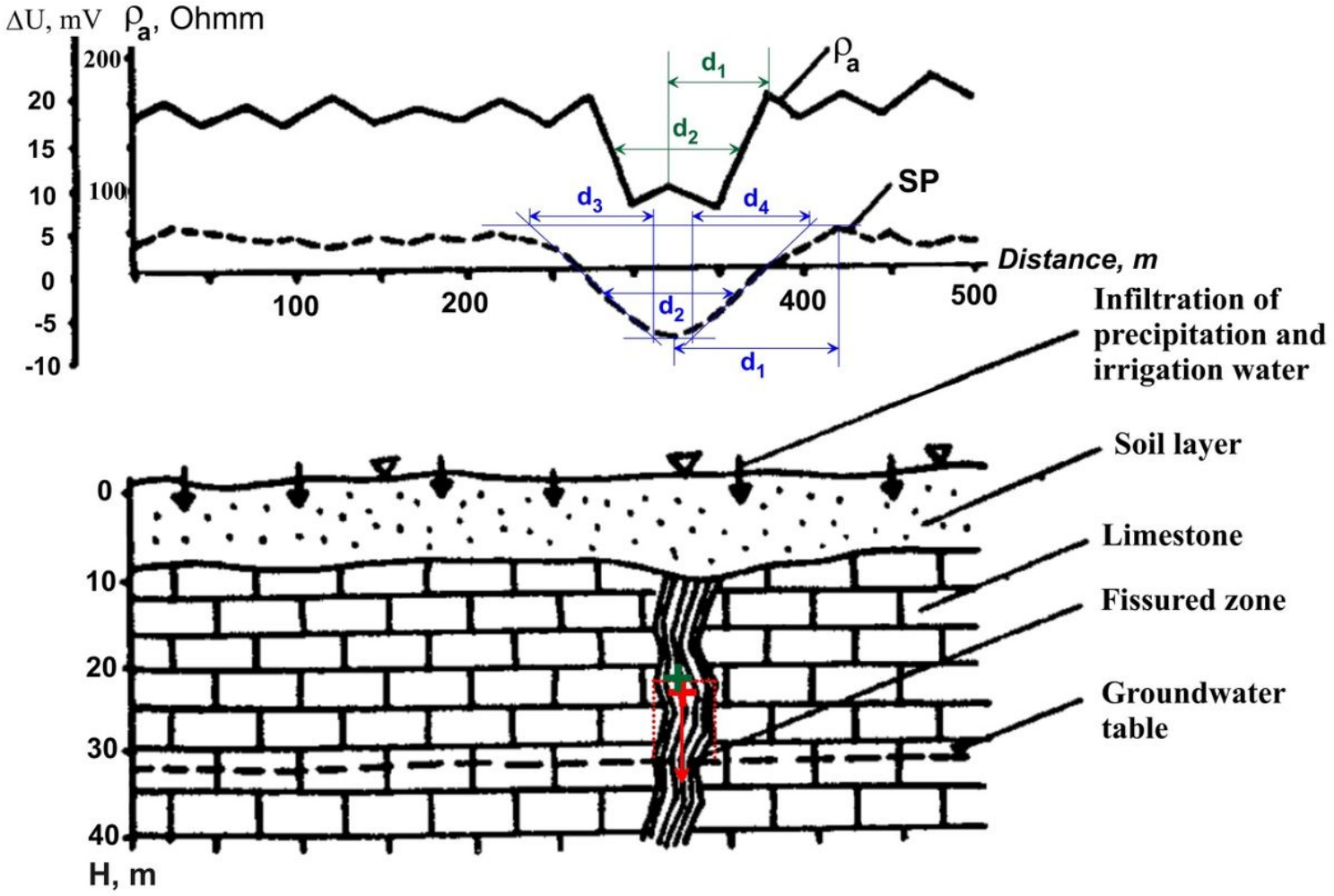

Figure 20

Interpretation of SP anomaly over the fissured zone (Russia) (resistivity and SP graphs and geological section are from Ogilvy and Bogoslovsky (1979)). Red and green crosses show the positions of the upper edge of the anomalous target determined from SP and resistivity curves, respectively. Red arrow indicates the position of self-potential vector

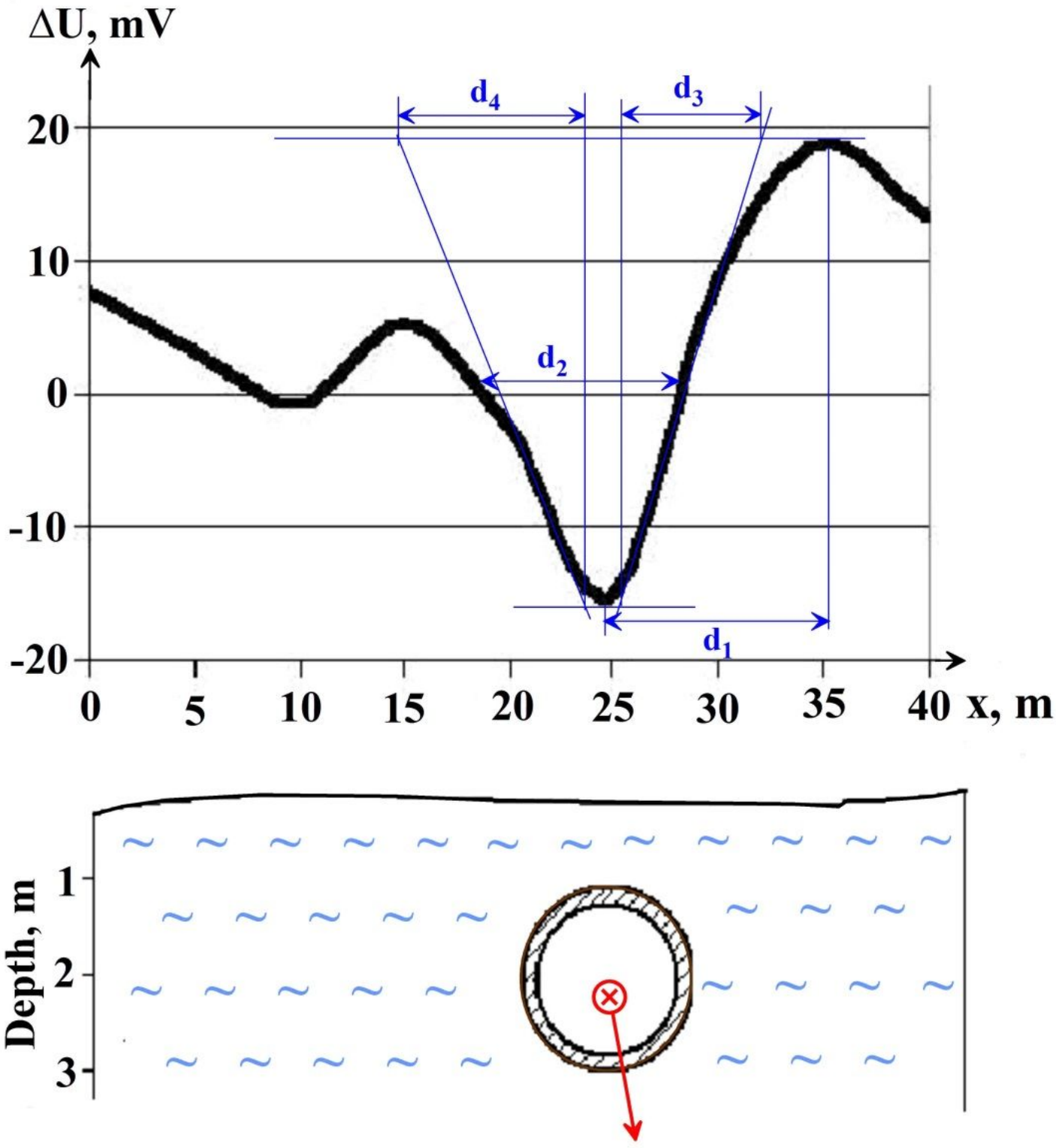

Figure 21

Quantitative examination of SP anomaly from the buried metallic pipe (southern Russia). Observed SP graph and environmental section are taken from Fomenko (2010). Red circle indicates determined position of the center of HCC, and arrow shows position of self-potential vector